UNIVERSITA' DEGLI STUDI DI PARMA

Dottorato di ricerca in Scienze e Tecnologie Alimentari

Ciclo XX

DEVELOPMENT OF NEW METAL CHELATES FOR ANIMAL NUTRITION AND OF ANALYTICAL METHODS FOR THEIR QUANTITATIVE DETERMINATION AND QUALITY CONTROL

Coordinatore:
Chiar.mo Prof. G. SanSebastiano

Tutors:
Chiar.mo Prof. C. Corradini
Chiar.mo Prof. G. Predieri

Dottorando:
Beltrami Diego

Anno 2008

In copertina: **Wassily Kandinsky - Composition VIII - 1923 -**
Fonte: http://www.writedesignonline.com/history-culture/bauhaus.htm

INDEX

1. Introduction

It is well known that much of the life chemistry is *inorganic* because standard growth, development, health of the living organisms imply the presence in the right concentration of inorganic elements (so called mineral nutrients or simply *minerals*), that is elements different from carbon, hydrogen, nitrogen, oxygen, sulphur, phosphorous, which are the constituents of fundamental biomolecules (protides, lipids, glucides and nucleotides). Most *mineral* elements are constituted by metals that develop various functions. To understand it better, it is necessary to take the periodic table of chemical elements as a reference; the metal ions of Groups 1 and 2 (Na^+, K^+, Ca^{2+}, Mg^{2+}) act as structural elements and as maintenance of osmotic balance charges. The ions of the transition metals in a single state of electric charge (oxidation state), such as zinc (2+), work as structural elements in enzymatic proteins or as activators for the protein activity. The transition metals which show different oxidation states behave as electron transporters (iron and copper ions respectively in cytochrome and in plastocianin). For all these reasons and for other reasons that will be illustrated afterwards, metals have been subjected to numerous studies (retrospective, *in vivo, in vitro* or in laboratory) focused mainly on the so-called trace metals, that is, those in concentrations close to parts per billion (ppb). Regarding the nutrition field (much more in the animal nutrition but also in the human one) in the past the trace metals elements *(mineral micronutrients)* were administered solely as integrators and in the form of oxides or inorganic salts, as they were less expensive, but especially stable and easily mixable in food. In fact trace elements have been observed and studied in Europe for more than 30 years. Currently, there are 23 mineral elements recognized and classified as having significance in nutrition.

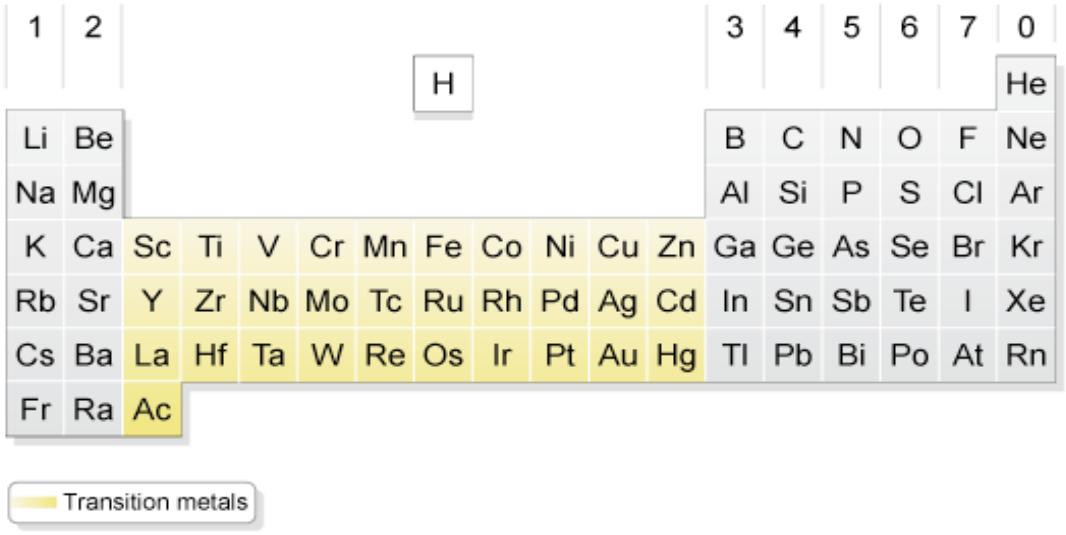

Fonte: http://www.bbc.co.uk/schools/gcsebitesize/science/edexcel/patterns/transitionmetalsrev_print.shtml

1.1. Minerals classification and basic knowledge about mineral nutrition

Minerals are generally classified by their presence in organisms and by their quantity required in the diet in: MACROMINERALS, required in high quantity in the organism, MICROMINERALS (or *microelements*) required in small quantities but nevertheless indispensable and OLIGOELEMENTS (or *trace* elements).
This is illustrated in Table 1:

MACROMINERALI	MICROMINERALI	OLIGOELEMENTI
calcium (Ca)	iron (Fe)	tin (Sn)
phosphorous (P)	manganese (Mn),	germanium (Ge)
magnesium (Mg)	cobalt (Co)	vanadium (V)
sodium (Na)	molybdenum (Mo),	tungsten (W)
potassium (K)	copper (Cu)	lithium (Li),
chlorine (Cl)	iodine (I)	nickel (Ni)
sulfur (S)	zinc (Zn)	arsenic (As)
	chromium (Cr)	lead (Pb)
	fluorine (F)	
	selenium (Se)	
	aluminum (Al)	
	boron (B)	
	cadmium (Cd)	
	silicon (Si)	

Table 1: Mineral classification

It is important to highlight that many minerals are fundamental for the vital processes. A number of micronutrients have been shown to affect of various aspects on physiological status: for example, the interactions between nutritional status, immunology and disease are extremely complex (Spears, 2000) and influenced by micromineral; or the case of reproductive performance by beef cows: its possible lowering under normal level is frequently attributed to subclinical deficiencies of a variety of trace minerals. Moreover the nutritionists have much to learn about regulating mineral intake, dietary mineral interactions, mineral availability from feedstuffs and capability of animal to store minerals in body tissue (Olson, 2007). Finally the National Research Council (NRC) has established dietary requirements or maximum tolerable levels for some mineral elements, even if what is unknown presently is the degree to which individual mineral elements are stored and how long it takes an animal to manifest a deficiency problem once intake of a particular

cases (McDowell, 2000). In fact the trace mineral status of animal depends not only on dietary allowance, but also on the efficiency of digestion and storage, which both can be affected by interactions with other food constituents. Hence, trace elements deficiencies are often suspected by veterinary surgeons in low performance herds, and when assessed, a deficient status is considered as the likely cause of disorders (Enjalbert, 2006).

1.2. Minerals properties

1.2.1. Role of the Elements in the organism

1.2.1.1. Minerals distribution

Generally, 96% of the body weight of a human being is made of elements contained in organic substances and water (carbon, hydrogen, nitrogen and oxygen). Among the macroelements, calcium represents 46% of the total concentration of minerals, while phosphorous represents about 29%. Potassium, sodium, chlorine and magnesium represent about 25% while the other trace elements cover less than 0.3%. However, the distribution of minerals in the body is not uniform as some tissues are selective according to the function they develop (Scott *et al.*, 1982). Bones, indeed, are the main stocking area for various essential reasons as 85%, of the minerals in the body are found in the bony tissue of the skeleton and it mainly consists of calcium salts, phosphorous and magnesium (Underwood, 1981). Moreover, the total mineral heritage depends on the general nutritional state and growth; after a malnutrition period or dehydration conditions, for example, a net increase in the mineral concentration can be observed. Or, as in the case of sodium, potassium and chloride, the concentration remains constant during the growth process from the embryo to the adult phase while, for elements such magnesium, calcium and phosphorous the concentration at the embryo state is

about half that of the adult state.
It is necessary, therefore, to take into account that the mineral quantity (characteristic for each element) must be kept constant in order to safeguard tissue integrity and animal health.

1.2.1.2. Minerals functions

Mineral elements have four main functions: structural, physiologic, catalytic and hormonal. The structural function is made explicit at the level of the bones which are constituted by hydroxylapatite, that is a containing calcium, magnesium and phosphorous, in protein matrix, which guarantees a suitable structural solidity but also an appropriate mobility to the whole skeleton. Magnesium, silicon, fluorine, which contribute to the elasticity and mechanical stability of bones and teeth, play another important role. Phosphorous, zinc and sulphur (this last one main constituent of amino acids, sulphides and coenzymes) give, instead, proteins structural stability. These proteins constitute various tissues especially membranes; zinc in proteins, for example, co-ordinates some amino acids of the peptide chain influencing the folding of the protein itself and being constituent of numerous enzymes, it is the activator of different enzymatic systems.
The physiologic role is played by many of the macro and microelements at muscular tissue level (sodium, potassium, chloride play the function of electrolytes in fluids and in soft tissues), in nervous tissue (calcium, potassium and sodium are mainly responsible of the transmission of the nervous impulse), in biological fluids (blood coagulation, composition of cerebrospinal liquid, maintenance of pH conditions, tissue hydration and osmotic pressure), in membrane permeability (mechanism of ionic pumps), in enzymatic reactions (iron, chromium, copper, molybdenum, zinc, manganese and magnesium are present in the catalytic site of numerous enzymes) in cell respiration, in vitamins (cobalt is present in vitamin B_{12}), in hormones (iodine is part of the main thyroidal hormones) and in nucleic acids (phosphorous is directly involved in many metabolic processes in the form of ATP and energy

transference) (Underwood, 1981).

It is important, therefore, to highlight that the functions of minerals are strictly correlated among them as the elements are combining in a synergetic way to carry out, in the best possible way, the function for which the elements are in biological processes. Therefore, sometimes it is necessary to talk of a set of functions, more than of a specific function, linked to element combination which finally represents the whole requirements of macro and microminerals in the organisms (Cao et al, 2000).

1.2.2. Role of the Elements in dietary

1.2.2.1. Bioavailability

All forms of life need inorganic compounds to develop normal vital processes; all animal physiological tissues and all diets have inorganic elements or minerals in different quantities and ratios. However, the presence of an element in food does not imply that the organism is capable of using it for its biological processes. Therefore, there is a difference between the chemical amount of an element and its bioavailability. This term indicates both the quantity of food which enters in the organism after its introduction in the diet, and the easiness with which is absorbed and it is, therefore, available to exercise the physiological activity. In order that a substance (contained in food or introduced as such in a diet) has its effect in the organism, it is necessary that sufficient concentrations are reached in organ receptors which must respond to its action.

Generally, the bioavailability is complete and quick with intravenously administration, while for all others administration ways it depends on many factors, elements related with the substance that must be absorbed, on the production processes and on the general conditions of the subject. Concerning the administration by mouth, instead, the administration time, gastrointestinal pH,

digestive tract motility, biochemical transformations that are taking place in the lumen and on the wall of the alimentary canal, bacterial flora, digestive enzymes, hepatic metabolization have huge influence. Furthermore, the overall diet formulation and its chemical form make more or less available the active principles contained in it and the individual characteristics of the organisms can influence their absorption. For example, pigs do not absorb more than 50% of the phosphorous resulting from vegetable feeding, while the need for phosphorous of the ruminants is completely met by the vegetable diet (Cunha, 1977). The quantity of iron, assessed with hematologic studies, for rabbit growth is 50 ppm although in actual terms, the quantity administered for an excellent growth must be of at least 85 ppm (Pallauf e Bock, 1990). Other examples are given by few studies that have compared the bioefficacy of a zinc/methionine complex to conventional zinc-sulfate (Hill et al (1986) and Pimentel et al. (1991)) or studies that observe the efficiency of absorption of many trace minerals and dietary factors that affect bioavailability of minerals differ greatly between ruminants and non-ruminants (Spears, 2003).

1.2.2.2. Mineral Integration

To understand the aspects of mineral integration, it is necessary to make reference to the concept of "mineral dosage". The mineral dosage in a diet is strictly related to the bioavailability of nutrients in it and can be expressed in different ways: daily quantity, for product units, body weight units or proportional to dry substance taken in the diet. Generally, the quantity of minerals introduced in the diet must allow the organisms not to draw from the physiological stocks and that defines the so-called minimum dose level; this is based upon objective criteria such as growth, health or production and it is the one sufficient to avoid the onset of a deficiency syndrome. Instead, the Optimal Level provides the animal with the possibility to better express its productive potentialities guaranteeing an optimal health state while beyond the Toxic Level you get toxic effects on the organism. The dosage,

moreover, must keep into account the homeostatic regulation of the superior organisms which tends to buffer the excesses or lacks, changing the efficiency of the absorbing and excretion mechanisms (Underwood e Mertz, 1987). For example, if a diet is too rich in calcium, the homeostatic mechanism reduces the absorbing efficiency of that ion by the organism.

From that, therefore, the need to regulate and integrate the diet contributing with what the diet itself cannot provide, as for micro and macro elements, in order to meet mineral requirements. However, different factors influence mineral requirements and as a consequence their dosage such as production quantity and quality, animal age, chemical form of the mineral to integrate, interaction with other nutrients, quantity of food an animal takes, reproduction cycle and animal adaptability (Long *et al.*, 1969; Thornton *et al.*, 1969; Underwood, 1981); in any case, the integrator dosage is not proportional, for example, to the cattle production regime because if the regime increases the animal takes more food products and therefore it takes more integrator. So the request for integration varies according to the adaptability criterion. On the contrary, as soon as the amount of mineral available for an animal is low for inadequate intake or drop of reserves, certain physiological processes, in competition among them, fail for inadequate integration (Underwood, 1981).

1.2.2.2.1. Indirect Methods of Integration

Indirect integration is applied especially in the breeding of the grazing cattle; it is implemented: fertilising the pasture with fertilizers rich in minerals, changing the pH of the soil and encouraging favourable plant growth. It was seen, for example, that the increase in soil pH is accompanied by the drop of concentration of elements, such as copper and cobalt and from an increase of selenium and molybdenum in the fodder.

The concentration difference of mineral elements in the various plant species, which grow on the same soil, can be used to integrate or diminish the availability

of some metals in the grazing cattle (McDowell and Valle, 2000). The indirect approach is difficult to implement because it is necessary to take in consideration many factors difficult to control, such as interaction of soil-plant-minerals and the climate conditions of the vegetable growth. Where the climate conditions, but also the economic ones, are favourable the focused soil fertilisation and the use of spray, which enrich leaves with minerals, are used with good results. If the pasture area is circumscribed and the vegetable species are limited, the mineral elements must be added directly to the soil when the plants are ready to extract them, otherwise the addition would not give results (Underwood, 1979). Moreover, in case of vast pasture areas, the mineral integration by means of fertilizers is expensive and not successful if we consider factors such as the low fodder production per surface unit, the variability of elements to integrate and the high cost of transport and application. Indeed, the persistence of the trace elements in the soil depends on different factors (Hannam e Reuter, 1987):

- From the soil conditions
- From the kind of mineral
- From the fertilisation technique

For example, the concentration of the remaining zinc can vary in a lapse of time that goes from two to ten years on a calcareous soil; in an acid soil can last more than ten years (Judson, 1996). A cobalt treatment of two kilograms per hectograms is sufficient for about three to four years; the application of a kilogram per hectogram of selenium is sufficient for two years (MacPherson, 2000). Moreover, the metal salt quantity depends on the kind of salt: 10 g per hectogram of barium selenate are sufficient for about 2 years, while the same quantity of sodium selenate does not last more than 15 months (Valle *et al.*, 2002). Copper, instead, is a very persistent, a dosage of two kilograms per hectogram is sufficient for twenty-three years. Another method to increase mineral element bioavailability is to spray integrators on the leaves that are subsequently cut to make hay (Judson, 1996).

Concluding, increasing the metal concentration by means of fertilizers brings different advantages; for example, it is assured the uniformity of mineral intake on behalf of animals and a greater food digestibility (especially in case of phosphorous) (Underwood, 1981). However, the technique of fertilisers rich in minerals is very expensive. Furthermore, there is the need to take into consideration the effects of toxicity of the elements themselves; for example, phosphates can contain toxic levels of fluorine and cadmium. The fluorine does not represent a serious problem, while the cadmium is dangerous for plants which constitute the pasture and for animals (Langlands *et al.*, 1988).

1.2.2.2.2. Direct Methods of Integration

Direct methods of integration foresee the mineral intake through the administration of fortified foods or integrators in animals as integrant part of the diet; indeed, metal elements can be added to feeds by creating mixtures or blends, or they can be administered in water solution or feeds, gelatine or glass pellets or through intramuscular injections (salts or organic complexes). The benefits and the disadvantages of these techniques were widely illustrated by McDowell (1976, 1996 a, 1997, 1999) and by Judson (1996).

To administer the integrator by means of water solution, for example, it is necessary that the metal salt is soluble in water and that water source, where the animals drink, is unique and localizable. This method allows to know accurately the integrator dosage that each animal intakes but it is not always suitable to be applied; indeed, if the implementing costs of the method are too high or if the animals are obliged to drink much it is better to adopt another method.

The pellets, instead, are prepared to integrate the metal bioavailability in the ruminants and to keep into account the fact that the integrators are maintained in the gastrointestinal tract and from there they release the elements. In general, the duration of a pellet in the gastrointestinal tract is directly proportional to the mineral content (Judson, 1996) and to the shape it takes: gelatine capsules or

soluble glass pellets. The former are used to administer copper oxide as they easily melt and the salt liberated is then assaulted by gastric juice and dissolved (MacPherson, 2000). The latter, instead, conditions the mineral release according to the material solubility grade (Ammerman and Henry, 1986). The elements administered with this system are: copper, cobalt, selenium, manganese, zinc and iodine and some vitamins such as A, D and E.

The intramuscular injections cure the deficiency of elements such as copper, selenium, zinc, iodine and they are very efficient. Generally, the organic complexes of these elements are slowly absorbed by tissues so they integrate the deficiencies for long periods. For example, copper deficiency is integrated with injections at intervals of three or six months. Iron deficiency is provoked by anaemia in the new born pigs; it can be cured with metal administration, orally or with intramuscular injection during the first three days of life. (Judson, 1996).

In spite of the different advantages surely the main disadvantage of this technique is that not all the elements can be administered individually: for example the sodium and the phosphorous are administered in mixture containing also calcium (McDowell e Conrad, 1991). Indeed, the integration of one element or few usually reach evident results when the deficiency of the element is considerable (Ammerman e Henry, 1986).

For example the cobalt deficiency in some areas of Australia and the lack of selenium in New Zealand can be cured with the administration of single elements.

1.3. Mineral Complexes

The growing interest for mineral integration to increase bioavalability brought the research to re-examine accurately the meaning that complexes and chelates can have for food industry (Nelson, 1988; Kincaid, 1989; Patton, 1990; Spears, 1991; Parks and Harmston, 1994; Ammerman *et al.*, 1995). This interest towards the so-called *organic* or *chelate* mineral forms to be used in diets, in particular those associated with amino acids, peptides or other organic molecules, was raised by the encouraging results obtained in different *in vivo* tests on animals of economic interest and fed with fodder containing minerals in the form of chelates. Such results, awarded to the improvement of metal bioavailability, include: (i) increase of growth, (ii) increase of the reproductive ability (iii) general improvement of the health state of animals (greater resistance to various diseases). Moreover, the use of metal chelates in animal nutrition, in replacement of conventional mineral integrators was encouraged by a series of reasons that have spread their use, even outside a necessary in-depth analysis of many scientific aspects. In parallel, after an initial period of scepticism, and on the basis of many practical results, the interest of the scientific community on the use of metal chelates in nutrition aroused, as it is shown by the remarkable increase of scientific articles written in the last ten years. Regarding this aspect, the Figure 1 shows the distribution of the articles appeared on international scientific publications in the last thirty years regarding copper and zinc.

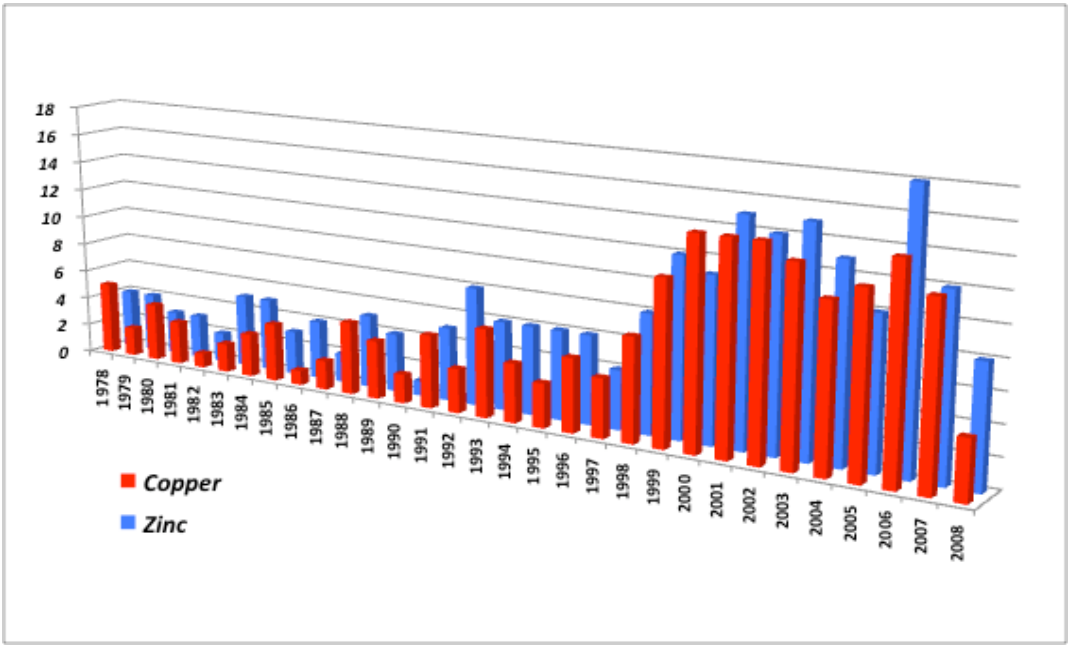

Figure 1: Number of international publications regarding Chelates studies, on Zinc and Copper, from 1978 to 2008

1.3.1. Nature of chelates and their characteristics

Metals in the biologic systems are present in the form of positive ions (cations). These in solution are not *naked* ions, but co-ordinate a certain number of molecules rich in electrons, both neutral and with a negative charge (anions), called ligands in order to minimize the excess of positive charges. The ligand molecules, such as ammonia, water and thiol must contain atoms capable of donating a couple of electrons such as N, O, S. When transition metals are considered (see Periodic Table page 2) the metal/ligand bond is defined *dative* and consists in the donation of a couple of electrons from the *ligand* to the ion. The species resulting from this interaction are called *complexes or co-ordination compounds;* to set an example, ammines are an important class of molecules containing nitrogen (N) as a donating atom. Metal complexes are therefore compounds in which the metal atom is bound by more than those suggested by its

valence and the number of these defines the *coordination number*, which depend on the nature of the donor atom and on the oxidation state of the metal.

Metal chelates are specific kinds of complexes in which at least one ligand, which may be an amino acid, co-ordinates on the metal cation through two or more dative bonds. This is accomplished owing to the presence of at least two donor centres rich in electrons like oxygen and/or nitrogen atoms present in the same molecule. The word *Chelates* results from the Greek *Che'le'*, chelae of a crab, a lobster or a scorpion. Morgan and Drew suggested this term for metal complexes in which the metal atom is complexed through more than an attachment point, just like the very grip of chelate. Figure 2 shows the comparison among the state of *naked* ion, never in a solution, the state of complex surrounded by water molecule, typical of water solution and the state in presence of an aminoacid anion, which, having two donor centres, is called *bidentate chelate*. Also water beliaves as a (monodentate) ligand through oxygen, donor of an electronic couple; Figure 3 shows the most common co-ordination geometries and the relating hybridations of the value orbitals of donor ligands (H_2O) around the metal atom. Instead, in case of non-metallic microelements like for example selenium and iodine, these elements, not being metals, do not form positive ions in solution and therefore they cannot form chelates (Kratzer, Vohra, 1986).

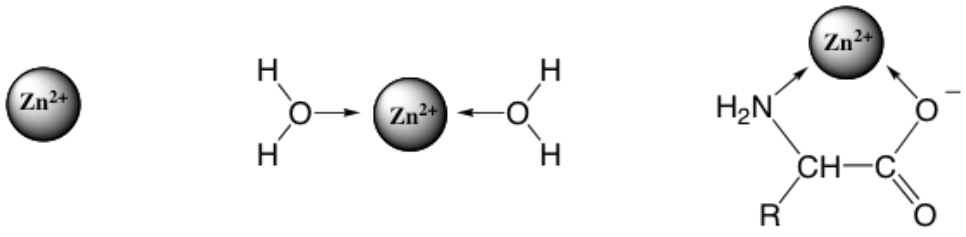

Figure 2: Possible states for a metal ion: (i) *naked*, rarely and only in gaseous phase; (ii) *complex,* in case of water solution surrounded by water molecules (the arrows show the dative bond that is the donation of a couple of electrons, possible in case of transition metals); (iii) *chelated complex,* in the specific example with an amino acid ion which behave like a bidentate chelating ligand

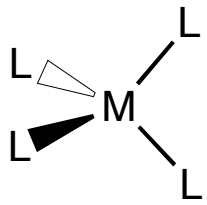

Tetrahedral coordination, sp^3

(M = metal cation; L = donor ligand; may be H_2O)

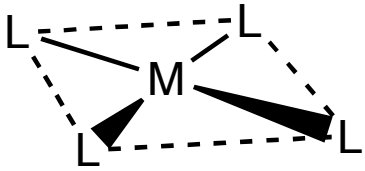

Square planar coordination, dsp^2

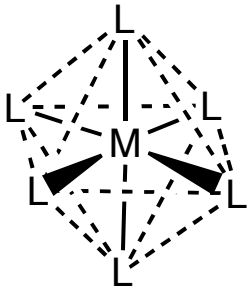

Octahedral coordination, d^2sp^3

Figure 3: Spatial distribution of donor ligands around the metal atom

Figure 3 shown three typical configurations of monodentate ligands (such as water) around a metal cation. In general, the electrons of coordinated water molecules are closer to the metal and hydrogen ion and can be more easily re-moved by a bounded water than by non-bounded water.

Beside the amino acids, among the typical bidentate chelates there are alpha-ketoacids (like pyruvic acid) and hydroxy acids, aliphatic and aromatic compounds (such as methionine hydroxy-analogue or lactic and salicylic acid) in their respective anionic forms; in addition, tetradentate chelates are well represented by porphyrins (hemoglobin, chlorophyll). Other coordination compounds of metals, present in nature, can result from: carbonhydrate (mono and polysaccharides), lipids, phosphates (phytic acid), fibres, proteins, surfactants and vitamins (vitamin B12) like vitamin C or ascorbic acid.

1.3.2. Stability constants or formation constants

Chelate formation constants measure the relative stability of various chelates in solution. These constants indicate quantitatively the affinity of a metal (M) to form complexes with ligands (L). *Formation constants* may be expressed in terms of concentrations and also indicated with *Kf* for their formation is commonly written as follows:

$$M^{2+} + L \rightarrow ML$$

$$Kf = \frac{[ML]}{[M^{2+}] \cdot [L]}$$

Thus K_f represents the number of moles of chelated metal in relation to the product of the moles of metal ion and of ligand in free state in the system. The log K_f is known as *Stability Constant* and in the table below values of some common chelates are shown:

Ligand	Cu^{++}	Ni^{++}	Zn^{++}	Co^{++}	Fe^{++}	Mn^{++}	Mg^{++}
Glycine	8.5	6	5	5	4	3	2
Cysteine	*	10	10	**	6	4	4
Histidine	10.5	9	7	7	5	4	4
Histamine	10	7	5	5	4	?	?
Ethylenediamine	11	8	6	6	4	3	?
EDTA	19	18	16	16	14	13.5	9
Guanosine	6	4	4.5	3	4	3	?
Oxalic acid	6	5.5	5	4.5	4.5	4	3
Salicylic acid	11	7	7	7	6	6	?
Tetracycline	8	6	5	5	5	4	4

* Cysteine is decomposed by copper.
** Cobalt-cysteine chelate is formed but only with 3:1 ratio of cobalt:cysteine, whereupon Stability Constant is 16.
From: Scott, Nesheim and Young, 1982.

Figure 4: Stability Constant and in the table below values of some common chelates are shown

Generally, the highest the value of $K_{f,}$ the more stable the chelate (Kratzer, Vohra, 1986). The well-known EDTA, exadentate chelate, capable of capturing all the metal cations and used in water sweetening is the chelate that indeed shows K_f values among the highest. The chelate stability depends on the nature of the electron donor atoms (N, O, S) which are present in the molecule, on the nature of the metal chelate, on the electric charges of the ligand and the metal and finally on the structure of the ligand molecule. Moreover, the chelating capacity strongly depends on water solution pH: indeed, increasing the acidity, such capacity strongly diminishes. All metal chelates tend to dissociate when they are dissolved in water. This trend is strictly related to the chelate stability and therefore to K_f *formation constant*. The chelate dissociation in water, big or small as it may be, is however an ineluctable fact that determines the difficulties in analysing chelates in solution. The trend towards dissociation, finally, exposes the chelate to the attack of other ligand molecules that can be present in food products or in gastric and intestinal fluids such as chloride ions, sulphate ions and phytates (Predieri, Ballarini, 2007). The natural digestion of food produces numerous ligands that can coordinate (chelate) the minerals in the diet, facilitating the passage from the intestinal lumen to the cells of the intestine wall, where, possibly, they are chelated with natural ligands which play the role of transporting the minerals in the organism. Unluckily, important quantities of minerals are chelated with ligands, which are not effectively absorbed and therefore are lost in the excretions. In any case, the introduction of metal chelates should in general increase the absorption. Therefore, in the animal digestive systems, organic minerals bound by organic ligands such as proteins, amino acids or carbohydrates can be more bioavailable than inorganic minerals (Parks e Harmston, 1994). There are numerous research reports, both from field trials and University studies reporting positive results of feeding chelates trace elements to various production animals. Intuitively, we would guess that there is a correlation between the stability of a chelate product and its effect on animal performance. However, there have not been conclusive studies conducted which verify this. Kratzer and his co-workers found that the availability of zinc for chickens in a purified diet which was deficient in zinc was

enhanced by the addition of EDTA to this diet. This has been confirmed by Scott and his associates who also indicate that natural chelating compounds are found in feed ingredients which may aid in the utilization of zinc by chicks. Kratzer and his associates determined that EDTA improved the utilization of zinc and other trace elements by acting as a carrier of the polyvalent transition group trace minerals. It has been shown that chelating agents are involved in moving required metal elements through the cell walls. Kratzer's group compared a variety of chelating agents in their effect on zinc utilization by chicks. The results of these studies are shown in the graph below.

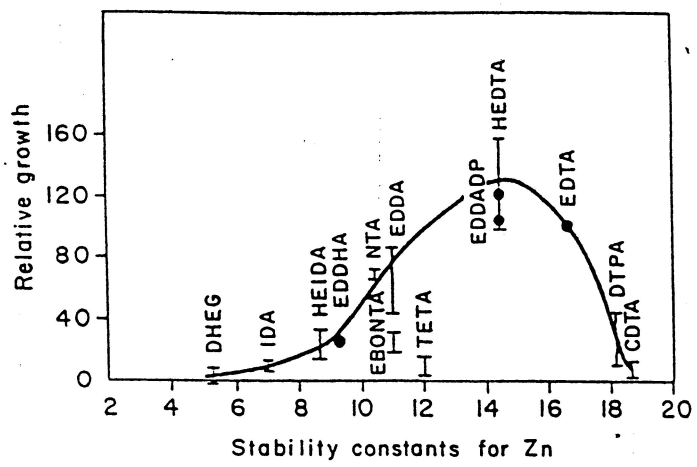

Figure 5: The relative growth of chicks fed chelating compound with a range of zinc stability constants

They tested chelating compounds which have stability constants both greater and lower than EDTA. It must be noted that the stability constants used for the products tested in these trials were not determined by these workers but were obtained from the literature. It is possible that some error was introduced by not determining what the stability constant was for each product made using a standard analysis. In these trials chelating agents with stability constant for zinc less than 11 did not improve zinc utilization most likely because natural chelating agents such as phytic acid in the intestinal tract were able to pull the metal

element out of the pre-formed chelate compound. Although the diets fed in these studies were purified diets deficient in zinc these studies are good indication that there is a relationship between chelated essential trace elements and animal performance.

1.3.3. Chelates classification and legislation

An important objective of the research on chelates consists in defining fast and effective analytical methods for the *recognition* and the *determination* of the chelate forms in the preparations for human and zootechnical feeding, or for the *evaluation of the metal chelating grade* (ratio between bounded and non-bounded metal) where the complexity of the mixing does not allow the univocal recognition of single species (Leach GA *et al*, 1997). To this purpose, the great variety of metallic complexes and chelates for animal nutrition on the market (especially the North American market) induced the "Association of American Feed Control Officials" (AAFCO, 2001: 282-3) to introduce classification of the different products:

- *Metal/amino acid complex*: product resulting from complexing of a soluble metallic salt with amino acids.
- *Metal/specific-amino acid complex*: product resulting from complexing of a soluble metallic salt with a specific amino acid.
- *Metal/amino acid chelate*: product resulting from the relation between a metallic ion of a soluble salt and amino acids with a molar ratio from 1:1 to 1:3 (preferably 1:2) to form coordinate covalent bonds. The average weight of the hydrolysed amino acids has to be approximately 150 and the resulting molecular weight of the chelate must not exceed 800.
- *Metal proteinate*: product resulting from the complexing of a soluble salt with amino acids and/or partially hydrolysed proteins.
- *Metal/polysaccharide complex*: product resulting from the complexing of

a soluble salt with a polysaccharide solution.

Instead, regarding chelates the European Union, by means of the Commission (OJEC, 1998), provided a definition only for the *Metal chelates of amino acid hydrate*, having the formula $M(x)^{1-3} \cdot nH_2O$. The European Commission has recently approved *iron, copper, manganese, zinc glicinates,* through the EFSA, as chelate forms (Official Journal of the European Union, OJEU, 24/3/2006, L 86/4-7). However, from a strictly chemical-analytic point of view, the chelate species present on the market (approved or going to be approved) can be classified as follows:

- Chelates of a single amino acid with a well-defined formula.
- Chelates of a single alpha-hydroxyacid (e.g. methionine hydroxy-analogue and lactic acid) with a well-defined formula.
- Chelates of amino acid *pool* in known percentage.
- Chelates of protein lysates (e.g. Soy meal).

More rarely, chelates of other organic molecules (saccharide or other).

The first two cases (i, ii) include pure chelate formed by a metal ion surrounded by a well-defined number of known chelate molecules; they are pure substances and as such they have a precise identification code (*Registry Number)* of the *Chemical Abstract Service*, that is the U.S. company that classifies all the world chemical literature and the new substances that are published. For these chelates, their recognition directly in the product like in the solid state is often possible; while for the cases (iii, iv, v), when more chelate species are present in the blend, the univocal recognition of single species is practically impossible and it is necessary to make chemical-physical characterising studies.

1.4. Commercial Chelates

Currently the commercial chelates are classified by two different market types: on one hand the American one more permissive and on the other hand the European one in which the European Union, together with EFSA, gave precise restrictions on patents and on the registration of some commercial products (OJEC, 1998 - OJEU, 24/3/2006, L 86/4-7). The main multinational corporations that deal with chelate production and sale are: ALBION minerals™ (Ferrochel®, MAAC® Facts, TRAACS™), PANCOSMA caring quality nutrition™ (Footprint®, B-TRAXIM®), ALLTECH...naturally® (BioPlex)®, ZINPRO corporation® (ZINPRO®, CuPLEX®, MANPRO®, COPRO®), BIOCHEM (BioKey®), JHBIOTECH (Buffermin®), NOVUS biologicals® (Mintrex®).

Moreover, it is possible to underline that the greatest interest of the feedstuff production industry, driven by the immediate possibility to put new products on the market, is addressed mainly to chelate species normally in the feedstuff for other functions and to those metals that can more easily induce deficiency stages in animals. This is the case of 2-hydroxy-4-methylthiobutanoic acid (MHA the so-called *methionine hydroxy-analogue*), that is an alpha-hydroxyacid largely used in animal nutrition as a source of methionine (Dibener, 1990); or Glycine, also used in the diet as an amino acid source. Concerning the metals, instead, the attention is addressed to the Zinc (Zn), copper (Cu) and Iron (Fe) for the physiological roles they play in animals and to a lesser extent also to Calcium (Ca), Magnesium (Mg), Manganese (Mn) and Cobalt (Co).

1.5. Aim of the work

Aim of this work was to complete the physico-chemical characterization of metal chelates of MHA, whose properties were till now not fully investigated. A prominent feature of MHA is the better stability of its metal chelates in acidic medium with respect to corresponding chelates of other ligands, in particular aminoacids. In this contest, an important goal of this investigations was to estabilish the effective chelation of MHA towards metal cations, both in solution and in the solid state.
In addition, this work deal with the attempts to set up reliable analytical methods in order to recognize and determine MHA metal chelates in commercial samples.

2. Experimental

2.1. Characterization of the MHA Chelates

2.1.1. Syntheses and characterization

Solvents, reagent grade metal salts were commercial products (Sigma-Aldrich group). 88% MHA in water is available as *Alimet feed supplement* from Novus International Inc. Elemental analyses were performed on a Carlo Erba CHNS-O EA 1108 automatic equipment. IR spectra (KBr discs) were recorded on a Thermo-Nicolet Nexus FT spectrometer by the KBr discs technique or by means of the Thermo Smart Orbit ATR diamond accessory. Single crystals FTIR analysis was performed recorded on a Thermo-Nicolet Continuum microspectrometer coupled with the aforementioned Nexus FT. Thermogravimetric analyses (under nitrogen, 10°/min) were performed with a Perkin-Elmer Delta series TGA 7 equipment. MHA metal chelates with various divalent metal cations were prepared by one-step reactions (MHA/M 2:1; M = Ca^{2+}, Mg^{2+}, Mn^{2+}, Co^{2+}, Cu^{2+} or Zn^{2+}) of commercial 88% MHA with divalent metal carbonates, suspended in small amounts of water at room temperature. Evolution of CO_2 is observed and the reactions are complete within one hour giving rough products as microcrystalline powders Complexes of formula $[\{CH_3SCH_2CH_2CH(OH)COO\}_2M]\cdot 2H_2O$ (satisfactory C, H, S elemental analyses) can be recovered after recrystallization in warm water, filtration and drying at 60° for two hours, with exception of copper, which gives an anhydrous complex (yields > 90%). They appears as microcrystalline powders (X-ray diffraction), sparingly soluble in cold water. The iron(II) bis-chelate derivative was prepared by reaction of the sodium salt of MHA with iron(II) sulfate.

A pale yellow precipitate was obtained which, after filtration, washing with water and drying, was recognized as $[\{CH_3SCH_2CH_2CH(OH)COO\}_2Fe]\cdot 2H_2O$ by elemental C, H, S analysis (yield 85% not optimized). Infrared data (solid state, KBr disc): n(OH)/ cm^{-1} 3101s (M = Ca), 3099s (Mg), 3265s (Mn), 3262s (Fe), 3290s (Co), 3050s (Cu), 3094s (Zn); $n_{as}(CO)/cm^{-1}$ 1579vs (M = Ca), 1577vs (Mg), 1597vs (Mn), 1595vs (Fe), 1580vs (Co), 1641vs (Cu), 1591vs (Zn)

Synthesis of the anhydrous zinc bis-chelate $[Zn(MHA_{-H})_2]$: a suspension of $ZnCO_3$ (51.8% Zn; 7.02 g, 55,8 mmol) in water (50 ml) is added with MHA (88% in water; 19.1 ml, 111.6 mmol). The mixture is stirred for 2 h at room temperature; during this time evolution of gas (CO_2) and formation of a white, caseous precipitate are observed. The precipitate is filtered, washed with cold water and dried at room temperature. It has been recognized as $Zn(C_5H_9O_3S)_2$ by CHS elemental analysis and TGA profile (yield 92%). Found (%): C, 32.7; H, 5.1; S, 17.2. Calculated for $C_{10}H_{18}O_6S_2Zn$ (%): C, 33.0; H, 5.0; S, 17.6. No significant weight loss is observed under 180°C, during the thermogravimetric analysis.

Synthesis of the dihydrate zinc bis-chelate $[Zn(MHA_{-H})\cdot 2H_2O]$: it is obtained nearly in the same way by doubling the amount of suspending water and by operating at 60°C. The product is obtained as a white microcrystalline powder which rapidly precipitates on cooling. It has been recognized by CHS elemental analysis and TGA profile as $Zn(C_5H_9O_9S)_2\cdot 2H_2O$. Found (%): C, 29.8.; H, 5.4; S, 15.7. Calculated for $C_{10}H_{22}O_8S_2Zn$ (%): C, 30.0; H, 5.5; S, 16.0. The weight loss observed during the thermogravimetric analysis is 9.0% at 100°C corresponding to the release of two water molecules.

The infrared spectra of the two products are reported in results session. The anhydrous form can be turned to the dihydrate one simply by dissolving it in hot water: the microcrystalline precipitate obtained by cooling is the dihydrate complex. On the other hand, the dihydrate can be turned to the anhydrous form by dissolving it in boiling ethanol (or methanol): the precipitate obtained by cooling is the anhydrous form.

2.1.2. X-ray diffraction analysis

Suitable crystals for the X-ray analysis of the bis-chelate, dihydrate zinc complex $[Zn_2(MHA)_4(H_2O)_3]\times H_2O$(**1**) were obtained by slow evaporation of a saturated aqueous solution of the anhydrous derivative. The intensity data were collected at 293(2) K with a K Philips PW1100 diffractometer (graphite monochromated MoK_a radiation, l = 0.71073 Å). Crystallographic and experimental details for the structure are summarized in Table 1. The structure was solved by direct methods (SHELXS-97) and refined by full-matrix least-squares procedures (based on F^2, SHELXL-97) (Sheldrick, 1997) with anisotropic thermal parameters for all the non-hydrogen atoms. The hydrogens belonging to carbon atoms were introduced into the geometrically calculated positions (SHELXS-97 procedures) and refined *riding* on the corresponding parent atoms. The hydroxyl hydrogens were introduced into the geometrically calculated positions and their torsion C-O-H angle refined. In view of the importance of the hydrogen bonding in the crystal packing, the water hydrogens, not found in the density maps, were introduced by the CALC-OH procedure (Nardelli, 1999), which takes into account combined geometric and force field calculations based on hydrogen bonding interactions, resulting in positions consistent with the connectivity shown e.g. in figure 1. The so-introduced hydrogens were then refined with constrained geometrical parameters. The C18-C19-S4-C20 chain was found disordered in two positions with equal occupancy factors.

Formula	$C_{20}H_{42}O_{15}S_4Zn_2 \cdot H_2O$
M_r	799.53
Crystal system, space group	Triclinic, *P*-1
Temperature(K)	293(2)
***a*, *b*, *c*(Å)**	16.990(1), 18.019(1), 5.7980(6)
α, β , γ(°)	96.651(5), 95.082(6), 72.919(8)
V(Å^3)	1682.5(2)
Z	2
ρ(g cm^{-3})	1.578
Radiation type	Mo$K\alpha$
μ(mm^{-1})	1.74
Crystal size(mm)	0.2 × 0.1 × 0.1
measured, independent, observed refl.	5855, 5855, 3733
θ_{max}(°)	25.0
$R[F^2 > 2\sigma(F^2)]$, $wR(F^2)$, S	0.050, 0.128, 0.96
parameters	432

Table 1: X-ray data collection and refinement parameters for 1.

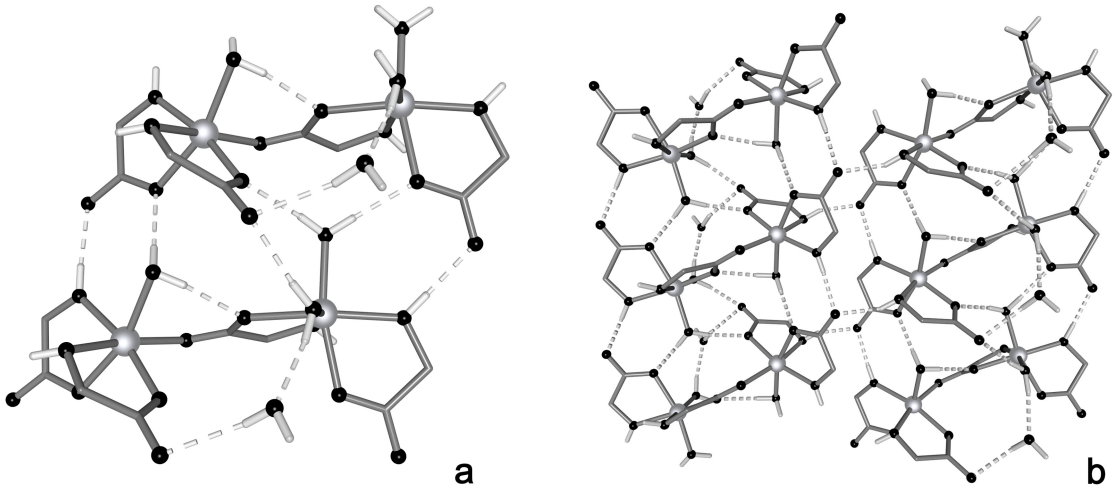

Figure 1: Packing diagram (view along c axis) of the crystal structure of **1** representing: (a) a couple of dinuclear complexes, interconnected by hydrogen bonds and (b) an extended view, depicting 6 dinuclear complexes. Thioether chains omitted for clarity. Gray spheres: zinc atoms; black spheres: oxygen, dark gray sticks: carbon; light gray sticks: hydrogen. Hydrogen bonds are represented by gray dashed lines. Symmetry operation generating equivalent molecules of figure a: -x, -y, -z

2.1.3. Methods and details of theoretical calculations

The Density Functional Theory calculations have been employed by the group of Professor R. Basosi (University of Siena) at the hybrid unrestricted uBecke3LYP functional level (Lee *et al*,.1988; Becke 1993). A mixed basis set (C,H,N,O=6-311+G(d,p) and Zn = LanL2DZ) has been used. Solvent effects have been taken into account by using the Polarizable Continuum Model (PCM) (Tomasi e Persico, 1994). The bulk solvent effect has been checked embedding the molecules under investigation in a continuum of dielectric constant e = 78.39. All calculations were performed with Gaussian03 (Frisch *et al.*, 2003).

2.1.4. NMR measurements

The MHA and $[Zn(MHA_{-H})_2]$ solutions were prepared at concentrations ranging from 8 to 10 mM. NMR measurements were performed either at 14.1 T with a Bruker Avance 600 MHz or at 9.4 T with a Bruker AMX 400 MHz spectrometers at controlled temperatures (± 0.2 K) using a TBI (Triple Broadband Inverse) or BBI (Broadband Inverse) probe. Water suppression was achieved by presaturation. Proton and carbon resonance assignment was checked by means of standard homonuclear and heteronuclear 2D experiments such as ^{1}H-^{1}H TOCSY, ^{1}H-^{1}H NOESY ^{1}H-^{13}C HSQC. Chemical shifts were referenced to internal TSP-d_4 (3-trimethylsilyl-[2,2,3,3-d_4] propionate sodium salt). Spin lattice relaxation rates were measured with inversion recovery pulse sequences. The same sequence was also used to measure the single-selective relaxation rates by means of suitably shaped p-pulses instead of the usual non-selective p-pulse. All rates were calculated by regression analysis of the initial recovery curves of longitudinal magnetization components leading to errors not larger than ± 3%. The diffusion coefficients were measured at 298 K by a PFG longitudinal eddy-current delay (LED) pulse sequence with bipolar gradients incorporating spoil gradients during both longitudinal storage periods (Wu *et al.*,1995; Gibbs *et al.*, 1991; Dingley *et al.*, 1995; Johnson, 1999) . The gradient

strength was incremented (with an initial value of 0.86 G cm^{-1} and a step size of 2.65 G cm^{-1} for 2 ms), while the separations of the field gradients and the total echo time were kept constant. A series of 16 spectra, with a number of scans ranging from 16 to 32, was recorded in 2D mode for each measurement, with a recycle time of 10 s between scans. The diffusion values were calculated by regression analysis of the signal decay leading to errors not larger than ± 2-5%. The strength of the B_0 field gradient was calibrated by measuring the self-diffusion coefficient of the residual HDO signal in a 100% D_2O sample at 298 K (Callaghan *et al.*,1993; Price1998). Spectra processing was performed on a Silicon Graphics O2 workstation using the XWINNMR 2.6 software.

2.1.5. Potentiometry and spectrophotometry

Stock solution of the ligand was prepared accordingly to the procedures reported in a previous paper (Predieri *et al.*, 2003). Solutions of Fe^{+3} and Cu^{2+} were prepared by weight from their chloride salts (Carlo Erba) and an appropriate amount of standardized HCl solution was added to prevent hydroxide precipitation. Concentration of both solutions was checked by titration with standard EDTA (ethylendiamminetetraacetic acid) solution. KOH and HCl aqueous solutions (*ca.* 0.2 mol dm^{-3}) were prepared by diluting concentrated Merck Titrisol ampoules and standardised with the usual procedure of this laboratory. [9bis] All solutions were prepared with freshly boiled, doubly distilled water. The titrations were carried out at T = 25 ± 0.1 °C and I = 0.1 mo1 dm^{-3} (KCl) under a stream of N_2, using 50 cm^3 samples. Potentiometric measurements were performed with the automatic apparatus previously described (Dallavalle et al., 1994). Hamilton combined electrode was calibrated in terms of $[H^+]$ by titrating HCl solutions with standard KOH solutions and the calculated pK_W value resulted to be 13.77(1). Absorption spectra were recorded with a Uvikon 941 Plus Kontron spectrophotometer using matched quartz cells of 1 cm pathlength and 0.1 mol dm^{-3} KCl as reference.

Solutions were passed from the potentiometric vessel to the thermostatted cuvette by means of a peristaltic pump. Potentiometric study of the Fe^{3+} / MHA (HL) system was performed by titration of four samples with Fe/L ranging from 1:4 to 1:11 (C_{Fe} = 0.5 – $2.3 \cdot 10^{-3}$ M) in the pH range 1.5 – 3.5. Spectrophotometric study in the visible range (400 – 800 nm) of the Cu^{2+} / MHA system was performed by collecting 17 spectra of solutions obtained by titrating a Cu^{2+} solution (C_{Cu} = $8 \cdot 10^{-3}$ M) with a $4 \cdot 10^{-1}$ M solution of MHA up to Cu / L ratio of 1:8.1 (pH ranging from 2.6 to 4.8). Protonation constant of MHA (HL) was determined in a previous paper (log ß = 3.56(1)). Potentiometric data were treated by the HYPERQUAD 2000 computer program (Gans *et al*, 1996). Spectroscopic (A = f(l)) data were processed with the program PSEQUAD (Zékany *et al.*, 2001). Distribution diagrams were calculated and plotted by the program HYSS (Alderighi et al., 1999).

2.1.6 Electrospray Ionization Mass Spectrometry (ESI-MS and ESI-MS/MS)

A Quattro LC triple quadrupole instrument (Micromass, Manchester, UK) equipped with an electrospray interface and a Masslynx v. 3.4 software (Micromass) was used for data acquisition and processing. The nebulizing gas (nitrogen, 99.999% purity) and the desolvation gas (nitrogen, 99.998% purity) were delivered at a flow-rate of 105 and 536 L/hr respectively. The operating parameters of the ESI interface were as follows: electrospray voltage 3.0 kV, cone voltage 8-120 V, rf lens 0.1 V, source temperature 50°C, desolvation temperature 50°C. ESI-MS analysis were performed by operating the mass spectrometer in positive ion (PI) mode acquiring mass spectra over the scan range m/z 80-600 using a step size of 0.1 Da and a scan time of 0.6 s. MS/MS product-ion scan mass spectra were recorded in the 30-600 Da mass range with a scan time of 1 s and an interscan delay of 0.05 s. Collision energy was varied in the 5-40 eV range (argon pressure 2.56 e^{-3} mbar).

2.2. Analytical methods for determination of the MHA chelates

2.2.1. HPLC - Mass Spectrometry

Reagents

- Deionized water with a Milli-Q (Millipore, Bedford, MA, USA);
- Ammonium acetate, 98% (Aldrich);
- Acetic acid (J.T.Baker);
- Ammonia, 35% (J.T. Baker);
- Acetonitrile, ultra gradient HPLC grade (J. T. Baker);
- Calcium carbonate, 99,5% (Carlo Erba);
- Methanol ultra gradient HPLC grade (Sigma-Aldrich);
- Trifluoroacetic acid, 99% (Aldrich).

Preparation of the standard solutions

The zinc-chelate $Zn(MHA_{-H})_2$, previously synthetized (see 2.1.1.), was solubilized in deionized water (1000 ppm, final concentration) and sonicated for 10 min.
Working solutions were prepared daily by dilution in water from the 1000 ppm solution (see Validation Procedure).

Preparation of the feedstuffs

The feed was prepared by following a standard procedure used for the growing of the littel pigs in the companies. The ingredients were singly blended before mixing. The blank matrix was prepared without adding the Zn-chelate and composition was shown in Table 2.

Ingredients	Composition
Calcium Carbonate	1,0
Bicalcicum Phosphate	0,5
Sodium Chloride	0,4
Brano of triticum durum	8,0
Wheat	19,0
Maize	25,0
Soia Oil	3,0
Barley	14,0
Whey	10,0
Soia	18,85
Premix for pig	0,25
Total	100

Table 2: Feedstuffs composition so called "blank"

Extraction procedure and SPE treatment

The samples used for the HPLC-ESI MS/MS and FIA-ESI MS/MS analysis were prepared by mixing the blank feed with known amount of $Zn(MHA_H)_2$. The extraction and purification procedure were as follows:

2 g of feedstuffs + 15 ml deionized H_20

↓

Homogenization (2 min)

↓

Centrifugation (5000 rpm,20° C, 5 minutes)

↓ ↓

Surnatant Residual

↓ ↓

5 ml of deionized H_20 Vent

↓

Vortex (2 minutes)

↓

Centrifugation (5000 rpm, 20° C, 5 minutes)

↓ ↓

Surnatant Residual

↓ ↓

Filtration (0,45 µm) Vent

↓

20 ml of filtered extract + 10 ml di methanol

↓

Store at 4°C (40 min)

↓

Centrifugation (5000 rpm, 4° C, 10 min)

↓

Add 10 ml di methanol

↓

Storage at 4°C (30 min)

↓

Centrifugation (5000 rpm, 4° C, 10 min)

↓

Filtration (0,45 µm)

↓

Evaporation under N_2

↓

Residual resuspended in 2 ml of water

The solid phase extraction was carried out off-line on the Supelclean® ENVI-C18 (6 ml, 0.5g) (Supelco®, Bellefonte, PA, USA) cartridges. The experimental conditions were the following:

- Cartridge conditioning: 5 ml of methanol and 5 ml water;
- Sample loading: 2 ml of extract;
- Analyte elution: 2 ml 100% acetonitrile.

The extracts were dried under nitrogen and re-suspended in 2 ml buffer solution (pH 5.5) before analysis.

Chromatographic conditions

A liquid chromatograph Alliance 2690 (Waters, Milford, MA, USA) equipped with a 120-vial capacity sample management system was used. Chromatographic separation was obtained using a C18 reversed-phase column (250 ´ 2.1 mm, 5 µm, Supelco, CA, USA) under isocratic conditions. The mobile phase was made up of 0.1% (v/v) trifluoroacetic acid aqueous solution (50%) and acetonitrile (50%) as the organic modifier delivered at the flow-rate of 0.2 ml/min.

Apparatus and conditions of MS analysis

A Quattro LC triple quadrupole-mass spectrometer (Micromass, Manchester, UK) with pneumatically-assisted electrospray interface was used. Acquisition data was performed in positive ion (PI) mode. Interface parameters were set as follows: capillary voltage 3.0 kV, cone voltage 35 V, source temperature 130°C, desolvation temperature 250°C, rf lens 0.1 V. The nebulizer and the desolvation gas (nitrogen, 99.999 % high-purity) were delivered at 60 l/hr and 550 l/hr respectively.

Experiments for optimization of ESI interface parameters were performed by directly infusing $Zn(MHA_{-H})_2$ solution in the ESI-MS system at a flow-rate of 6 mL/min. Full-scan analyses were carried out in the 40-550 Da mass range. Operating in MS/MS mode, product-ion scan mass spectra of the molecular ions of $Zn(MHA_{-H})_2$ were acquired in the 40-400 m/z mass range. Multiple reaction

monitoring (MRM) analyses were performed acquiring the following transitions: m/z 363®261, m/z 365®263 and m/z 367®265. For MS/MS analysis it was operated at a collision energy of 40 eV. For the acquisition and processing data the Masslynx v3.4 software was used.

Validation procedure

Single-laboratory validation of the LC-ESI-MS/MS and FIA-ESI MS/MS method was carried out following EURACHEM guidelines [The Fitness for Purpose of Analytical Methods (1998)]. Instrumental performance was evaluated by analyzing analyte standard solutions. To achieve data on real samples validation was also performed on matrice (feed). Validation was performed in terms of detection limits, quantification limits, linearity and accuracy (trueness and precision). Detection limit (y_D) and quantification limit (y_Q) were calculated as signals based on the mean blank ($\overline{x_b}$) and the standard deviation (s_b) of the blank signals as follows:

$$y_D = \overline{x_b} + 2\, s_b \qquad\qquad y_Q = \overline{x_b} + 10\, s_b$$

Ten blank measurements were performed to calculate and s_b. Using an appropriate calibration function, yD and yQ were converted from the signal domain to the concentration domain to estimate LOD and LOQ respectively. The precision was calculated on two concentration levels in terms of RSD% on five replicated measurements.

2.2.2. FTIR-HATR investigations

- Matrix preparation -

Premix

The Premix was prepared by following a standard procedure used for the growing of the littel pigs in the companies. The ingredients were singly blended before mixing. The blank matrix was prepared without adding the Zn-chelate and composition was shown in Table 3.

Ingredients		Composition	
Vitamin	A	U.I	4400
	D	U.I	440
	E	mg	32
	K3	mg	1
	B1	mg	2
	B2	mg	7
	B6	mg	3
	B12	mg	0,035
Niacin		mg	30
Pantothenic Acid		mg	20
Folic Acid		mg	0,6
Biotin		mg	0,1
Zinc (from solfate)		mg	80
Iron (from solfate)		mg	100
Copper (from solfate)		mg	1
Manganese		mg	4
Selenium		mg	0,3
Iodine (from potassium iodine)		mg	0,14

Table 3: Premix composition so called “blank”

Feedstuffs

The Feedstuffs was prepared by following a standard procedure used for the growing of the littel pigs in the companies. The ingredients were singly blended before mixing. The blank matrix was prepared without adding the Zn-chelate and composition was shown in Table 4.

Ingredients	Composition
Calcium Carbonate	1,0
Bicalcicum Phosphate	0,5
Sodium Chloride	0,4
Brano of triticum durum	8,0
Wheat	19,0
Maize	25,0
Soia Oil	3,0
Barley	14,0
Whey	10,0
Soia	18,85
Premix for pig	0,25
Total	100

Table 4: Feedstuffs composition so called "blank"

- Sample Preparation for MIR and NIR investigations -

Premix

The samples was prepared by mixing the $Zn(MHA_{-H})_2$ and Premix in order to have a concentration corresponding to amount of chelate in the commercial products, or else 100000 – 110000 ppm (10-11%); the levels of concentration considered was: 0

(*blank*) – 10000 – 20000 – 30000 – 50000 – 70000 – 80000 – 110000 - 130000 - 150000 ppm (0 – 15%), both validation and calibration curves. The samples was used to collect the two dataset using by MIR and NIR analysis.

MIR analysis was carried out by means a Simple linear calibration (according to: legge di Lambert Beer) and a Multiple linear calibration separately. A sub-dataset of four levels (2%, 5%, 8% and 13%, 36 spectra, named validation data set) was distinguished from the original data set and used for validating the model. The remaining 5 levels constituted the training dataset. MIR data (1557 sampled wavelengths) for Multiple linear calibration were normalized by means of multiplicative scattering correction (MSC) in order to correct variability of the baselines due to scattering phenomena. MSC was carried out employing the customized software of the spectrophotometer.

NIR analysis was carried out by means a Multiple linear calibration. A sub-dataset of four levels (2%, 5%, 8% and 13%, 36 spectra, named validation data set) was distinguished from the original data set and used for validating the model. The remaining 5 levels constituted the training dataset.

Validation, in the case of Simple linear regression, was performed in terms of detection limits, quantification limits, linearity and accuracy (trueness and precision). Detection limit (y_D) and quantification limit (y_Q) were calculated as signals based on the mean blank ($\overline{x_b}$) and the standard deviation (s_b) of the blank signals as follows:

$$y_D = \overline{x_b} + 2\, s_b \qquad\qquad y_Q = \overline{x_b} + 10\, s_b$$

Ten blank measurements were performed to calculate and s_b. Using an appropriate calibration function, y_D and y_Q were converted from the signal domain to the concentration domain to estimate LOD and LOQ respectively. The precision was calculated on all concentration levels in terms of RSD% on nine replicated measurements derivated from three indipendent weigh.

Feedstuffs

The samples was prepared by mixing the $Zn(MHA_{-H})_2$ and Feedstuff in order to have a concentration corresponding to amount of chelate in the commercial products, or else 100-110 ppm; the levels of concentration considered was: 0 (blank) – 70 – 100 – 130 – 160 – 190 – 220 – 250 – 280 – 310 – 340 – 370 – 400 – 430 – 460 - 490 ppm both validation and calibration curves. The samples was used to collect the two dataset using by MIR and NIR analysis.

MIR analysis was carried out by means a Multiple linear calibration. A sub -dataset of four levels (2%, 5%, 8% and 13%, 36 spectra, named validation data set) was distinguished from the original data set and used for validating the model. The remaining 5 levels constituted the training dataset. MIR data (1557 sampled wavelengths) for Multiple linear calibration were normalized by means of multiplicative scattering correction (MSC) in order to correct variability of the baselines due to scattering phenomena. MSC was carried out employing the customized software of the spectrophotometer.

NIR analysis was carried out by means a Multiple linear calibration. A sub -dataset of four levels (100 ppm, 190 ppm, 220 ppm and 310 ppm, 36 spectra, named validation data set) was distinguished from the original data set and used for validating the model. The remaining 11 levels constituted the training dataset.

Validation, in the case of Multiple linear regression, was performed in terms of linearity and accuracy (trueness and precision). The precision was calculated on all concentration levels in terms of RSD% on nine replicated measurements derivated from three indipendent weigh.

- Instruments and Calculation software -

MIR spectra were recorded on a Thermo-Nicolet Nexus FT spectrometer by means of the Thermo Smart Orbit ATR diamond accessory. FTIR analysis was performed recorded on a Thermo-Nicolet Continuum microspectrometer coupled with the aforementioned Nexus FT. DA was performed on MSC-corrected data by means of

the statistical package SPSS 14.0 for Windows (SPSS, Chicago, IL, USA). The stepwise regression method (Wilks' Lambda) was used for DA. Also Multiple linear calibration and statistics data was carried out with the same software.

NIR spectra were recorded on a BÜCHI NIRLab®-N200 MSC 100 spectrophotometer working in reflectance mode. Samples of premix and feed were placed in glass Petri dishes, continuously rotating during the acquisition of the spectra. The spectra for each sample were acquired by the customized software of the spectrophotometer (NIRLAB 2000). Multiple linear calibration and statistics data was carried out with NIRCal 4.21 software.

2.2.3. Use of $Zn(MHA_{-H})_2$ as standard for the HPLC determination of MHA

Procedure for the standard

In order to calibrate the analytical procedure, 88% MHA obtained by the supplier, coul be used for preliminary study according to Rinda R. *et al.*, 1987. The sample was solubilized in water on hot plate in order to reach a MHA concentration of about 820 ppm and was injected in the HPLC system.

Moreover, standard used is the anhydrous zinc bis-chelate of MHA (pure), $Zn(MHA_{-H})_2$ previously syntetized (see 2.1.1.): MHA content 82.03 % (determined by stechiometrich calculation), zinc content 17.97 % (determined by AAS, Atomic Absorption Spectrometry or ICP-AES, Plasma emission spectrometry after mineral digestion of the sample - AOAC Official Methods of Analysis (17th Ed.)) (i.e. See Table 4, Page 42). It can be used as MHA standard through extraction of MHA via acidic hydrolysis and the procedure is following: the zinc chelate (36.3 mg) is stirred in a 50 ml becher containing warm water (10 ml) till dissolution (about 5-7 min) on an hot plate at 50°C; then 20 µl of HCl 37% (molar ratio HCl/$Zn(MHA_{-H})_2$ 2:1) are added and the acidic solution is stirred for additional 5 min. The solution is filtered with a nylon filter (0.45 µm) and diluted in order to reach a MHA concentration of about 820 ppm (corresponding to 1000 ppm of the chelate) and then 20 µl of the filtrate are injected in the HPLC column though an injection loop.

Chromatographic conditions

A liquid chromatograph Alliance 2690 (Waters, Milford, MA, USA) equipped with diode array detector was used. Chromatographic separation was obtained using a Amino column (250 ´ 2.1 mm, 5 µm, phenomenex®, USA) pre-column Amino (phenomenex®) under isocratic conditions. The mobile phase was made up of 77% 0,01 M aqueous phosphoric acid adjusted to pH 3,25 with ammonium hydroxide and 23% acetonitrile delivered at the flow-rate of 0.2 ml/min. The run time is about 30 min and the UV Wavelength considered is 210 nm.

2.3. *In vitro* tests with Caco-2 cells

The human intestinal Caco-2 cell line was obtained from Prof. Alain Zweibaum (INSERM, Villejuif, Paris, France). Caco-2 were grown and maintained as previously described (Ferruzza et al., 1999) in Dulbecco Modified Minimum Essential Medium (Biochrome KG, Milano, Italy) containing 25 mM glucose, 3,7 g/l $NaHCO_3$ and supplemented with 4 mM L-glutamine, 1% non-essential amino acids, 1 x 10^5 U/l penicillin, 100 µg/l streptomycin and 10% heat inactivated fetal calf serum (Euroclone, Wetherby, West Yorkshire, UK) (complete culture medium). For toxicity and transport experiments cells were seeded on polycarbonate filter cell culture inserts (Figure 2) (Transwell, 24 mm diameter, 4.71 cm^2 area, 0.45 µm pore diameter, Costar Europe, Badhoevedorp, The Netherlands), at a density of $4x10^5$ cells/cm^2 and were left to differentiate for 17 days after confluence; the medium was regularly changed three times a week. For toxicity and transport experiments cells were treated from the AP compartment with balanced salt solution (BSS: 137 mM NaCl, 5.36 mM KCl, 1 mM $CaCl_2$, 1 mM $MgCl_2$, 5.6 mM glucose) containing 20 mM morpholinoethane sulfonic acid (MES) at pH 5.5 with or without the addition of 100 and 250 µM Fe^{3+}MHA or Fe^{3+}NTA for 3 hours in a water bath at 37°C. The iron complexes were freshly prepared by dropwise addition of 40 mM $FeCl_3$ in 0.5 N HCl under continuous vortexing to 80 mM NTA (nitrilotriacetic acid) or MHA in 1 mM HCl. The complexes were then diluted in BSS to the required concentration and the pH adjusted at pH 5.5. The BL compartment contained BSS additioned with 20 mM N-2-hydroxyethyl piperazine-N-4-butanesulfonic acid (HEPES) at pH 7.4 with 50 µM human apo-transferrin. These pH conditions were chosen to reproduce the pH gradient existing *in vivo* across the mucosa of the small intestine. During treatment, the permeability of the cell monolayer was monitored by measuring the transepithelial electrical resistance (TEER) at 37°C, using a commercial apparatus (Millicell ERS; Millipore, Bedford, MA, USA) as previously described (Ferruzza *et al.*, 1995). TEER was expressed as Ω x cm^2 after subtracting from the reading the resistance of the supporting filter and multiplying it by the surface area of the

monolayer (Figure 3). At the end of the incubation period BL media were collected, filters transferred on ice and rapidly washed twice with Fe chelating solution (140 mM NaCl, 10 mM piperazine-N,N'-bis ethanesulfonic acid) pH 6.7, containing 5 mM $Na_2S_2O_4$, 5 mM bathophenanthroline disulfonic acid (Glahn et al., 1995) at 4°C; the filters were carefully removed from the plastic ring, cells collected in distilled water and samples sonicated 3 times for 5 s at 20 kHz frequency (Sonicator vibracell VC100, Sonic and Materials). Fe content in cells and BL media was determined by atomic absorption spectrometry (AAS) after Microwave digestion (reported in the table below) and expressed as nmol Fe/filter. One filter has an area of 4.71 cm^2 and contains 1.33 ± 0.16 mg protein. In the case of Zn^{2+} and Cu^{2+}, toxicity studies were performed treating differentiated cells grown on filter with chelates and relative solfate salt (200-400 µM) for 2 h from the apical chamber and measuring variation in trans-epithelial electrical resistance (TEER).

Step	Tempo [min]	Potenza [W]
1	2:00	250
2	2:00	0
3	6:00	250
4	5:00	400
5	5:00	600
Vent 5:00	Rotorctrl on	Twist on

Table 4: Microwave digestion program. The bomb was prepared with 1,5 ml of sample, 4 ml of HNO_3 65% and 1ml of H_2O_2 35%. Running time: 30 minutes

Figure 2: The Caco-2 cells on filter

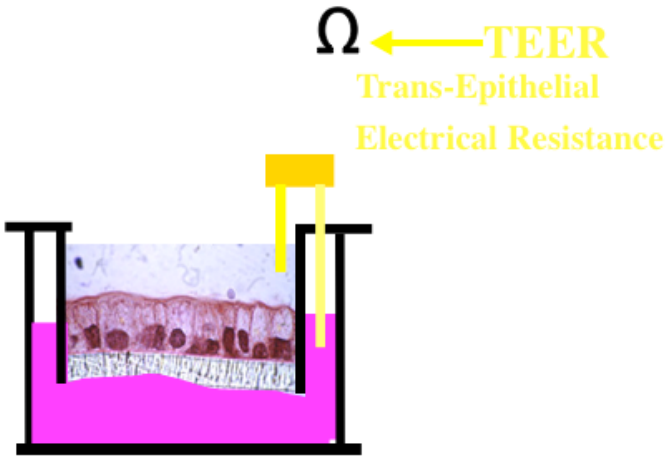

Figure 3: How to measure tight junction permeability

2.4. *In vivo* trials with rats

Carried out by Dr. Giacomo Biagi at DIMORFIPA, Università di Bologna

Twenty four adult rats (initial average live weight, 317 g) were used. First, six animals were euthanized with an overdose of urethane and liver, spleen, kidneys, femur, and a sample of blood were collected. Immediately after collection, all samples were frozen. Prior to being frozen, blood samples were centrifuged. Zinc content of the collected samples was determined. The remaining animals were fed a zinc-deficient diet (5 mg Zn/kg feed DM) for 21 days. After this period, six animals were sacrificed to verify that a zinc deficiency had been induced. Liver, spleen, kidneys, femur, and plasma samples were analysed for their zinc content. The remaining 12 animals were then divided into two groups (six animals each). Treatments were the zinc-deficient diet added with a) zinc sulfate ($ZnSO_4$) or b) Zn-MHA, $[\{CH_3SCH_2CH_2CH(OH)COO\}_2Zn]\cdot 2H_2O$, CAS RN: 292140-29-5 (ACT IONE Zn®, Agristudio Srl, Italy), to reach a final zinc concentration of 20 mg Zn/kg feed DM. Animals were kept individually in metabolic cages that allowed separated collection of urine and faeces. Diets were fed *ad libitum* for seven days and feed intake was recorded. Deionised water was provided *ad libitum*. Urine and faeces were collected daily. Subsequently, animals were sacrificed and Zn content of liver, spleen, kidneys, femur, plasma, urine and faeces was determined. Zinc concentration in the diets was determined digesting feed samples with a 90% solution of nitric acid using a microwave oven (CEM MDS-2000, CEM Corporation). Zinc concentration in the mineralised samples was measured using an atomic absorption spectrophotometer (SP-9, Philips S&I). Plasma zinc concentration was determined using a commercial colorimetric kit (Zinco Sentinel; Sentinel CH). Samples were read using a spectrophotometer (Ultrospec 3000, Amersham Pharmacia Biotech) at 560 nm. Faeces collected from each animal during the seven days of collection were pooled, weighed and then dried in an oven at 62°C for 24 h. Urine samples from each animal were pooled, weighed and then freeze-dried. All collected samples were then digested with a 90% solution of nitric acid using a

microwave oven (CEM MDS-2000, CEM Corporation). Zinc concentration in the mineralised samples was determined using an atomic absorption spectrophotometer (SP-9, Philips S&I). Data were analysed by one-way ANOVA using the program GraphPad Prism 3.0 (GraphPad Software). The differences among means of groups were analysed using the Student-Newman-Keuls test. Differences were considered statistically significant at $P < 0.05$.

3. Results and Discussion

3.1. Preface

As pointed out in the Introduction, interest in using alternative mineral sources, particularly those chelated with proteins or aminoacids, has recently increased due to their reported higher availability compared to conventional (inorganic) sources (Ashmead *et al.*, 1993) In fact, metal chelates of transition metal ions, in particular zinc(II), iron(II or III) and copper(II) with aminoacids and peptides are widely used in animal feeding, as they appear to induce a faster growth and a better resistance to various deseases in comparison with the simple inorganic salts (Kratzer e Vohra, 1986). It has been suggested that these effects are correlated with the improved metal bio-availability (Wadekind *et al.*, 1992). For example, it has been found that ruminants respond (increased growth, milk production etc.) to certain trace mineral complexes or chelates (Spears, 1996) and that aminoacid chelates show a higher availability than the inorganic compounds when fed to rainbow trouts, even in presence of phosphates and phytates (Apines *et al.*, 2003). Many forms of metal complexes with aminoacids (AA) and hydrolysed proteins are commercially available categorized respectively as metal AA chelates and complexed chelated (metal) proteinates (CCP). However, there are still contentions both regarding improved bio-availability and integrity of metal chelates at the low pH of the first digestive tract. In addition, recent studies raise some doubts regarding both improved metal bio-availability and structural integrity for AA chelates and CCP in the case of zinc and copper respectively (Cao *et al.*, 2000; Pastore *et al.*, 1999). Rergarding the second aspect, which evidently affect the first one, it has been suggested that hydrolysis of the starting proteins must be as complete as possible and in a large excess to keep metal complexes stable even at the low pH found in the first digestive tract. This important drawback can be overcome by using a chelating ligand able to give metal chelates adequately stable at low pH values. 2-hydroxy-4-methylthiobutanoic acid (MHA; the so-called *methionine hydroxy-*

analogue), an alpha-hydroxyacid largely used in animal nutrition as a source of methionine (Dibner *et al.*, 1990), has the requested features. It forms bis-chelate complexes of formula $[\{CH_3SCH_2CH_2CH(OH)COO\}_2M]\cdot nH_2O$ (M = Ca^{2+}, Mg^{2+}, Mn^{2+}, Fe^{2+}, Co^{2+}, Cu^{2+} or Zn^{2+}).

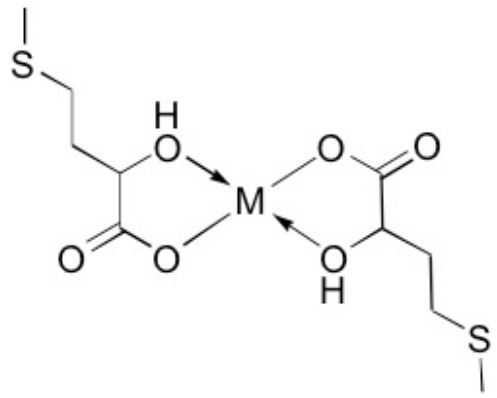

Scheme 1: Molecular sketch of the MHA_{-H} metal bis-chelates

Morever, potentiometric investigations on Zn/MHA complexes, in the presence of glycine as competing ligand, have shown that at pH<5 the unique chelates present in solutions are the MHA chelates. In order to gain insight into bio-availability of MHA metal chelates, both in vivo and in vitro studies have been programmed by our research groups. In this context, this thesis deals with:

(i) the characterization of MHA metal chelates by IR and mass spectrometry

(ii) studies on these species by means of potentiometry and ESR spectroscopy (ESR for Cu^{2+}) in order to detect the distribution of the iron and copper species in solution in the presence of MHA at various pH values

(iii) structural investigations on the MHA zinc chelates spectroscopy and single-crystal X-ray diffraction in the solid state and nuclear magnetic resonance (NMR) in solution.

(iv) the *in vivo* effect of MHA/Zn supplementation on rats

(v) the *in vitro* study regarding exposure of Caco-2 cells to the MHA chelates.

3.2. Characterization of Metal chelates of 2-hydroxy-4-methylthiobutanoic acid

3.2.1. Characterization of the MHA metal chelates by FTIR

MHA/M 2:1 (M = Ca^{2+}, Mg^{2+}, Mn^{2+}, Co^{2+}, Cu^{2+} or Zn^{2+}) chelates were prepared by reaction of MHA with divalent metal carbonates suspended in water. Complexes of formula $[\{CH_3SCH_2CH_2\ CH(OH)COO\}_2M]\cdot 2H_2O$ can be isolated, with exception of copper, which gives an anhydrous complex. They appears as microcrystalline powders (X-ray diffraction), sparingly soluble in water. The iron(II) bis-chelate derivative dihydrate was prepared by reaction of the sodium salt of MHA with iron(II) sulfate. This species is apparently air stable only when dried; wet samples undergo progressive browning probably as a consequence of iron(II) oxidation, evidenced by Moessbauer spectroscopy (see 2.2.7.). In all these chelates two deprotonated MHA molecules should coordinate to the metal cations through two oxygen atoms from the caboxylic and the hydroxylic group respectively, producing two penta-atomic chelation rings. In this regard, the FTIR spectra of all complexes show strong absorption bands due to the asymmetric stretching of the carboxylic group (ranging from 1580, in the case of Co^{2+}, to 1641 cm^{-1}, in the case of and Cu^{2+}), significantly shifted to lower frequencies with respect to free MHA (1720 cm^{-1}), as expected for deprotonation and coordination. On the other hand, evidence for the coordination of the OH group comes from the significant shifts to lower energies of the relevant stretching bands: 3410 cm^{-1} in free MHA; from 3050 in the copper derivative to 3290 cm^{-1} in the cobalt derivative. As expected, IR data for the COO^- and OH groups are well comparable to those reported for the corresponding glycolate complexes (Fischinger *et al.*, 1969). TGA analyses throw light on the structural role of the water molecule in MHA chelates. In the case of Ca^{2+} and Mg^{2+} the two water molecule are completely lost before 100°C suggesting they are involved in simple hydrogen bonds and not in coordination; these metal cations should experience tethraedral environment determined by the two MHA *O,O'*-

chelation rings. On the other hand, in the case of Mn^{2+}, Co^{2+} and Fe^{2+} the two water molecule are completely lost only at 250°C suggesting that they are directly coordinated to the metal cations, which should exhibit hexacoordination as occurs for the corresponding Mn^{2+} glycolate complex (Melikyan *et al.*,2000). In the case of Cu^{2+} the structure should be the same of that observed for the bisglycolato complex, where two bidentate ligand determine a square-planar environment completed to bipyramidal through interaction with carbonyl oxigens of adjacent molecules (Forrest *et al.*, 1968).

In the case of zinc the water loss during TGA analysis occurs before 100° C; however single-crystal structural analysis reveled that $Zn(MHA_{-H})_2 \cdot 2H_2O$ is a dimer in the solid state, three water molecules beign coordinated to the zinc cations. The zinc bis-chelate, $Zn(MHA_{-H})_2$ can be isolated in two forms: dihydrate and anhydrous (Scheme 2).

The two forms, which can be easily converted into each other (see experimental section), exhibit rather different X-ray powder diffraction patterns and infrared spectra. Their IR spectra, allow their rapid and univocal recognition and determination also in commercial products when their concentration is not lower than 5%.

In particular, whereas the dihydrate form displays a single very strong peak due to n_{as}(CO) and d(OH) at 1591 cm^{-1}, the anhydrous one displays two peaks of the same intensity at 1580 and 1637 cm^{-1}. In both cases absorption frequencies are significantly shifted to lower values with respect to free MHA (1720 cm^{-1}) as expected for deprotonation and coordination. This was exhaustively described in an previous study on glycolate, lactate and mandelate solid complexes with divalent metals (Hahn e Baker 1993). It is worthy to note that the ATR-FTIR spectrum in the fingerprint region of the saturated solution of **1** in water is rather comparable to that of solid state spectra (Figure 2) supporting the presence of chelate complexes also in solution.

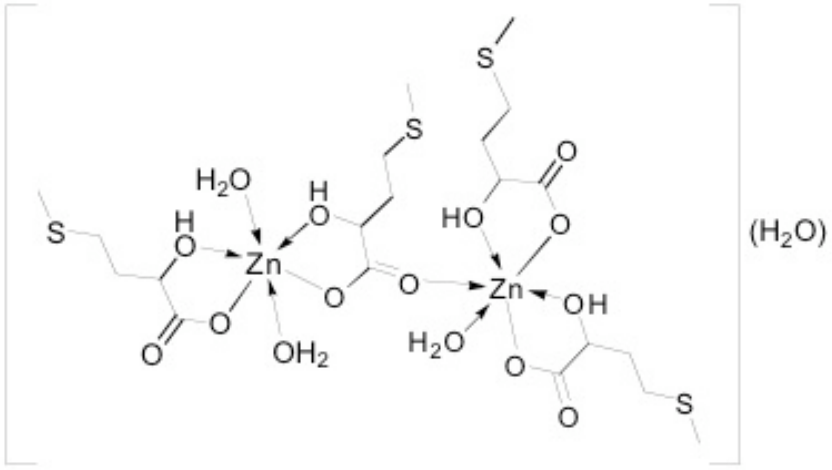

Scheme 2: Molecular sketch of **1**

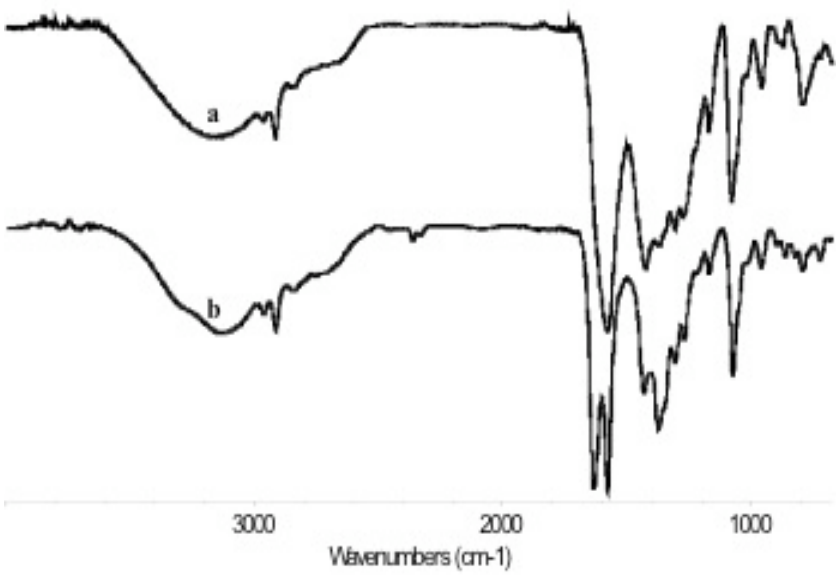

Figure 1: Comparison between the FTIR spectra in the solid state of (a) $[Zn_2(MHA_{-H})_4(H_2O)_3]H_2O$ (**1**) and (b) $[Zn(MHA_{-H})_2]$

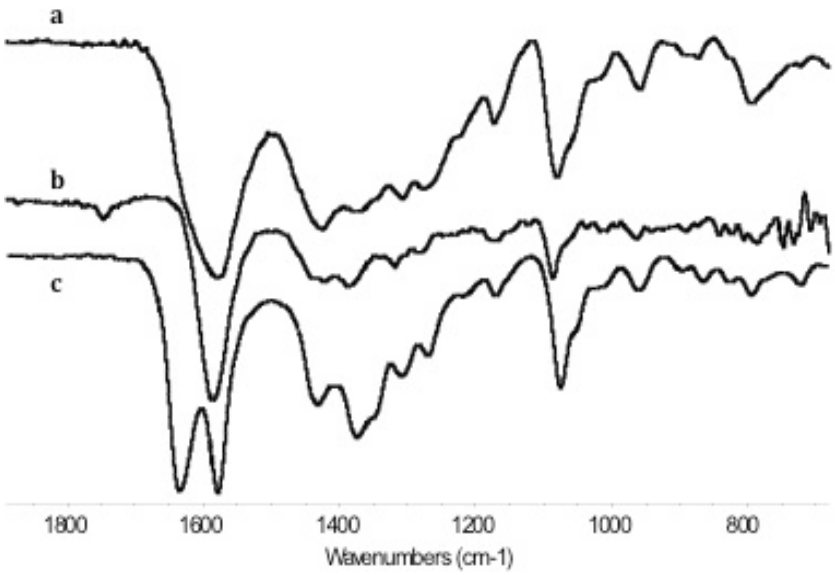

Figure 2: Comparison among the ATR-FTIR spectra in the fingerprint region of (a) the dinuclear hydrate bis-chelate **1**, (b) the MHA_{-H} /zinc bis-chelate saturated solution in water, and (c) the anhydrous bis-chelate

3.2.2. Potentiometric and ESR spectroscopy investigations

As spontaneous oxidation occurs on wet solid samples of MHA:Fe(II) complex, the iron(III) complex is the ultimate source of iron when used for metal ion supplementation. Thus, the system Fe^{3+} / MHA (HL) was studied by potentiometry in aqueous solution at T = 25 °C and I = 0.1 M (KCl) in pH range 1.5 – 3.5. At higher pH the instability in pHmeter reading and further precipitation of an insoluble material was observed even at Fe^{3+} / MHA 1:11 ratio and $C_{Fe} = 0.5\times10^{-3}$ M. The calculated formation constants for the Fe^{3+} / MHA system are reported in Table 1. Literature formation constants for the Zn^{2+} / MHA system are also reported (Predieri *et al.*, 2003). A representative distribution diagram is reported in Figure 3.

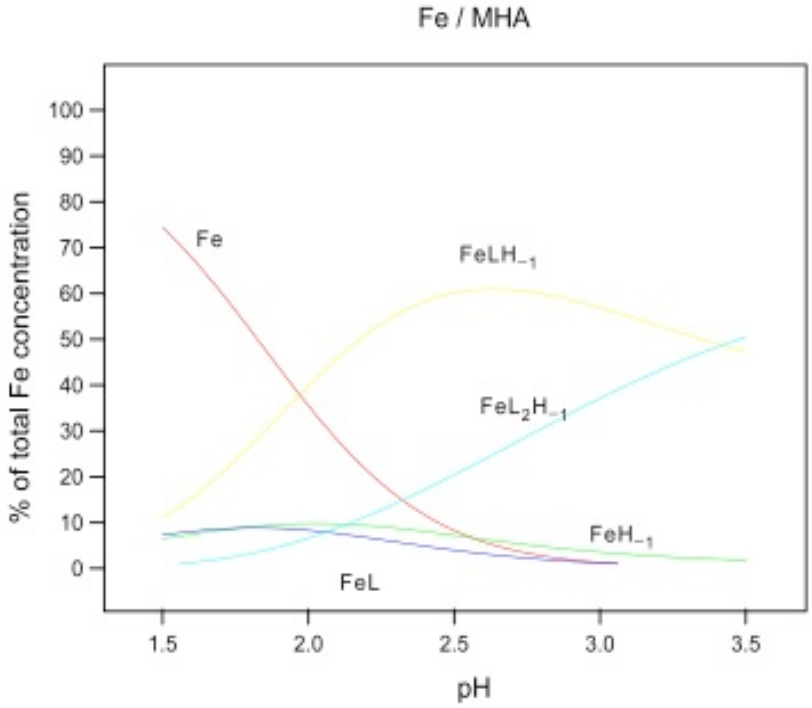

Figure 3: Distribution diagram of the Fe^{3+} / MHA (HL) system (Fe / L = 1:8, $C_{Fe} = 2.3\times10^{-3}$ M)

In the case of Fe^{3+}, and differently from Cu^{2+} (vide infra) and Zn^{2+} (Predieri *et al.*, 2003), no free Fe^{3+} is present at pH > 2.5, and this is in agreement with the *hard* properties and great coordination capabilities at low pH of MHA. In the species $[FeLH_{-1}]^{+}$ and $[FeL_2H_{-1}]$, one MHA ligand is probably deprotonated on the OH group. This behaviour was observed only in the case of Fe^{3+}. This is also in agreement with literature data for glycolic and lactic acids (Martell e Smith, 2001). The hydroxide species $[FeH_{-1}]^{2+}$ ($[Fe(OH)]^{2+}$) is present even at very low pH and it is almost coexhistent with the $[FeL]^{2+}$ species. The concentration of this hydroxide species reduces upon formation of the more stable $[FeLH_{-1}]^{+}$ and $[FeL_2H_{-1}]$ species. The $[FeL_2H_{-1}]$ species becomes predominant at pH higher than 2. The system Cu^{2+} / MHA (HL) was studied by spectrophotometric titrations in aqueous solution. The calculated formation constants are reported in Table 1. A representative

distribution diagram is reported in Figure 4.

The stechiometries of the species formed with Cu^{2+} and Zn^{2+} are the same, but the ones with Cu^{2+} are more stable, as expected. (Predieri *et al.*, 2003) However, also in the case of Cu^{2+} the precipitation of the hydroxide is observed at pH higher than 5. As observed for Zn^{2+}, the chelation capabilities in acidic pH of MHA are remarkably high than those of amino acids (Figure 5-6). However, even in excess of ligand, only with iron(III) complete complexation of the metal can be observed. In the case of Cu^{2+} and Zn^{2+} a small amount of free metal is still present at a M / L ratio up to 1:8.

Table 1: Logarithms of complex formation constants for the Fe^{3+}, Cu^{2+} and Zn^{2+} / MHA (HL) systems [a]. *T* = 25 °C, *I* = 0.1 M (KCl). Standard deviations are given in parentheses. Charges of the species are omitted for clarity

	Fe^{3+}	Cu^{2+}	Zn^{2+} [a]
[ML]	3.1(1)	2.57(2)	1.83(3)
[ML_2]	-	3.97(3)	3.1(2)
[MLH_{-1}]	1.78(1)	-	-
[ML_2H_{-1}]	4.73(2)	-	-
n [b]	238	1683	-
σ [b]	1.05	$6.85 \cdot 10^{-3}$	-

[*] *Protonation constant of the ligand (log β = 3.56(1)) and formation constants for the Zn^{2+} / MHA system were published in ref. [8]* [b] $\sigma = [\Sigma w_i(E_i^o - E_i^c)^2/(n-m)]^{1/2}$ *= sample standard deviation;* $w_i = 1/\sigma_i^2$, *where* σ_i *is the expected error on each experimental e.m.f. value* (E_i^o); *n = number of observations; m = number of parameters refined.*

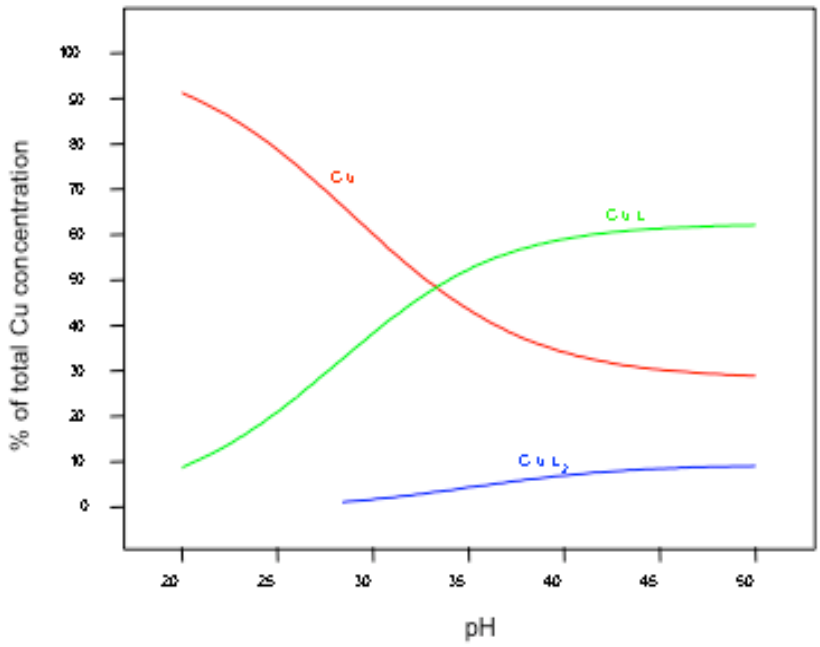

Figure 4: Distribution diagram of the Cu^{2+} / MHA (HL) system (Cu / L = 1:8, C_{Cu} = 8×10^{-3} M)

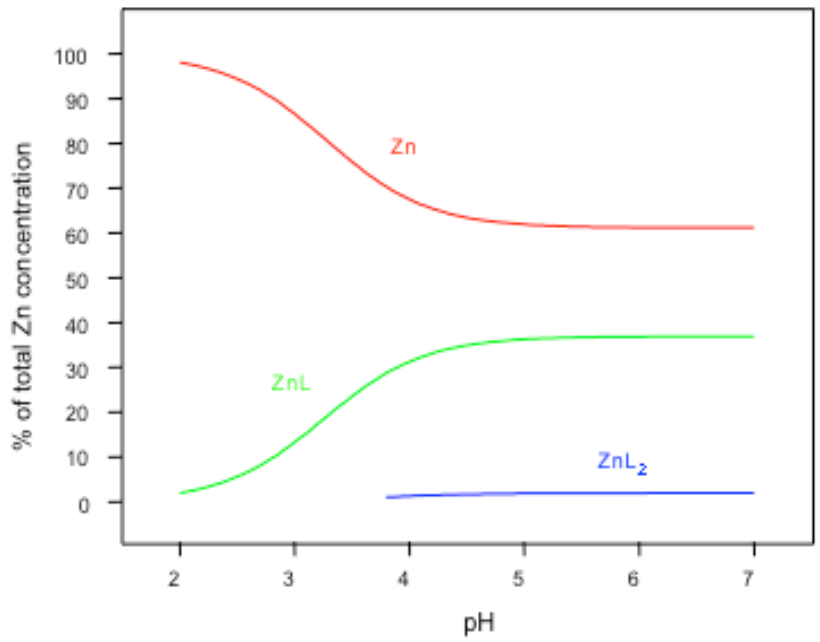

Figure 5: Distribution diagram of the Zn^{2+} / MHA (HL) system (Zn / L = 1:8, C_{Zn} = 8×10^{-3} M)

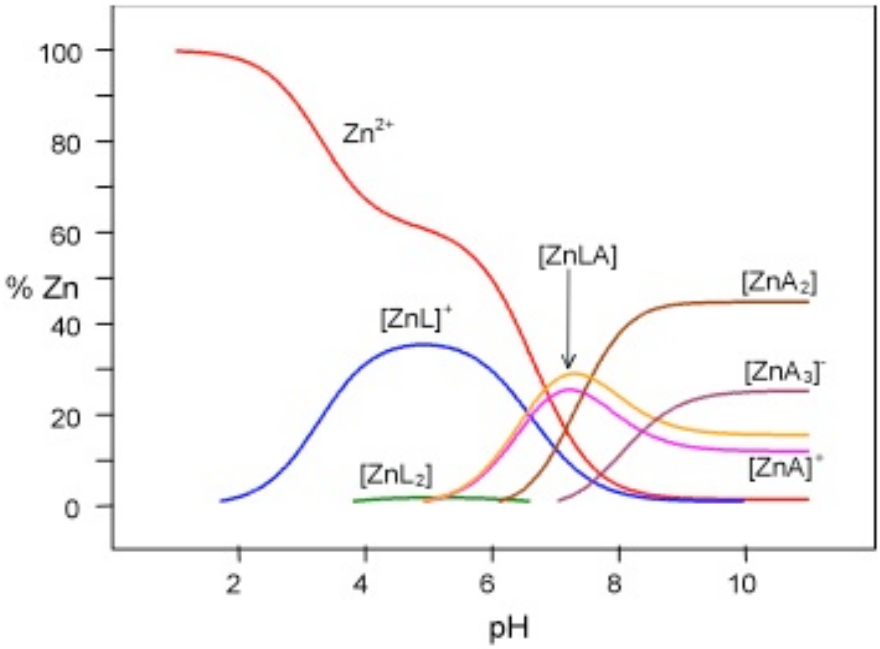

Figure 6: Distribution diagram of the Zn^{2+} / MHA (HL) / Amino acid (A) system (Zn / L / A = 1:8, C_{Zn} = 8×10^{-3} M)

In order to gain more insight into the structural features of copper chelates in solution have been undertaken on these species by means of ESR spectroscopy (ESR for Cu^{2+}) by the group of Professor Riccardo Basosi, at University of Siena. The spectra at pH=5.5 and 4.5 are typical of Cu^{+2} complexes and show the presence of $Cu(MHA_{-H})_2$ and $Cu(MHA_{-H})^{+}$ species; the spectrum at pH=2 shows the presence of the Cu^{2+}aquo-complex as the predominant species with a little amount of $Cu(MHA)^{+}$ that is evident from the distorted lineshape (Figure 7). The results are in agreement with the potentiometric measurements.

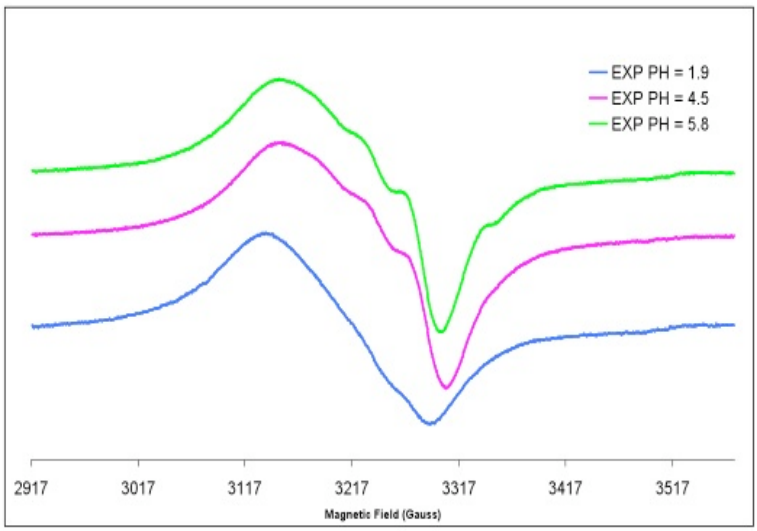

Figure 7: EPR spectra of $Cu(MHA_{-H})_2$ in aqueous solution at different pH

3.2.3. Characterization of MHA metal chelates by mass spectrometry

Characterization of the Iron(III) complexes in solution was also performed by ESI-MS analysis. Iron(III) complexes were obtained by reaction of Iron(III) sulphate (10^{-4}M) and Methionine Hydroxy Analogue (MHA) (1:3 stoichiometry) and directly infused into the electrospray mass spectrometer system and analysed both by ESI-MS and ESI-MS/MS. In order to determine experimental conditions that provide the best sensitivity and admit to maintain the complex integrity during the electrospray process, the cone voltage was varied between 8 and 120V. The formation of 1:1, 1:2 and 1:3 metal to MHA complexes was observed (Figure 8) through peaks at m/z 205, 355 and 505 respectively. The signal at m/z 151 was attributed to free protonated MHA. The relative intensities of the metal/MHA complexes were detected and optimized by ESI-MS, scanning the sampling cone voltage in the 8-120 range (Figure 9). In fact, species having different degrees of complexation showed a different stability towards cone voltage. In particular, a signal at m/z 151 was present in ESI-MS full-scan spectra up to 50 V. The signal of 1:1 complex was present from 30 up to 80 V, the 1:2 was observed up to 50 V. The 1:3 (m/z 505) was very labile and completely disappeared at cone voltages higher than 15V.

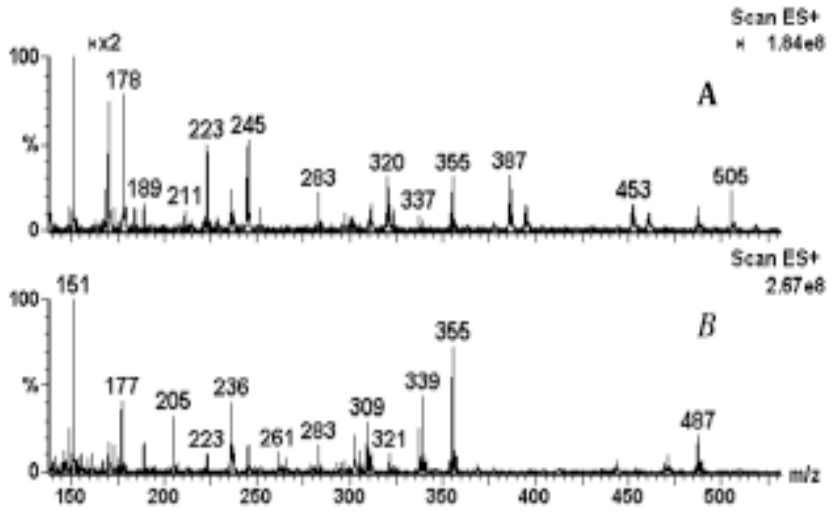

Figure 8: ESI-MS full-scan spectra of Iron (III) complexes obtained by reaction of Iron (III) sulphate (10^{-4}M) and MHA (1:3 stoichiometry) and acquird at a cone voltage of (A) 8V and (B) 30V

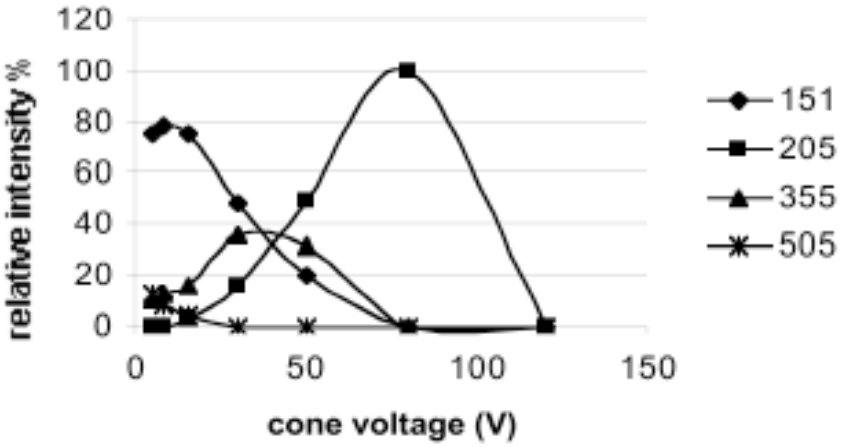

Figure 9: Relative intensity vs. cone voltage of MHA (m/z 151) and for 1:1 (m/z 205), 1:2 (m/z 355) and 1:3 (m/z 505) Iron (III) to MHA complexes

Signals occurring at m/z 205, 355 and 505 could be explained on the basis of an electrolytic reduction process of Fe(III) to Fe(II) that take place in the metal ESI capillary. Under this hypothesis the 1:1 complex between one deprotonated molecule of methionine hydroxy analogue and Fe(II), is observable as a singly positively charged ion at m/z 205. This finding is consistent with that observed for the first time by Van Berkel et al. about metal porphyrins (Van Berkel *et al.*, 1991), according to the Kebarle's description of the ESI ion source as an electrolytical cell (Blades *et al.*, 1991). In the case of 1:2 and 1:3 complexes, the signals observed at m/z 355 and m/z 505 could be explained on the basis of both the reduction process of Fe (III) and the acquisition of one and two protons, respectively. The complexes, were further characterized by tandem mass spectrometry, in order to confirm their identity according to their fragmentation pattern. ESI-MS/MS product-ion spectrum of the ion at m/z 151 (free MHA) shows a fragment at m/z 103, probably attributable to the loss of the CH_3SH group and one at m/z 85, due to the further loss of a water molecule. The presence of a fragment at m/z 61 is presumably attributable to a $[CH_3SCH]^{\cdot+}$ group. In the ESI-MS/MS product-ion spectrum of the ion at m/z 205 (1:1 complex), the loss of a water molecule and of a CO, could explain the presence of the ion at m/z 159. At low m/z values, fragments at 61 and 103 are in common with the fragmentation pattern of free MHA. The loss of a water and a CO molecules, accounts also for the formation of the ion signal at m/z 309 from the fragmentation of the 355 (1:2 complex). The protonated molecular ion of the 1:1 and some of its fragments (m/z 129, 159, 177) are also present in the ESI-MS/MS product-ion spectrum of the 1:2. Finally, the fragmentation pattern of the 1:3 complex (m/z 506) evidences the presence of a signal at m/z 355 attributable to the 1:2 complex and of many of its fragments (m/z 261,223,177).

Zn(II) complexes obtained by the reaction of $ZnCO_3$ (10^{-4} M) and $ZnSO_4$ (10^{-4}M) and MHA were characterized by ESI-MS both in the PI and NI modes. ESI(+)-MS experimental conditions were optimized, with particular attention to the cone voltage, that was varied between 10 and 80 V. By analyzing the solution of complexes obtained from $ZnSO_4$ and operating at a cone voltage of 10V the 1:2 and

1:3 metal to MHA complexes were observed at m/z 363 and 513, respectively at almost the same relative intensity (20%). By increasing the cone voltage at 30 V the 1:3 complex disappeared and an increase of the 1:2 specie (90% relative intensity) was observed. In addition, under these conditions the 1:1 complex appeared at m/z 213 (relative intensity of 18%). All complexes appear as ion distributions, due to the presence of the Zinc ion. The good fitting between the observed distributions and the theoretical isotopical models contribute to increase the confidence in the identification. Further evidence for this assignment comes from tandem mass spectrometry. ESI(+)-MS/MS product-ion spectrum of the ion at m/z 213 (corresponding to 1:1 complex) shows fragments at m/z 185 and 167, probably due to the loss of one and two water molecules respectively. These signals are also present in the fragmentation pattern of the 1:2 complex (m/z 363), together with a signal at m/z 213 attributable to the 1:1. ESI(-)-MS spectra showed at a cone voltage value of 10V the presence of only the 1:3 complex as singly negative charged ion at m/z 511 (10% relative intensity). The 1:2 complex started to appear at a cone voltage of 50V as $[M-H]^+$ ion at m/z 361 (30% relative intensity). By increasing cone voltage to 80V the 1:2 complex become the base peak and the 1:1 specie appeared at m/z 213 (55% relative intensity). The presence in the ESI(-) spectra of the 1:1 specie having a net positive charge could be explained on the basis of a reduction process involving $2e^-$ occurred at the electrospray capillary. The ESI(-)-MS spectra of the solution obtained from $ZnCO_3$ (cleaner than those obtained from $ZnSO_4$) showed, at a cone voltage of 30V, the presence of the 1:2 and 1:3 species at m/z 361 (5% relative intensity) and 511 (20% relative intensity) respectively. By increasing the cone voltage to 60V the 1:2 specie appear as the base peak. The 1:1 complex appeared at m/z 213 with a relative intensity of 15%, whereas the 1:3 resulted present at a relative intensity lower than 5%. Considering that the 1:3 species have not been detected by potentiometric experiments (reported above for iron and in ref 8 for zinc), in spite of the higher concentrations, it is likely that aggregations occur during analyte desolvation in ESI conditions. On the other hand, 1:3 species with a bidentate ligand like MHA are expected in solution, mainly in the case of iron at pH values higher than the limit

(3.5) adopted in collecting potentiometric data. The 1:3 species appear rather unstable as they tend to disappear by increasing the cone voltage, when the 1:2 species is the major one.

3.2.4. X-ray crystal structure of the Zinc bis-chelate

A view of the dinuclear complex $[Zn_2(MHA_{-H})_4(H_2O)_3]$ present in the crystal structure of **1** is reported in Figura 10. Table 2 report selected bond distance and angles. In this species both metal centres are chelated by two anions derived from MHA through the hydroxyl oxygen and one of the carboxyl oxygen atoms, forming five-membered chelation rings. One of the MHA_{-H} anions bound to Zn1 is also connected with Zn2 through the second carboxylate carbon. The coordination over the metal centres is completed by two water molecules for Zn1 and one for Zn2. The Zn-O bond lengths are in good agreement with those typically found in the literature [CCDC Zn-O average bond distance (over 3605 structures containing Zn-O bonds): 2.050 Å]; average Zn-O bond length in **1**: 2.097(4) Å]. The O2-Zn1 [2.185(4) Å] and O11-Zn2 [2.184(4) Å] bonds are significantly longer than the other Zn-O bonds and in particular the other two hydroxyl ones [2.107(3) Å for Zn1-O5 and 2.102(4) Å for O8-Zn2]. The O-Zn-O chelation angle [average: 75.6(1)°] is also in good agreement with those reported in the literature for chelating a-hydroxyacids. A common feature of this class of ligands, such as glycolate, malate and lactate, is to bridge two metal centres by using all the oxygen atoms for coordination. Examples of this coordination fashion can be found in the literature for Zn(II) coordination polymers (Templeton *et al.*, 1985; Smith *et al.*, 1985; Xiong *et al.*, 1999; Inomata *et al.*, 1999; Tsuji *et al*.1991; Chen *et al.*, 2000). On the other hand, in the presence of ancillary ligands (including water molecules) mononuclear bis-chelate compounds bearing two ancillary ligands are rather common (Fischinger e Webb, 1969; Singh *et al.*, 1975; Fleck *et al.*, 2001; Carballo *et al.*, 2004). To our knowledge, the structure of **1** represent the first reported example of a discrete dinuclear complex

with a-hydroxyacid ligands as bridge.

Packing energies could play a major role in determining crystal and molecular structure of **1**. Ten hydrogen bonds interconnect one molecule of $[Zn_2(MHA_{-H})_4(H_2O)_3]$ with the neighbors (Figure 11). One intramolecular hydrogen bond involves O3W and O1 [O×××O separation: 2.715(6) Å], while the free water molecule interacts with O2W as acceptor and with O12 as donor [O2W×××O4 and O12×××O4W separations: 2.704(7) and 2.896(7) Å]. The shortest hydrogen bond is present between O8 with O9 [O×××O separation: 2.652(5) Å]. The hydrophilic moieties (water molecules, carboxylic and alcoholic groups) are interconnected in such a way that layers of dinuclear complexes are formed. Moreover, the thioether chains are oriented in the same direction, thus forming lipophilic layers (Figure 12). This two-dimensional separation is reminiscent of that of micelles, in which the separation between the hydrophilic and lipophilic moieties results in spherical three-dimensional supramolecular structures. The thioether chains do not show significant close contacts between each other, the minimum C×××C separation [C10×××C15] being 3.752(6) Å and the minimum S×××C [S4×××C10] being 3.591(4) Å, resulting from a non classical hydrogen bond between the C10 methyl and S4. The gain in reticular energy that stem from the packing features described above may then be the reason for the particular $[Zn_2(MHA_{-H})_4(H_2O)_3]$ formulation of the discrete units (Predieri *et al.*, 2008).

Table 2. Selected observed (X-ray structure) and calculated[a] (via DFT methods) bond lengths (Å) and angles (°) for **1** and the corresponding model $[Zn_2(OC(O)CH_2CH(OH)CH_2CH_2SCH_3)_4(H_2O)_3]$; estimated standard deviations in parentheses

Structural parameters	X-ray structure	DFT structure[a]
Zn1-O1	2.052(3)	2.074
Zn1-O1w	2.048(3)	2.166
Zn1-O2w	2.065(4)	2.161
Zn1-O4	2.095(3)	2.002
Zn1-O5	2.107(3)	2.279
Zn1-O2	2.185(4)	2.347
Zn2-O10	2.049(4)	2.094
Zn2-O3	2.072(4)	2.237
Zn2-O7	2.097(4)	2.026
Zn2-O8	2.104(4)	2.232
Zn2-O3w	2.111(4)	2.223
Zn2-O11	2.184(4)	2.222
O7-Zn2-O8	75.70(13)	74.6
O10-Zn2-O11	75.95(14)	74.0
O1-Zn1-O2	75.28(14)	70.3
O5-Zn1-O4	75.84(13)	73.7

[a] The computed DFT bond lengths and angles are not strictly comparable with the X-ray parameters, as in the crystals the molecules are connected through a network of hydrogen bonds

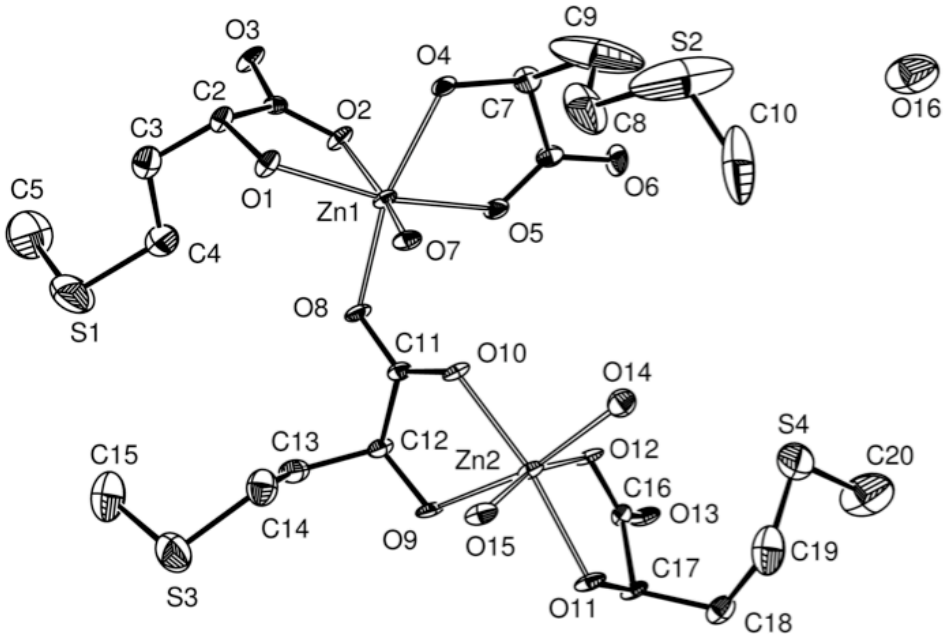

Figure 10: Ortep view of the dinuclear complex $[Zn_2(MHA_{-H})_4(H_2O)_3]$ present in the crystal structure of **1**. Thermal ellipsoids include 30% of the electron density. Free water molecules and hydrogen atoms omitted for clarity. A selected list of bond distances (Å) and angles (°) is reported in Table 2

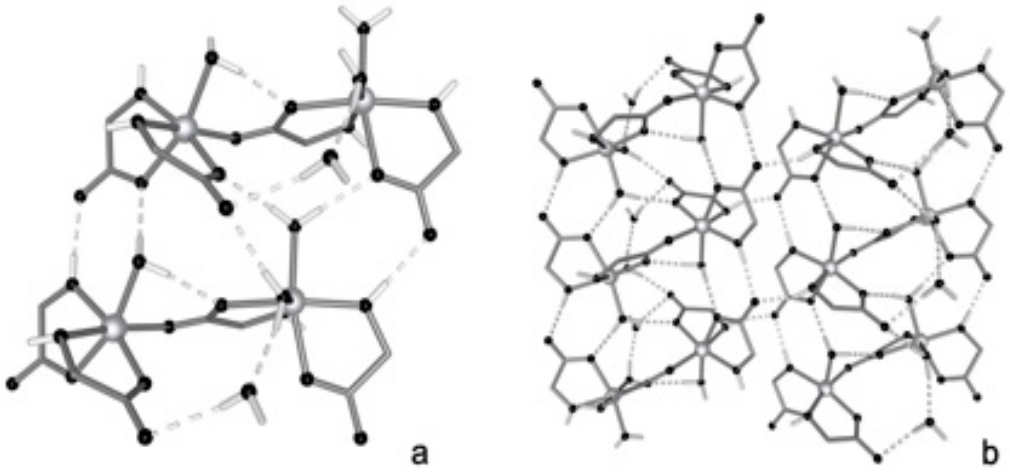

Figure 11: Packing diagram (view along c axis) of the crystal structure of **1** representing: (a) a couple of dinuclear complexes, interconnected by hydrogen bonds and (b) an extended view, depicting 6 dinuclear complexes. Thioether chains omitted for clarity. Gray spheres: zinc atoms; black spheres: oxygen, dark gray sticks: carbon; light gray sticks: hydrogen. Hydrogen bonds are represented by gray dashed lines. Symmetry operation generating equivalent molecules of figure a: -x, -y, -z

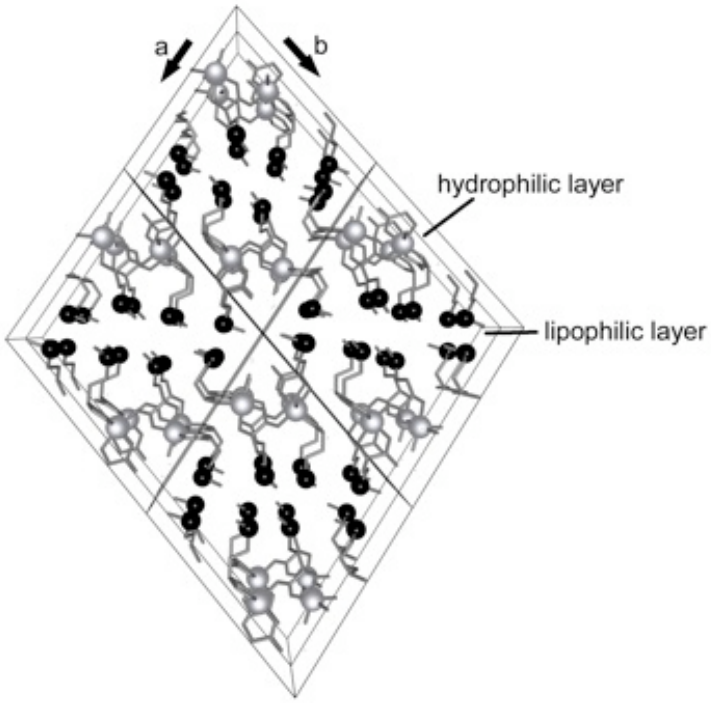

Figure 12: View of the packing diagram of the crystal structure of **1** along axis c emphasizing the separation between lipophilic layers (black spheres represent S atoms) and hydrophilic ones (gray spheres represent Zn atoms)

3.2.5. DFT computational analysis

A molecular computational analysis has been performed via density functional theory (DFT) on three Zn(II) complexes of MHA_{-H} (the dinuclear bis-chelate observed in the solid state, the mononuclear one and the monochelate-tetraaquo complex) with the aim to study the structural features of coordination to metal and to gain insight into the possibility that the dinuclear arrangement observed via X-ray single crystal studies could exist also in aqueous solution.

For the study of the dinuclear form $[Zn_2(MHA_{-H})_4(H_2O)_3]$, we performed a full geometry optimization using the X-ray structure as a starting model (Figure 8), at the B3LYP/6-311+G* level of theory, using the LANL2DZ basis set for the Zn(II) ion. The equilibrium structure is in good agreement with the dinuclear arrangement of **1** (with a bridging carboxylate) where both zinc atoms display hexacoordination. Selected computed distances and angles are reported in Table 2. The differences among the experimental and theoretical data are due to the fact that computations were performed in gas phase, whereas the X-ray data were obtained in the solid state where molecules are connected by a network of hydrogen bonds.

We then investigated the possible existence in solution of the the bis-chelate-diaquo mononuclear species $[Zn(MHA_{-H})_2(H_2O)_2]$. The model structure was obtained from the geometry of the dinuclear one (Figure 13). We performed a full geometry optimization at the same level of theory of the dinuclear form. In order to check the relative stability in solution of the mononuclear form compared to the dinuclear one, we simulated the solvent effects using the Polarizable Continuum Method (PCM). The bulk solvent effect has been evaluated embedding the molecules under investigation in a continuum of dielectric constants ε=78.39 (water).

The analysis has been performed considering the following reaction scheme:

$$2\,[Zn(MHA_{-H})_2(H_2O)_2] \rightleftharpoons [Zn_2(MHA_{-H})_4(H_2O)_3] + H_2O$$

The computation shows that the mononuclear species in water (left side of the reaction) is more stable than the dinuclear one for about 11 Kcal/mol.

For the sake of completeness we studied also the mono-chelate tetraaquo-complex $[Zn(MHA_{-H})(H_2O)_4]^+$. The presence in solution of the monochelate species has been suggested by potentiometric and mass-spectral data (Predieri *et al.*, 2003-2005). The resulting optimized structure is reported in Figure 14.

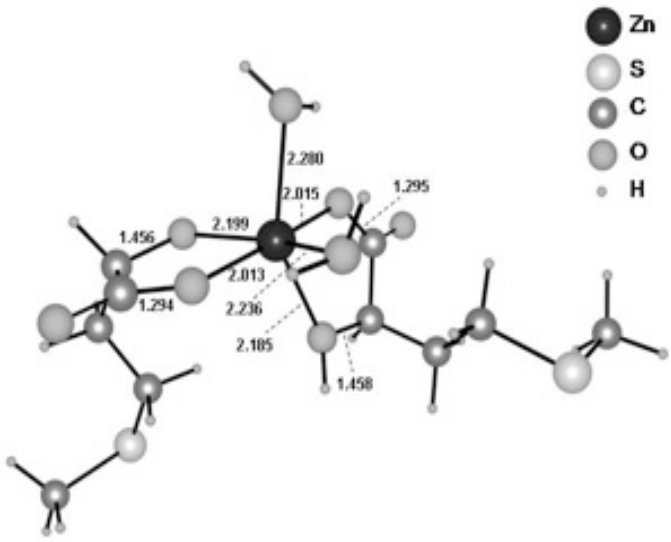

Figure 13: Optimized geometry and selected bond lengths for the mononuclear bis-chelate complex $[Zn(OC(O)CH_2CH(OH)CH_2CH_2SCH_3)_2(H_2O)_2]$ obtained at B3LYP/6-311+G*(C,H,O,S), LANL2DZ (Zn) level of theory. Selected computed bond lengths are reported in Å

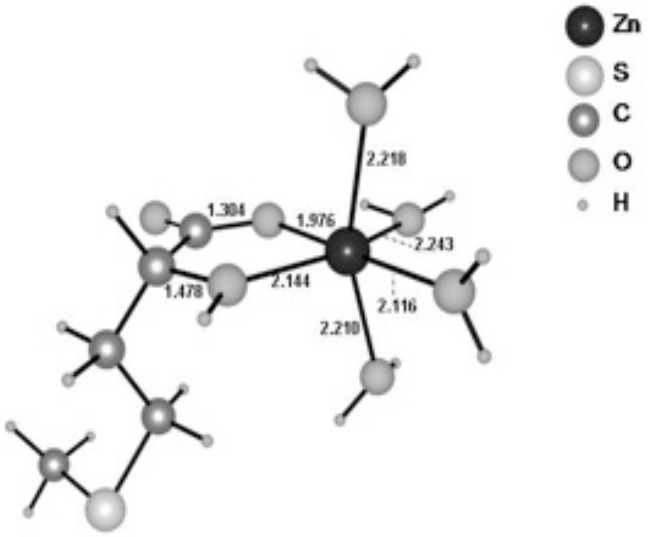

Figure 14: Optimized geometry and selected bond lengths for the mononuclear mono-chelate cation $[Zn(OC(O)CH_2CH(OH)CH_2CH_2SCH_3)(H_2O)_4]^+$ obtained at B3LYP/6-311+G*(C,H,O,S), LANL2DZ (Zn) level of theory. Selected computed bond lengths are reported in Å

3.2.6. NMR investigations

The proton and carbon assignments of MHA and $[Zn(MHA_{-H})_2]$ in solution are reported in Table 3. The 1D ^1H and ^{13}C spectra of the two compounds are very similar with the exception of the significant chemical shift variation experienced by the proton (+0.07 ppm) and carbon (-0.6 ppm) in alpha position. Such chemical shift perturbations arise from the diversity in chemical environment and suggest binding of Zn(II) to the carboxyl and/or hydroxyl moieties of MHA_{-H}.

Also the proton spin-lattice relaxation rates (Table 3) are consistent with the formation of a metal complex. In fact, selective and non selective relaxation rates are faster in $[Zn(MHA_{-H})_2]$, consistently with the occurrence of a longer correlation time, which is strictly dependent upon the molecular weight. The correlation time was calculated at t_c= 80 ± 10 ps and t_c= 140 ± 15 ps for MHA and $[Zn(MHA_{-H})_2]$ respectively from the value of the cross-relaxation rate s, of the b-CH_2 protons (Hall e Hill, 1976) and from the ratio between non-selective and selective

relaxation rates of alpha and beta protons of MHA (Freeman *et al.*, 1974).

In order to gain additional information on the molecular size of the two species, diffusion coefficients (D) were also calculated. D is given by:

$$D = \frac{k_B T}{6\pi\eta r_H}$$

where k_B = 1.380658x10^{-23} J/K is the Boltzmann's constant, η is the viscosity of the medium and r_H is the hydrodynamic radius of the molecule, here assumed of spherical shape (Stilbs e Lindman, 1981). The use of TSP as internal diffusion reference allows to take into account the variation in solvent properties while comparing solutions differing for solute concentration or solvent composition and makes it possible to correct the measured diffusion values for any change in the viscosity (Cabrita, 2001). The slight decrease in D in [Zn(MHA$_{-H}$)$_2$] solutions suggests an increase of the hydrodynamic radius which might be consistent with the simultaneous presence of both bis- and mono-chelate complexes in fast exchange with each other in the time scale of NMR experiments.

Table 3. ^{1}H and ^{13}C NMR assignment, ^{1}H spin-lattice non-selective and selective relaxation rates, diffusion coefficient of MHA and [Zn(MHA$_{-H}$)$_2$] solutions. The measurements were performed in D_2O T=298, pH 6.

	^{1}H (δ ppm)	^{13}C (δ ppm)	^{1}H R_1^{nsel} (s)	^{1}H R_1^{sel} (s)	D×10^{10} m^2 s^{-1}	D×10^{10} m^2 s^{-1} TSP
MHA						
Xα	4.12	71.8	0.31		6.0	5.5
Xβ	1.98	33.9	0.80	0.57	5.8	
Xγ	2.59	29.2	0.70		5.9	
Xε	2.11	14.2	0.33		5.8	
[Zn(MHA$_{-H}$)$_2$]						
Xα	4.19	71.2	0.53		5.4	5.5
Xβ	2.02	33.6	1.19	0.92	5.4	
Xγ	2.62	29.0	0.94		5.5	
Xε	2.12	14.0	0.36		5.5	

3.2.7. Moessbauer investigations on the iron MHA chelates

A major question concerning MHA iron chelates is the oxidation state of the metal cations. The question is if the oxidation state +2 of iron is stable in the MHA chelates and this could have tsome relevance in the nutritional characteristics of the iron chelates. In fact, it is well known that iron(II) metal chelates with *O*- or *N*-donor ligands are prone to easy transformation into iron(III) species in water media, in the air.

As pointed out in 2.2.1 the iron(II)-MHA bis-chelate derivative, prepared by reaction of the sodium salt of MHA with iron(II) sulfate, is apparently air stable only when dried; wet samples undergo progressive browning probably as a consequence of iron(II) oxidation. This has been confirmed by Mössbauer spectroscopy investigations carried out by Dr. Fabrizio Cavatorta in the Physics Deparment of Parma University on three samples of iron(II)/MHA chelates, listed below. The obtained spectra were compared with that recorded for the pure iron(III) chelate, prepared by reacting the sodium salt of MHA with iron(III) sulfate.

The following products were selected for Mössbauer investigations; industrial products were manufactured by Società S. Marco, Pegognaga (MN) by scaling up the laboratory procedure:

Iron(II) derivatives

(1) $Fe(MHA)_2$, industrial product (Fig. **predier1**)

(2) $Fe(MHA)_2$, industrial product, suported and dried on silica (Fig. **predier2**)

(3) $Fe(MHA)_2$, laboratory product (Fig. **predier3**)

Iron(III) derivatives

(1) $Fe(MHA)_2^+$ laboratory product (Fig. **predier4**)

The relevant Mössbauer spectra ere reported in Figures predier1-4 where the green component of the profiles is due to iron(III) and the red one to iron(II).

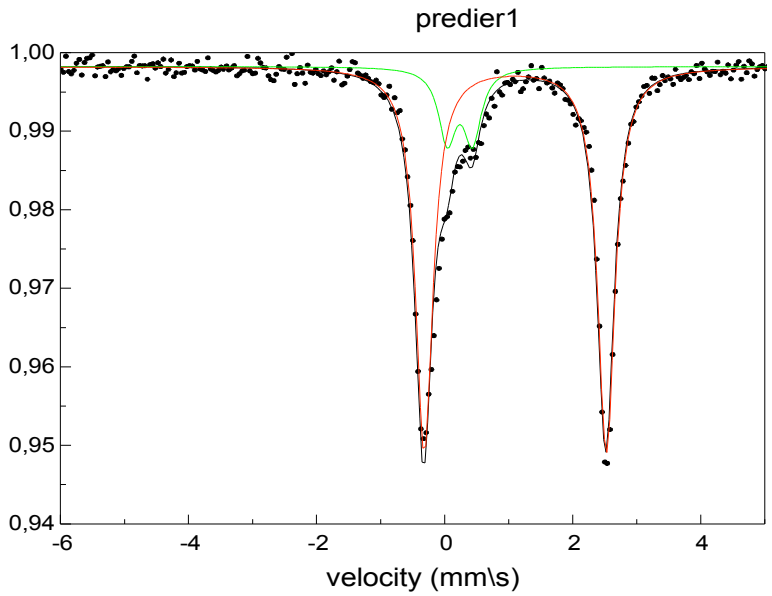
predier1
1,00
0,99
0,98
0,97
0,96
0,95
0,94
-6
-4
-2
0
2
4
velocity (mm\s)

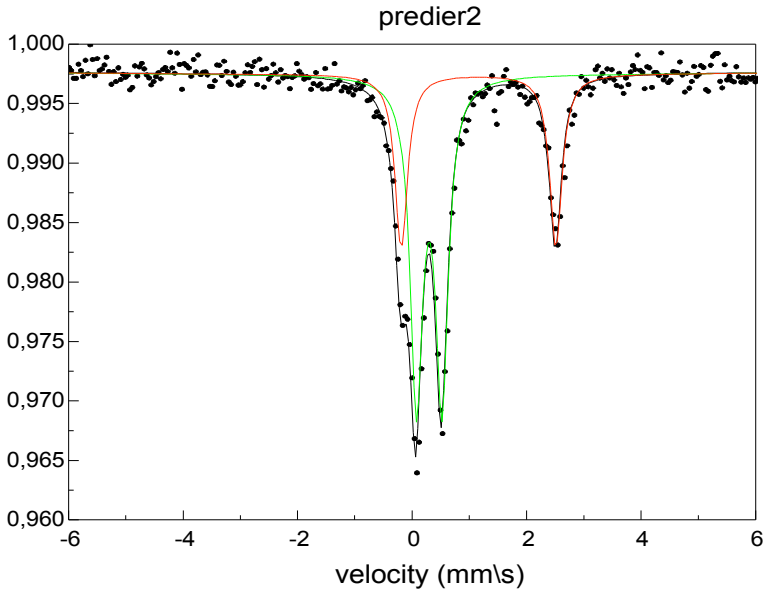
predier2
1,000
0,995
0,990
0,985
0,980
0,975
0,970
0,965
0,960
-6
-4
-2
0
2
4
6
velocity (mm\s)

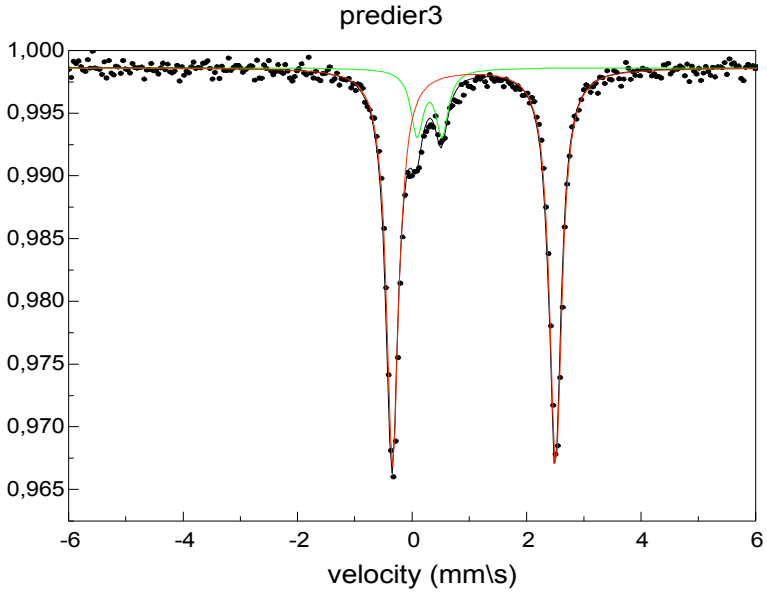
predier3
1,000
0,995
0,990
0,985
0,980
0,975
0,970
0,965
-6
-4
-2
0
2
4
6
velocity (mm\s)

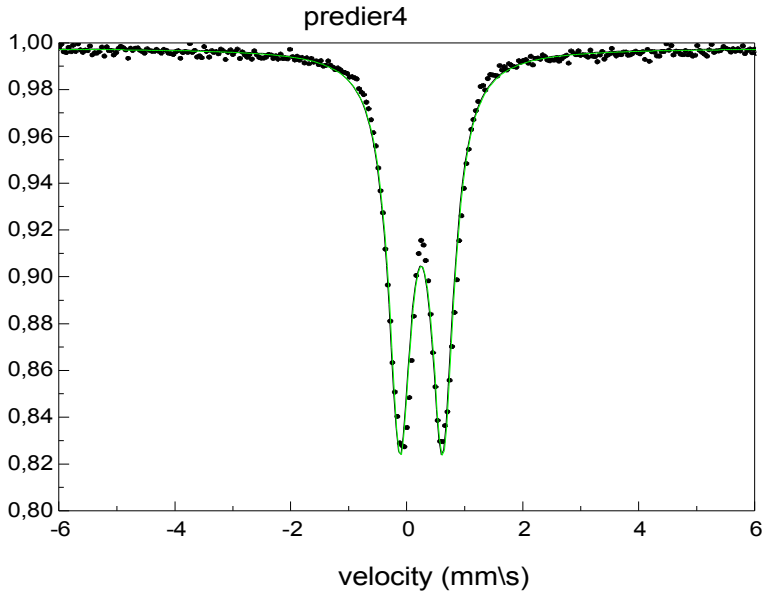
predier4
1,00
0,98
0,96
0,94
0,92
0,90
0,88
0,86
0,84
0,82
0,80
-6
-4
-2
0
2
4
6
velocity (mm\s)

By examining the three spectra of the iron(II) derivatives, it clearly appears that they easily undergo oxidation to iron(III) species and that this occurs just during the preparation procedure in the air, in the presence of water, even if in scarce amount. Actually, the fresh sample prepared in our laboratory, under controlled conditions, exhibits a content of iron(III) (14%, Fig.predier3, calculated by the Mössbauer peaks area) similar to that observed in the industrial product (17%, Fig.predier1).

Regarding the supported sample (Fig.predier2), the Mössbauer profile reveals that it is more liable to air oxidation, as the presence of iron(III) species reaches the extent of 65%. Probably the fine dispersion of the iron(II) chelates onto the silica surface makes them more labile and vulnerable to oxygen attack.

Finally, the spectrum of the iron(III) derivative does not any detectable trace of iron(II) species, confirming that iron(III) chelates with *O*-donor ligands are more stable than the corresponding ones with iron(II).

3.3. Analytical methods for determination of the MHA chelates

Another task of this research work concerned the development of new and reliable analytical methods for the rapid identification and determination of MHA metal-chelate species in commercial samples produced for animal feeding purposes (see Introduction).

In particular, the attention was paid to the analysis of the $Zn(MHA_{-H})_2$ complex as the most commercially important chelate. For this reason, feed-stuffs used for piglet feeding during the growing phase and directly provided by the manufacturer companies (see Experimental section) have been considered.

From the analytical point of view two different approaches were followed: the first one based on the solid-liquid extraction of the metal chelate from the matrix and HPLC analysis, the second based on the direct characterization of the target analyte by infrared spectrophotometry.

3.3.1. HPLC - Mass Spectrometry

In a first part of the work a solid phase extraction method was developed for the extraction and purification of the Zn-chelate from the samples followed by the HPLC-ESI-MS analysis. Excellent recovery values (91±7 %, R.S.D. 8,26 %) were obtained by fortifying the samples at the 290 ppm concentration level. A significant matrix effect did not allowed to calculate the recovery value at the 100 ppm concentration level (concentration level of the Zn-MHA chelate in the real samples).

The first studies carried out on the chelate stability established the dissociation of the complex in the HPLC ESI-MS system in four different forms: the 1:2 complex, the 1:1 complex, the free ion and the free ligand (see also 3.2.3.).

These preliminary results highlighted the necessary to optimize the sample purification procedure with the aim to reduce the matrix effect, improve the ESI-

MS analysis and to obtain LOD and LOQ values suitable for the determination of the Zn-chelate in the real samples.

The solid-liquid extraction method here developed (see Experimental) allowed to eliminate the proteic and the the lipidic fraction from the extract. A further SPE purification step was optimized on C18 cartridges by evaluating different solvent elution mixtures. The use of an acetonitrile/water (70/30, v/v) mixture (2 ml) allowed the quantitative elution of the Zn-chelate from the SPE support and, the fast removing of the acetonitrile, by evaporation under nitrogen from the final extract, prevented the complex dissociation. The final sample volume was then adjusted at 2 ml with a buffer solution (pH 4.8) for the optimal complex stability.

In order to optimize interface parameters, direct infusion of a standard solution of $Zn(MHA_{-H})_2$ in the ESI interface was performed. The FIA method allows to eliminate the effects of the chromatographic column on the complex dissociation equilibria by providing excellent ESI-MS and MS/MS signals with respect those obtained by HPLC.

Under PI ESI conditions, mass spectrum showed the protonated molecular ion having the typical Zn isotopic pattern without fragmentation (Figure 15).

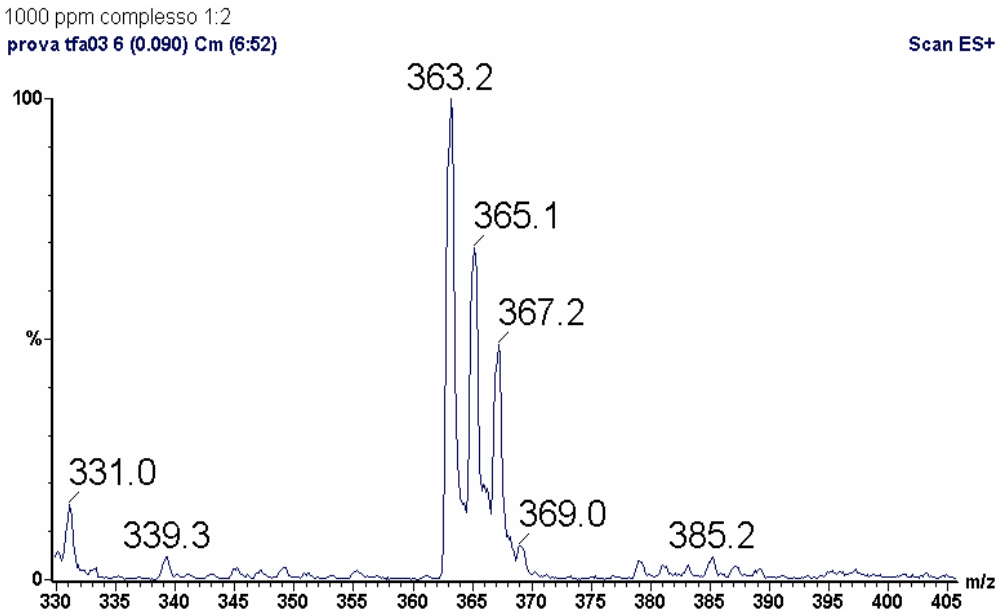

Figure 15: ESI(+)-MS spectrum of a standard solution of Zn(MHA-H)2 (1000 ppm) evidencing the isotopic distribution

For MS-MS analysis in product-ion scan the molecular ions of $Zn(MHA_{-H})_2$ complex were isolated as the precursor ions and fragmented by collision induced dissociation (CID). The main dissociation of $Zn(MHA_{-H})_2$ involves the fragmentation of one MHA at the carboxylic acid end, leading to a loss of 103 amu. The product-ion mass spectra are shown in Figure 16.

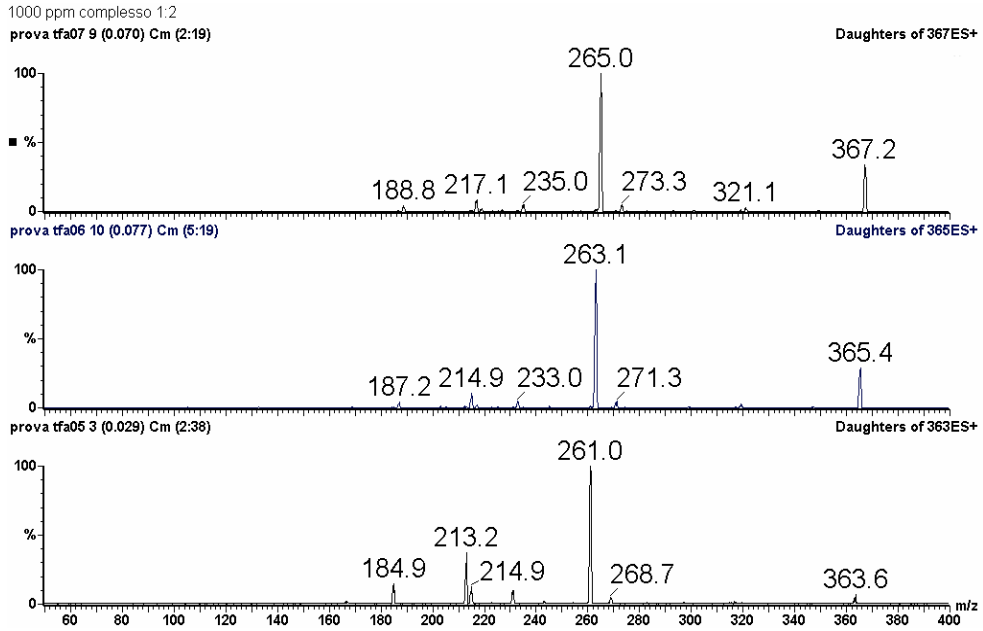

Figure 16: ESI(+)-MS/MS product-ion mass spectrum of the $Zn(MHA)_2$ complex and isotopic distribution of the most intense ion

Consequently, for quantitative determinations, two characteristic MRM (Multiple Reaction Monitoring) transitions of the $[M+H]^+$ ions were acquired.

In developing the chromatographic procedure, the main goal was to achieve a good retention of $Zn(MHA_{-H})_2$ while separating it from matrix constituents. For this purpose, preliminary trials were carried out analyzing both standard solutions and animal feed sample extracts on reversed-phase partitioning using narrow-bore columns containing C18 stationary phases. In these conditions, the chromatographic behaviour of the $Zn(MHA_{-H})_2$ complex exhibited the occurrence of a partial

dissociation leading to the formation of the 1:1 $Zn(MHA_{-H})_2$ complex and the free ligand.

For this reason, the high selectivity of the MRM detection was used to develop a flow-injection analysis (FIA)-ESI-MS/MS method.

Under the optimized MRM conditions, a detection limit lower than 1 mg/kg was calculated by analyzing $Zn(MHA_{-H})_2$ standard solution with excellent repeatability (RSD<5%) (Figure 17).

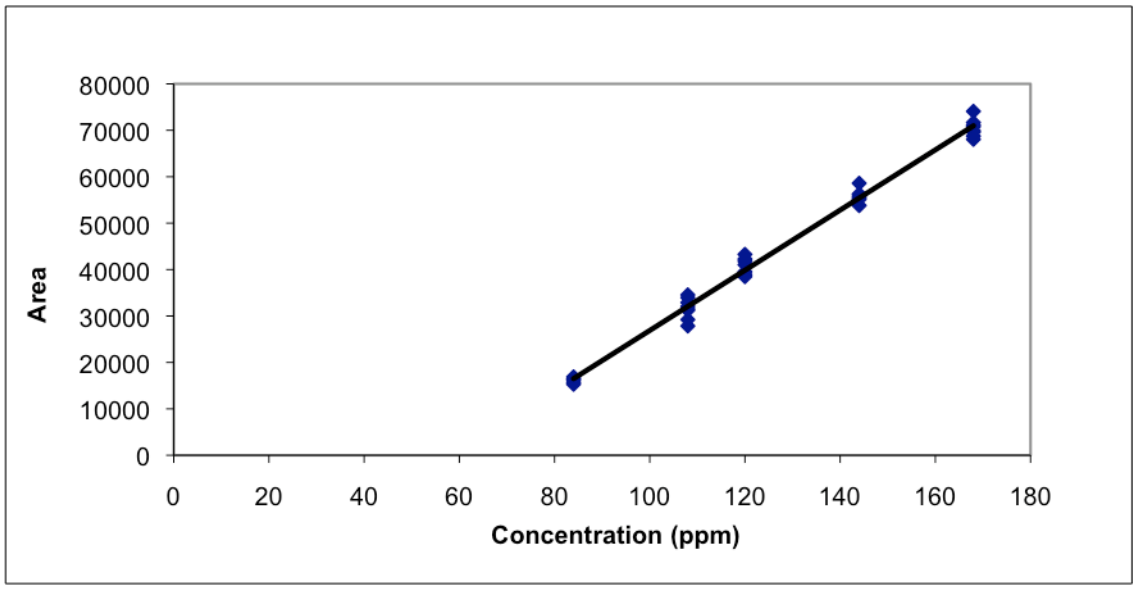

Figure 17: Instrumental calibration curve obtained by FIA ESI-MS/MS: y=648,4x-37957, R2=0,9919, n=40

However, by applying the method to the detection of $Zn(MHA_{-H})_2$ in the real sample the influence of the matrix significantly affected the detection limits by a strong signal suppression effect. In particular, the matrix should be diluted ten times to be analyzed by increasing the LOD value to 0.7 g/kg level.

The matrix-matched calibration curve was obtained by spiking blank extract samplesat different $Zn(MHA_{-H})_2$ concentration levels. The results evidenced a strong matrix effect affecting the noise level and the repeatability of the analysis. In order to decrease the matrix effect the sample extracts were diluted from 5 to 10

times. A significant reduction of the matrix effect was observed by diluting extracts 10 times and the linearity was observed starting from the 340 ppm concentration level (Figure 18).

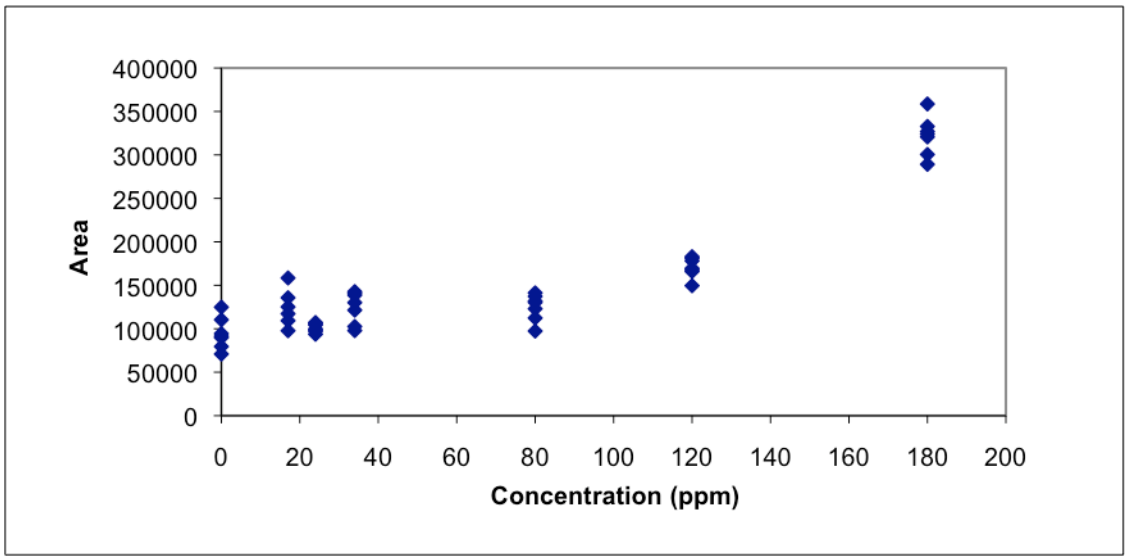

Figure 18: Matrix-matched calibration curve obtained by FIA ESI-MS/MS (matrix diluted 10 times) from 0 (blank sample) to 180 ppm

It can be inferred that the stability of the Zn-MHA complex is strongly dependent from a dynamic equilibrium establishing the release and the uptake of a molecule of ligand from the complex. This effect depends from the concentration of the chelate and the presence of matrix interferents that can compete with the MHA ligand for the Zn complexation.

The results obtained in this part of the research work demonstrated that the FIA-ESI-MS/MS method developed is suitable for the identification and determination of the $Zn(MHA_{-H})_2$ complex with a LOD and a LOQ value (see Experimental section) of 240 and 800 ppm, respectively (Figure 19).

The extraction and purification method was developed and optimized with success allowing to obtain excellent recovery values.

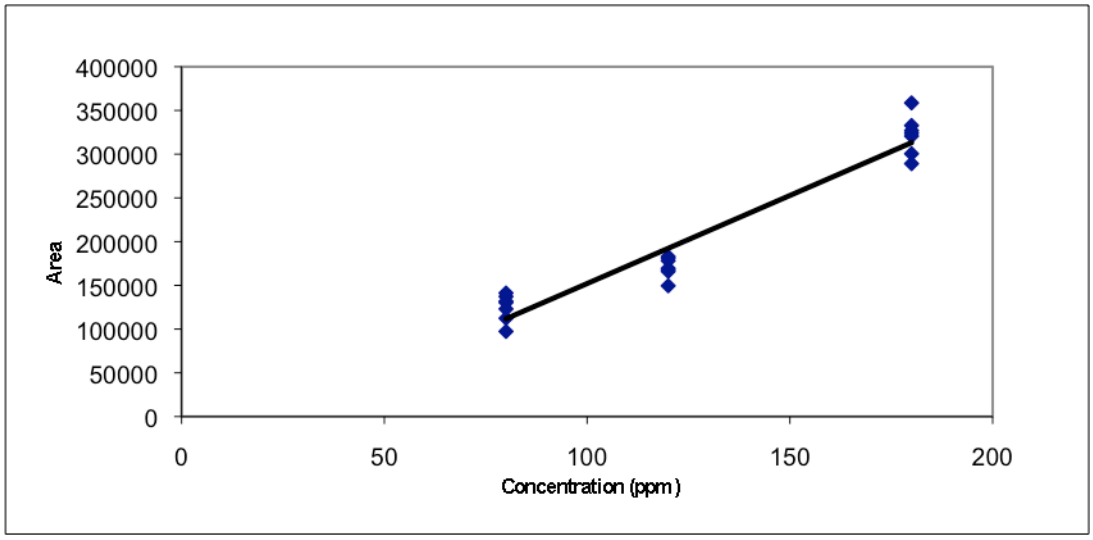

Figure 19: Matrix-matched calibration curve obtained by FIA ESI-MS/MS (matrix diluted 10 times): y=2013,8x-49306, R2=9,9667, n=24

3.3.2. MIR e NIR spectrophotometry investigations

The development of rapid methods for quality control in food industry is a current topic of high interest. IR spectrophotometry is nowadays a widespread technique used in many fields of analytical chemistry, including the quality control of feedstuffs. In addition, in the last two decades, the application of NIR analysis as routine quality control analysis was improved thanks to the possibility of its on-line implementa- tion by means of multivariate calibration techniques, allowing a reliable selection of analytically useful spectral variables. In comparison with other analytical techniques, IR analysis is essentially a rapid, cheap and non-destructive method. For example, NIR spectrophotometry has been extensively used in the field of cereal analysis for the evaluation of many quality variables, such as protein, moisture, dietary fibre contents, and wheat hardness. Quantitative methods are usually based on multivariate chemometric procedures like partial least-square regression or multiple linear regression (MLR) to build up their calibration models. The calibration is normally based on the correlation between the absorbances of the samples at certain wavelengths and the target molecule concentrations. Although discriminant analysis (DA) has been extensively used as powerful multivariate technique for qualitative discrimination of different kinds of samples, as oils, fats, flours, etc., in this study it was carried out on the NIR dataset in order to reduce the number of original variables by selecting those that were able to discriminate between the samples of different chelates concentrations. With the so selected variables a multivariate calibration model was then obtained by MLR. Many models were obtained by MLR which was applied with the "all subsets" procedure, and the best one was chosen according to its prediction power (Giannetto *et al.*, 2007).

The spectra obtained (see Experimental section) both in the case of feedstuff and premix was analized by means a Simple linear calibration (Univariate method according to the Lambert Beer law) and a Multiple linear calibration in the Medium

(4000-200 cm^{-1}) and Near Infrared region (14285-4000 cm^{-1}). The methods currently used in order to determine multivariate calibration models are partial least square analysis, principal component regression or MLR, carried out on the whole dataset of the variables furnished by the analytical method. With the aim of achieving the best predicting model with the lowest number of variables as possible, a set of linearly independent or uncorrelated variables (absorbances at the 1557 sampled wavelengths) had to be identified at first. Discriminant analysis was exploited for the purpose. As explained in Experimental Section, a sub-data set of four concentration levels (36 spectra), both in the case of premix and feedstuff, randomly chosen, was dropped from the variable selection procedure and used as validation dataset. In particular, in this study we used DA as a tool for identifying the spectral key variables, namely the wavelengths and the corresponding absorbances able to discriminate and classify the 90 spectra in 10 groups of 9 objects, in the case of premix and 135 spectra in 15 groups of 9 objects each, i.e. to allow each feedstuff and premix sample to the group of its chelate concentration. In order to correct the spectra for the variability of the baselines due to scattering phenomena, the MSC normalization procedure of reflectance IR spectra has been used for quantitative calibrations.

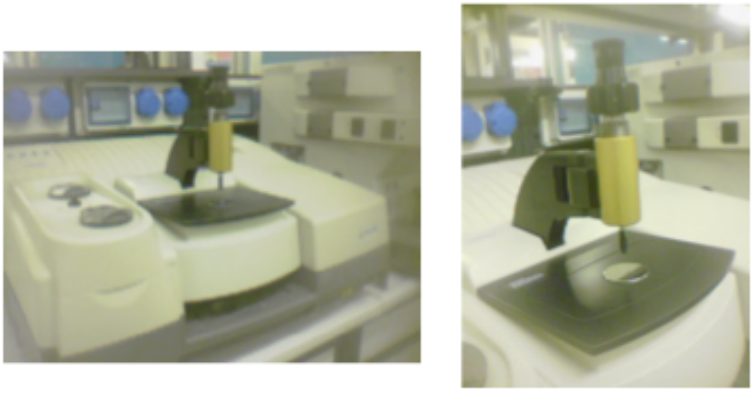

Thermo-Nicolet Nexus FT-MIR spectrometer equipped with the Thermo Smart Orbit ATR diamond accessory

BÜCHI NIRLab®-N200

3.3.2.1. Premix investigations

Simple linear calibration approach

In the case of simple linear calibration two wavelengths were considered corresponding to the carbonyl stretching in MHA in particular: 1577 cm^{-1} and 1626 cm^{-1}. The calibration curve was obtained by correlating the concentration with absorbance, according to the Lamber-Beer law. The Figure 20 shown the detail of the scpectra obtained with premix at the two wavelengths considered, in concentration range 0 to 150000 ppm.

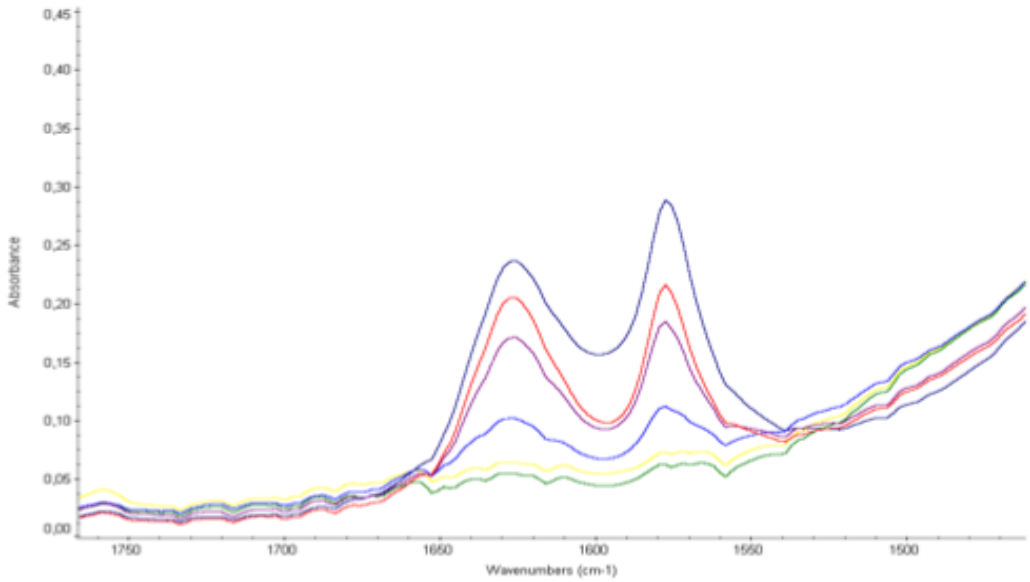

Figure 20: IR Spectra, in the carbonyl stretching region, of complex mixtures containing different concentrations of $Zn(MHA)_2$ (range 0 – 150000 ppm)

The absorbance values at each concentration level result disperded around the mean value probably because of casual errors mainly due to sampling procedure and data collection. The position of the sample on the diamond crystal of the HATR device may be a source of errors.

The results obtained demonstrated that the Simple linear calibration is suitable for the identification and determination of the $Zn(MHA_H)_2$ complex with a LOD and a LOQ value (see 2.2.2. Experimental section) of 2,8% and 9,3%, respectively for 1577 cm^{-1}, and 2,5% and 8,3%, respectively for 1626 cm^{-1}. The precision, calculated as RDS %, gives a mean value of about 12% for both wavenumbers (rather high dispersion around the mean value).

Figures 21; 22 show validation straight lines for both frequency values (expressed as wavenumber 1577 cm^{-1} and 1626 cm^{-1})

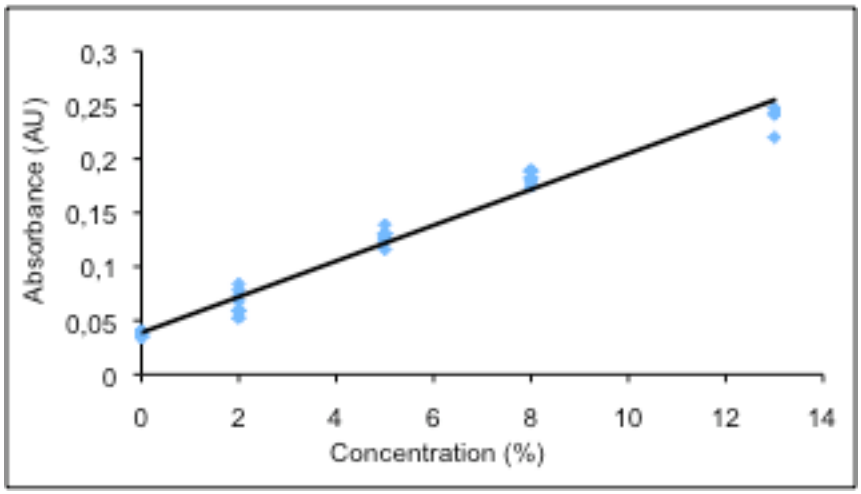

Figure 21: Matrix-matched calibration curve obtained by simple linear calibration (Picco 1577 cm-1):y = 0,0164(±0,0007)x + 0,0435(±0,0054), R2=0,9738, n=36

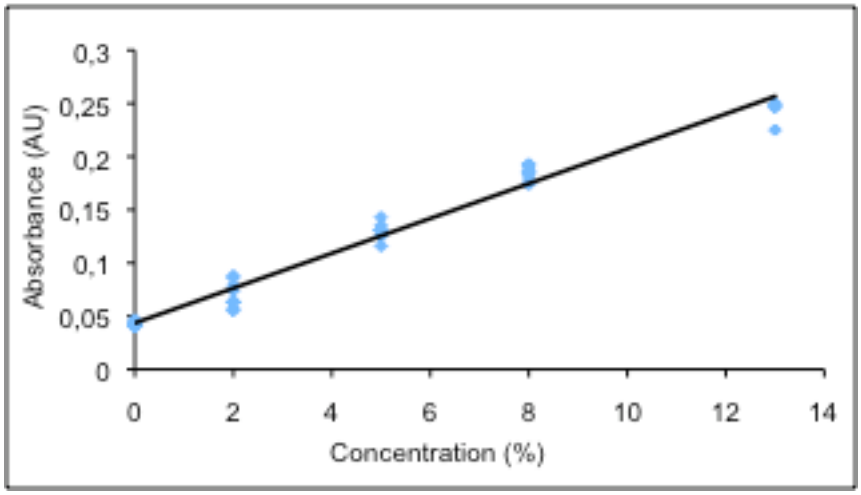

Figure 22: Matrix-matched calibration curve obtained by simple linear calibration (Picco 1626 cm^{-1}):y = 0,0166(±0,0006)x + 0,0435(±0,0048), R^2=0,9726, n=36

Multiple linear calibration approach in MIR region

Regarding multivariate approach, obtained results allowed to build up a model in which the fitting degree between predicted and calculated concentration is 98%. Precision and accuracy levels are statistically accepatble.

In Figure 23 calibration and validation straight lines are compared; the relevant equations, reported in the figure caption, show valuable coefficients of calibration and accuracy (slope and intercept of the equations), indicating that the experiemental concentration value is close to tha calculated by the model.

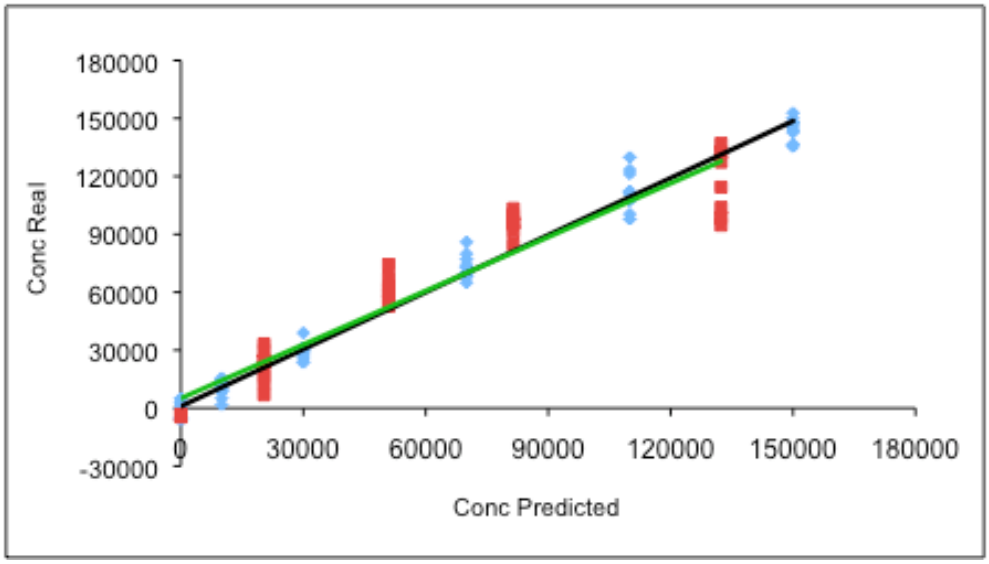

Figure 23: Matrix-matched calibration curves obtained by multiple linear calibration: Calibration: y = 0,9849 (±0,0171)x + 966,18(±55); R2 = 0,9849 (n=45); Validation: y = 0,9816(±0,0471)x + 507,18(±171); R2 = 0,9183 (n=36)

Multiple linear calibration approach in NIR region

NIR investigation confirm the results obtained by MIR. In addition NIR studies, besides finding a good fit between original and predicted cancentration values, estimates a standard error of prediction (SEP) of about 0,65%. In other words the predicted value is affect by a standard deviation of 0,65%

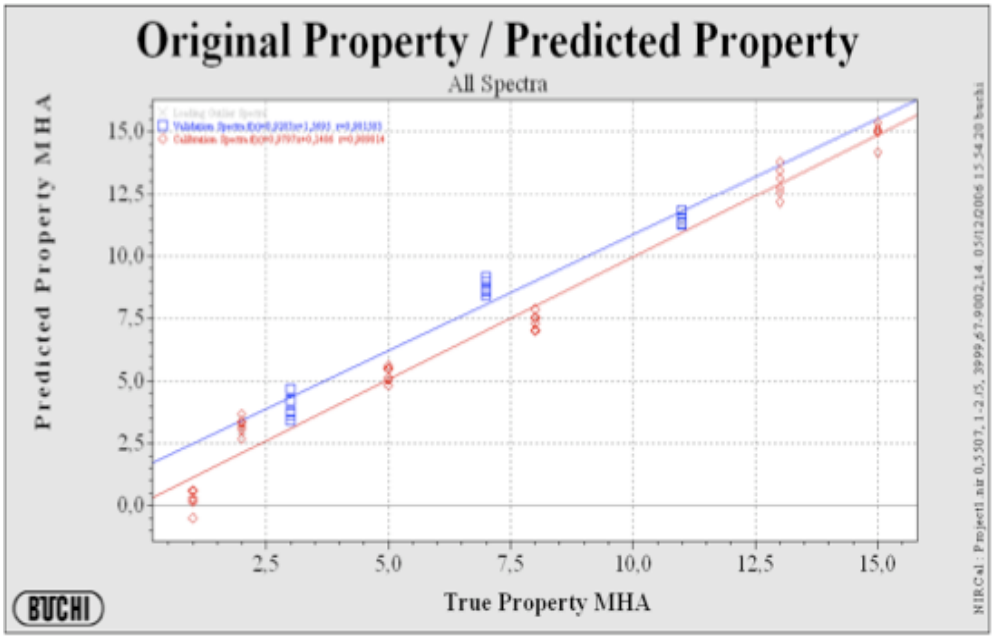

Figure 24: Matrix-matched calibration curves obtained by multiple linear calibration: Calibration: y=0,9797x + 0,1486; R^2 = 0,9898 (n=15); Validation: y=0,9283x + 1,5695; R^2 = 0,9816 (n=12); Standard error of prediction (SEP): 0,65 %

3.3.2.2. Feedstuffs investigations

Simple and Multiple linear calibration approach in the MIR region

In the case of feedstuffs, the instrumental detection limit is higher with respect to the premix. Lambert Beer approach is unsatisfactory below 10000 ppm, making this approach unapplicable in practice, as commercial feedstuffs contain lower level of metal chelate.

Morover, also the multiple linear calibration approach does not allow to afford a valuable model owing to the low concentration level of metal chelates in feedstuffs.

Multiple linear calibration approach in NIR region

In the NIR region, it is possible to find and to validate a model obtaining a standard error of prediction (SEP) of abuot 11 ppm. Taking into account tha the real concentration is abuout 110 ppm percentual SEP results abuot 10%. The relevant plot is reported in Figure 25

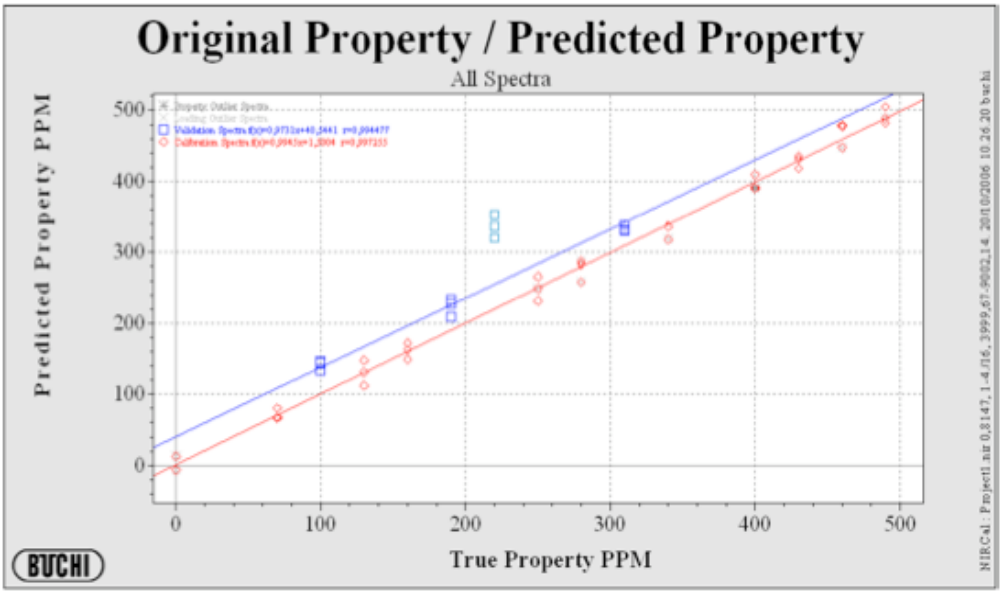

Figure 25: Matrix-matched calibration curves obtained by multiple linear calibration: Calibration: y=0,9947x + 1,5004; R2 = 0,9972 (n=54); Validation: y=0,9731x + 40,5441; R2 = 0,9945 (n=12); Standard error of prediction (SEP): 11,61 ppm

In conclusion the NIR approach permits to carry out quantitative determination af mineral chelates also at concentration levels much lower than those present in the premixes. This preliminary approach reveals that multivariate methods in the NIR region is reliable to afford quantitative data for metal chelates. This is very encouraging for going on towards the development of a reliable analytical methods for metal chelates in commercial feedstuffs.

Such information cannot be achieved by direct selection of characteristics absorbances, as for MIR spectroscopy, but a multivariate approach is fundamental in order to identify the signals correlated with the concentration of the analyte.

3.3.3. Use of $Zn(MHA_{-H})_2$ as standard for the HPLC determination of MHA

The determination of MHA is conveniently performed by HPLC according to a published procedure (Rinda R. *et al.*, 1987) and the chromatografic conditions are described in Experimental section. When this sustance is present in its anionic form in the zinc chelate $Zn(MHA_{-H})_2$, it is necessary to carry out an acidic hydrolysis to liberate completely MHA in its acidic form. Hydrolysis should be performed carefully in a hot HCl solution according to the proposed procedure. However, 88% MHA obtained by the current suppliers is a mixture of the monomer (65%) and the two diastereoisomeric dimers (23%). The three peaks are shown in the chromatogram reported below (Figure 26)

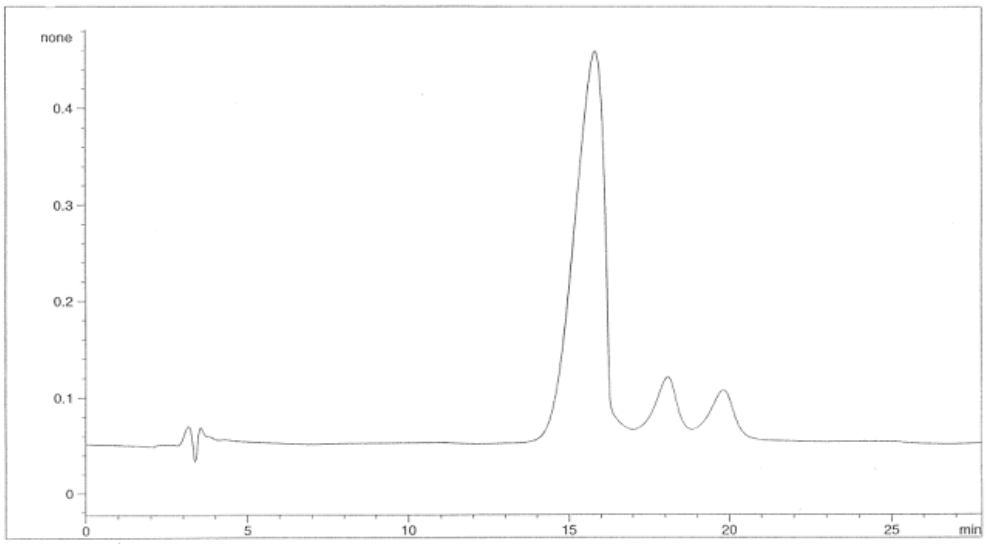

Figure 26: The chromatogram shows signals due to the solvent in the first five minutes and three peaks due to: Monomer and 2 Diemers with retention time 15,83 min, 18,09 min and 19,83 min respectively

The formation of the dimers occurs in concentrated solutions of MHA in water; MHA freshly obtained by hydrolysis of the zinc chelat is only in its monomer form. Therefore, the anhydrous zinc bis-chelate of MHA, $Zn(MHA)_2$, (a white powder, MHA content 82.03 %), can be used as MHA standard through extraction of MHA via acidic hydrolysis. Conditions of analysis are described in Experimental section and the

chromatogram reported below show the peak corresponding to MHA from hydrolysis.

Figure 27: The chromatogram shows the peak due to MHA ligand (Monomer) with retention time 15,83 min. Dimers are not present because the chromatographic conditions was different than Figure 26

This procedure was also applied for the determination of MHA content in the commercial sample Act-ione Zn 100®. From the amount of MHA it is possible to obtain the amount of the Zinc chelate by simple calculatig.

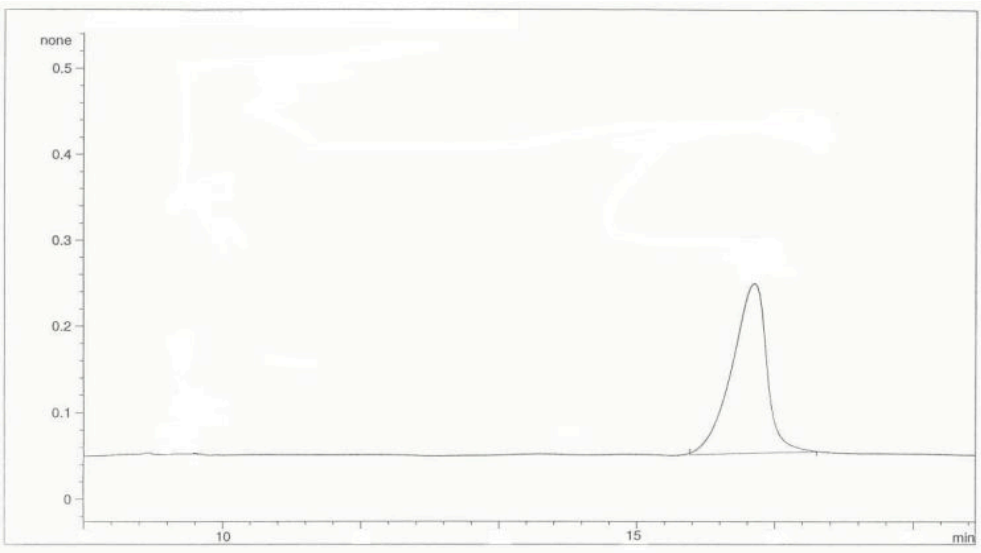

Figure 28: Chromatogram of the sample Act-ione Zn 100®

3.4. *In vitro* tests with Caco-2 cells

The intestinal mucosa is the main site of absorption of nutrients into the body but it also acts as a first line of defence against the uncontrolled entry of potentially harmful substances into the blood circulation. The barrier function of the intestinal epithelium is guaranteed by the presence of apical (AP) junctional complexes, highly specialized structures joining adjacent epithelial cells. Tight junctions (TJ) are the most AP component of the junctional complex, they form a selective permeability barrier along the paracellular pathway of epithelial cells (Anderson *et al.*, 1993; Ballard *et al.*, 1995). Under normal physiological conditions, several molecules, including some nutrients (i.e. glucose), are able to regulate TJ permeability (Nusrat *et al.*, 2000). Heavy metals represent an interesting case as they are often taken as nutritional supplements to improve the quality of the diet but, if taken in higher doses, can exert toxic effects at the level of the intestinal mucosa. Caco-2 cell line, derived from a human colon adenocarcinoma, undergoes spontaneous *in vitro* differentiation leading in two to three weeks to the formation of a monolayer of highly polarised cells, joined by functional TJ, exhibiting several morphological and functional characteristics of mature enterocytes (Pinto *et al.*, 1983). Caco-2 cells grown and differentiated on microporous filter supports, form a two compartment system where the cell monolayer separates the AP compartment, corresponding *in vivo* to the intestinal lumen, from the basolateral (BL) compartment, *in vivo* the blood capillaries space. This system allows full accessibility to both sides of the cells and represents a well-established model for the study of intestinal transport and toxicity of nutrients and xenobiotics, including trace elements (Zucco *et al.*, 1997; Sambuy *et al.*, 2001)) It has been previously shown that the micronutrients Zn, Cu and Fe were able to increase TJ permeability in differentiated Caco-2 cells (Rossi *et al.*, 1996; Ferruzza *et al.*, 2002; Ferruzza *et al.*, 2003) and that copper effects on tight junctional permeability are related to the AP uptake of copper (Ferruzza *et al.*, 1999). Many forms of iron complexes are given as dietary supplements to improve the quality of the diet so it is important to

consider any potential disadvantages of ligands for supplying iron and to establish the effects of iron complexes at the level of the intestinal mucosa.

We have used the human intestinal Caco-2 cell line to investigate the toxicity of Fe^{3+} NTA and Fe^{3+}MHA to the TJ by measuring the TEER of the cell monolayer. These tests were performed at INRAN Institute (Rome) by the group of Dr. Maria Laura Scarino. Cells were treated from the AP compartment with BSS at pH 5.5 with or without the addition of 100 and 250 μM Fe^{3+}NTA or Fe^{3+}MHA for 3 hours in a water bath at 37°C and TEER was monitored at set times during the course of the experiment. As shown in Figure 29, neither Fe^{3+}NTA nor Fe^{3+}MHA altered the permeability of TJ at the concentrations tested, indicating that this compounds are non toxic for the intestinal cells during the period of treatment.

In addition, since the bioavailability of nutrients depends on their efficient transport across the intesinal mucosa, we have also investigated the AP uptake and the AP to BL transport of Fe^{3+}NTA and Fe^{3+}MHA across Caco-2 cells. Cells were treated from the AP compartment with BSS at pH 5.5 with or without the addition of 100 and 250 μM Fe^{3+}NTA or Fe^{3+}MHA for 3 hours and Fe content in cells and BL media was determined by AAS. As shown in Figure 30, the intracellular Fe content increased with concentration and was much high for Fe^{3+}MHA than Fe^{3+}NTA. In addition, as shown in Figure 31, the AP to BL transport of Fe increased with concentration and no differences were observed between the two Fe^{3+}complexes.

In conclusion, results indicate that the amount of Fe^{3+}MHA taken up by the cells was higher than that of Fe^{3+}NTA. This is of particular interest considering that the NTA ligand was found to be more effective in determining iron retention from milk diets in mice than the citrate and EDTA ligands (Kwock *et al.*, 1984). However, both Fe^{3+}MHA and Fe^{3+}NTA are transported to the BL compartment in this experimental system and the transepithelial transport of Fe^{3+}MHA appear not different from that of Fe^{3+}NTA.

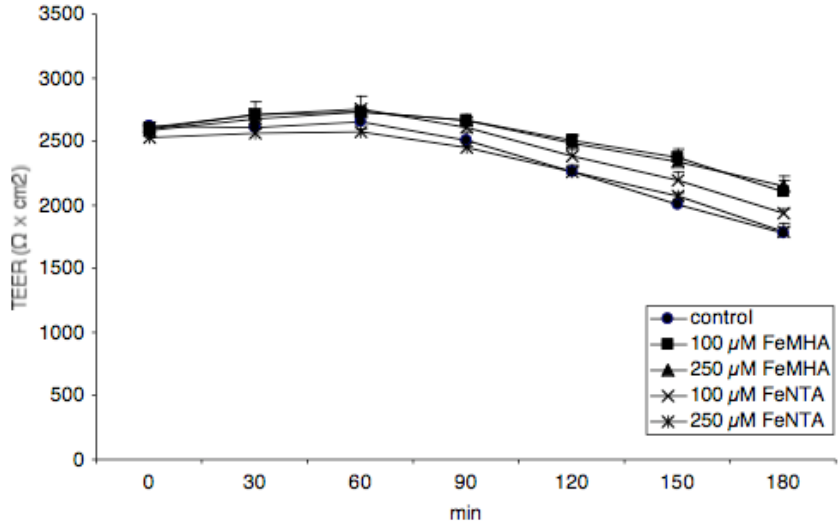

Figure 29: Effect of different Fe^{3+}chelates on tight junction permeability in human intestinal Caco-2 cells. Cells were treated in the AP compartment with 100 and 250 μM Fe^{3+}NTA (1:2) or Fe^{3+}MHA (1:3) for up to 3 h in BSS at pH 5.5 in a water bath at 37°C. TEER was monitored at set times during the course of the experiment and values expressed as Ω x cm^2. Data are the means ± SD pop from a representative experiment performed in triplicate

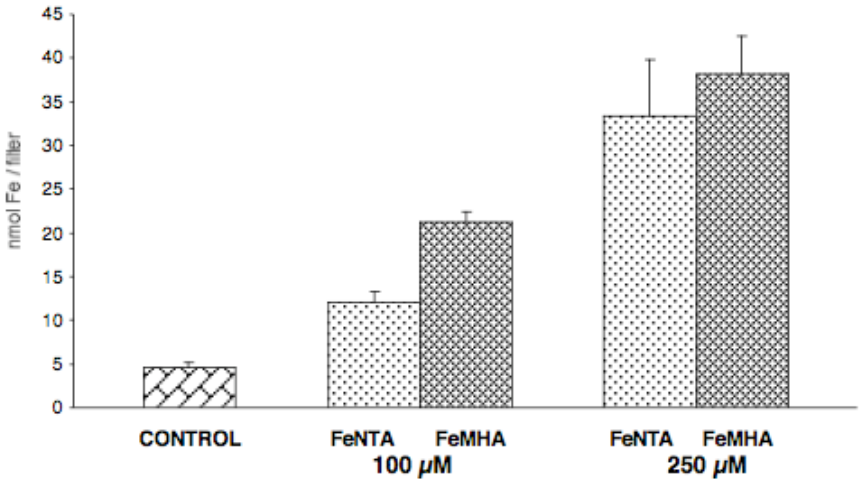

Figure 30: Intracellular Fe content in differentiated Caco-2 cells treated with Fe^{3+}NTA or Fe^{3+}MHA. Cells were treated in the AP compartment with 100 and 250 μM Fe^{3+}NTA (1:2) or Fe^{3+}MHA (1:3) for 3 h in BSS at pH 5.5 in a water bath at 37°C. After 3h of treatment cells were washed twice with Fe chelating solution at 4°C and collected in distilled water. Fe content in cells was determined by AAS and expressed as nmol Fe / filter. One filter has an area of 4.71 cm^2 and contains 1.33 ± 0.16 mg protein**.** Data are the means ± SD pop from a representative experiment performed in triplicate

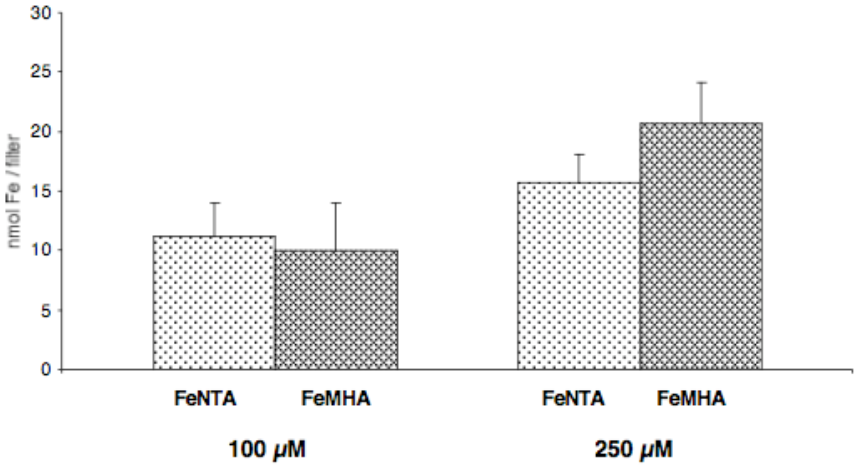

Figure 31: Transepithelial (AP to BL) transport of Fe^{3+}NTA or Fe^{3+}MHA across Caco-2 cell monolayers. Cells were treated in the AP compartment with 100 and 250 μM Fe^{3+}NTA (1:2) or Fe^{3+}MHA (1:3) for 3 h in BSS at pH 5.5 in a water bath at 37°C. After 3h of treatment BL medium were collected and Fe content in samples was determined by AAS and expressed as nmol Fe / filter. One filter has an area of 4.71 cm^2 and contains 1.33 ± 0.16 mg protein. Data are the means ± SD pop from a representative experiment performed in triplicate

Considering the MHA iron chelate in the oxidation state +2, indicated by Fe(II)MHA, it results non toxic at the same extent found for the corresponding iron(III) chelate, Fe(III)MHA. However, by comparing the *in vitro* bioavalability of Fe(II)MHA, Fe(III)MHA and $FeSO_4$ (Figure 32) it has been found that bioavailability of Fe(II)MHA is comparable with that displayed by $FeSO_4$ and larger than that of Fe(III)MHA. Transport to the basolateral compartment was undetectable by the analytical method employed.

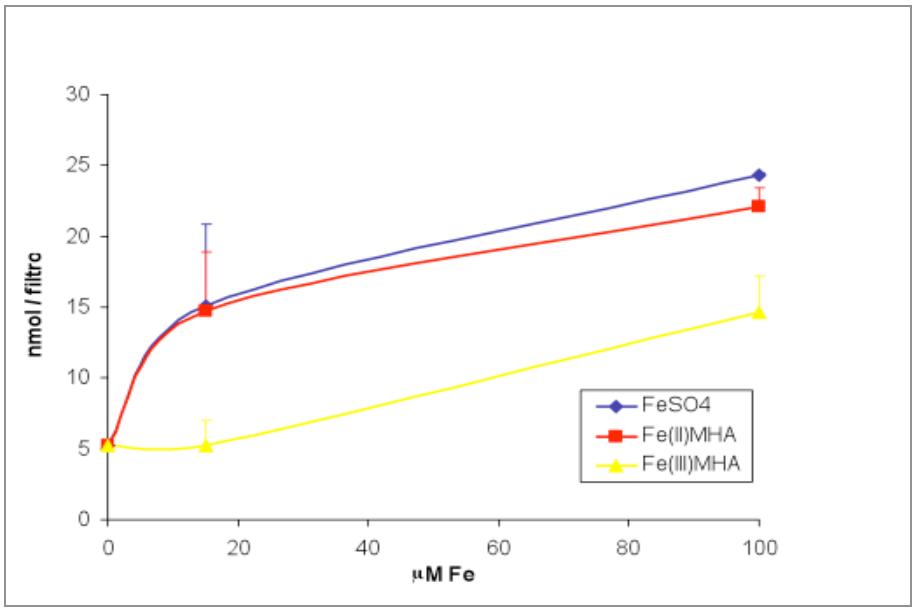

Figure 32: Iron uptake by Caco-2 cells treated with Fe(II)MHA, Fe(III)MHA and $FeSO_4$ at various concentrations for 120 min

The intestinal bioavailability of ZnMHA with the human intestinal cell line Caco-2 was also investigated. Toxicity studies were performed by treating differentiated cells grown on filter with ZnMHA and $ZnSO_4$ (200-400 µM) for 2 h from the apical chamber and by measuring variation in trans-epithelial electrical resistance (TEER). Toxicity of ZnMHA chelate for the Caco-2 cells is comparable with that of the inorganic salt $ZnSO_4$ at concentrations lower than 300 µM; on the other hand, at the concentration level of 400 µM the toxicity of the inorganic salt is slightly, but significantly, higher than that of the organic chelate as shown in the Figure 33.

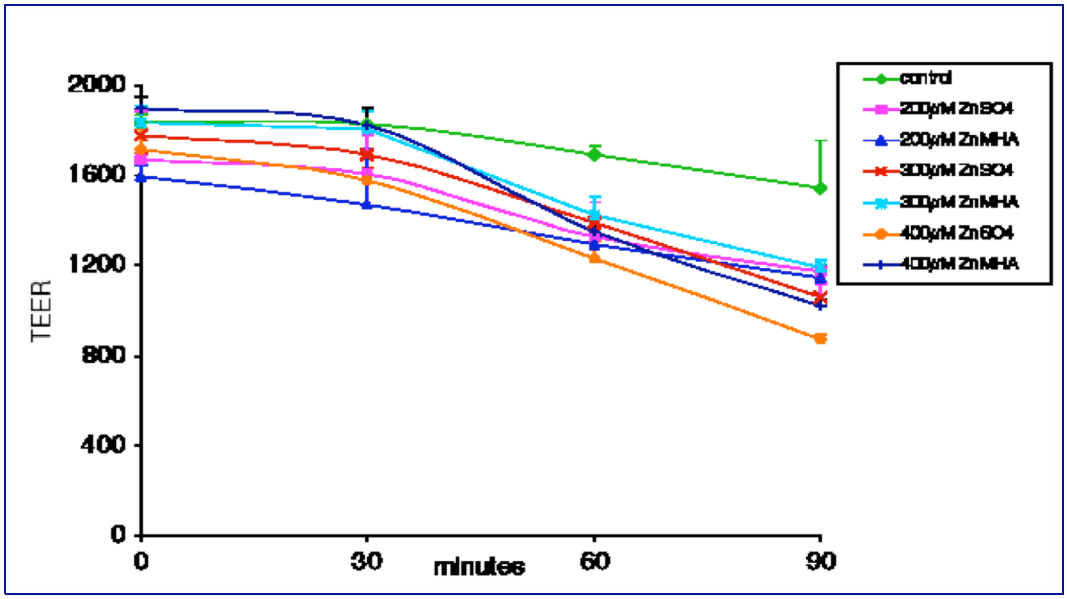

Figure 33: Effect of $ZnSO_4$ and ZnMHA at different concentrations on tight junction permeability in human intestinal Caco-2 cells

The study of the intestinal bioavailability has shown that the apical uptake of Zn increased from 200 to 300 µM, reaching a plateau between 300 and 400 µM for both $ZnSO_4$ and $Zn(MHA)_2$, as shown in Figure 34.

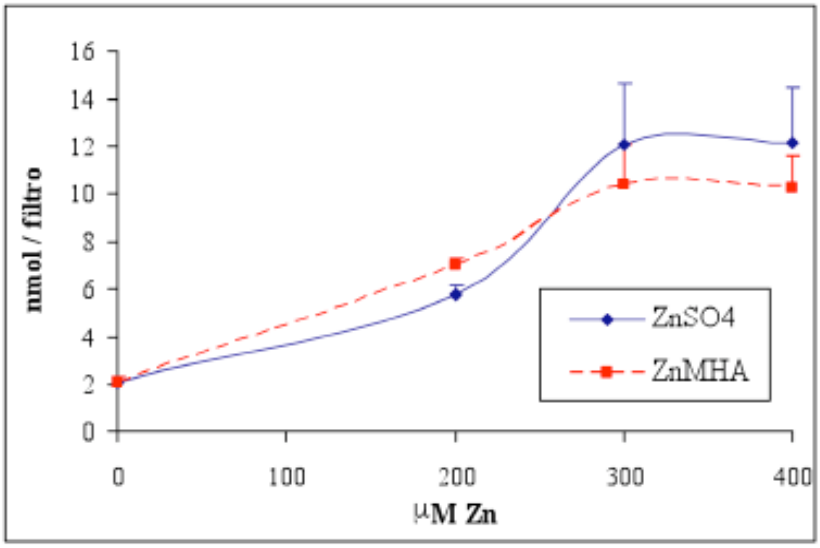

Figure 34: Zinc uptake by Caco-2 cells treated with ZnMHA and $ZnSO_4$ at various concentrations for 90 min

Basolateral transport increased with concentration for both chelates as indicated in Figure 35. The higher transport of 400 µM $ZnSO_4$, compared to $Zn(MHA)_2$, may be due to the higher paracellular permeability observed in the $ZnSO_4$ treated cells.

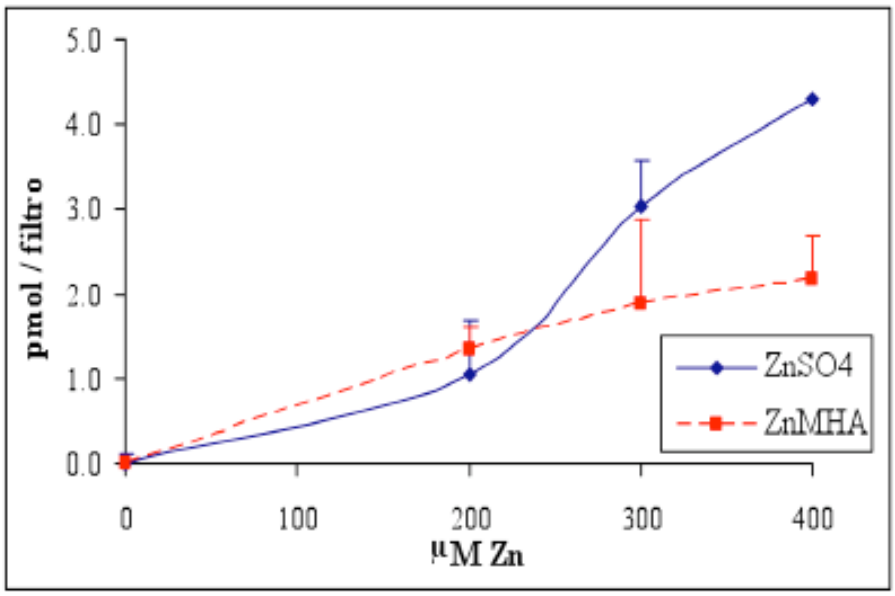

Figure 35: Zinc transport in the basolateral compartment at various concentrations of ZnMHA and $ZnSO_4$

Finally, toxicity studies were performed by treating differentiated Caco-2 cells grown on filter with CuMHA and $CuSO_4$ (25-100 µM) for 2 h from the apical chamber and by measuring variation in trans-epithelial electrical resistance (TEER). Toxicity of CuMHA chelate for the Caco-2 cells is well comparable with that of the inorganic salt $CunSO_4$ in the concentration range explored, as shown in Figure 36.

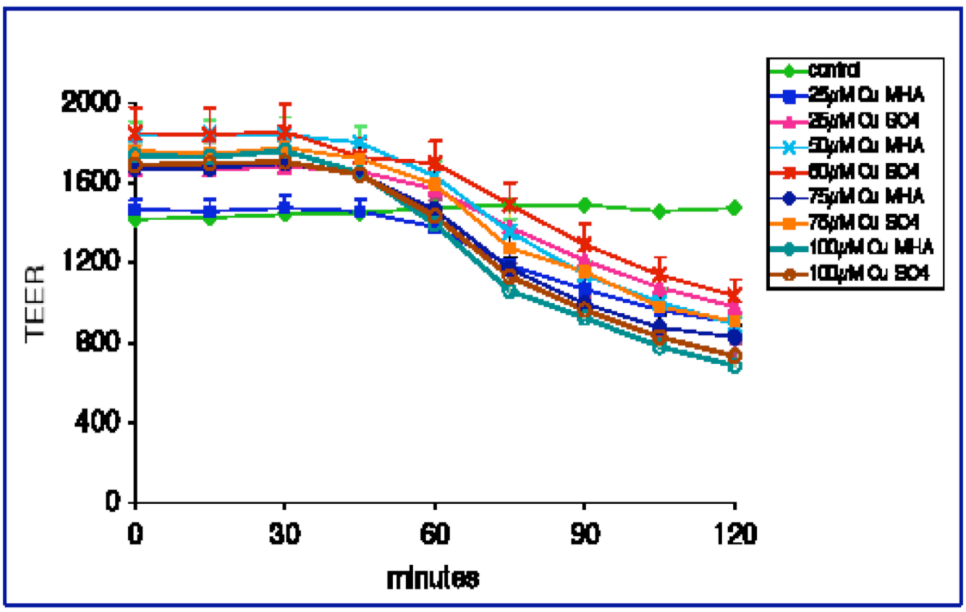

Figure 36: Effect of $CuSO_4$ and CuMHA at different concentrations on tight junction permeability in human intestinal Caco-2 cells

The apical uptake of copper slowly increased from 25 to 100µM for both CuMHA and $CuSO_4$, with no major differences between the organic chelate and the inorganic salt (Figure 37). Transport to the basolateral compartment was undetectable by the analytical method employed.

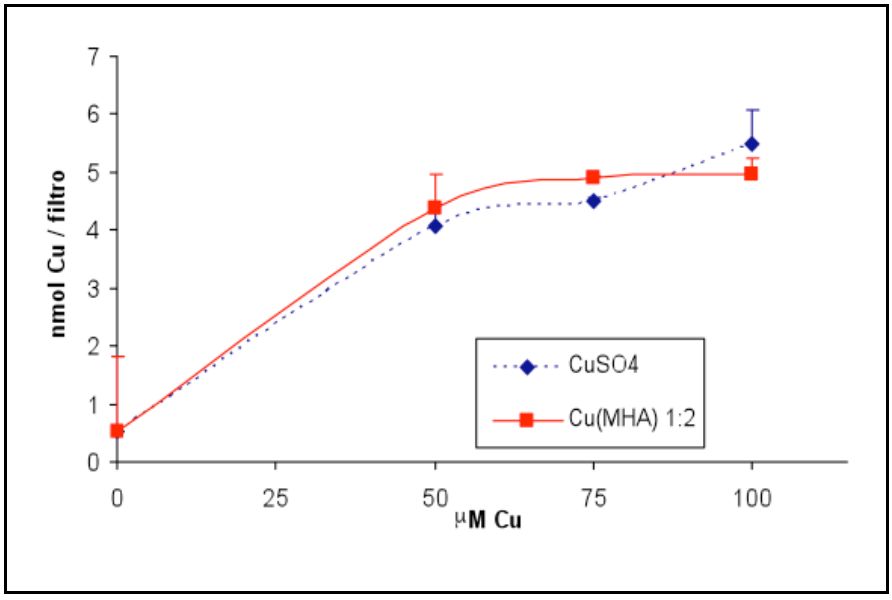

Figure 37: Copper uptake by Caco-2 cells treated with CuMHA and $CuSO_4$ at various concentrations for 120 min

In conclusion, *in vitro* experiments with Caco-2 cells have shown that MHA chelate of iron, zinc and copper do not display better biavailability with respect to the corresponding inorganic sulfates.

In fact, such experiments allow to establish the direction towards which different factors, like phytates, polyphenols, ascorbates, modify bioavailability of iron, zinc and copper, but often fail in determining the extent of these phenomena.

In order to properly determine the bioavailability of MHA metal chelates compared to the correspaonding inorganic salts, *in vivo* trials have to be performed taking into account that more complex interactions occur than *in vitro* systems.

3.5. *In vivo* trials with rats

After feeding the zinc-deficient diet for three weeks (see experimental section), zinc content of liver, spleen, and kidneys was significantly lower ($P < 0.05$; Table 4) than at Time 0. Zinc content of bones was not significantly reduced by the zinc-deficient diet. This finding can be explained by the fact that zinc concentration in bones declines at a slower rate than in other tissues, such as blood and hair (Bobilya *et al.*, 1994). Data regarding feed intake, zinc content of faeces and urine, and the percentage of dietary zinc retained by the animals are reported in Table 5.

Table 4: Zinc content of liver, kidneys, spleen, femur and plasma in rats at Day 0 and after a zinc-deficient diet was fed for 3 weeks (average of 6 animals ± SD)

	Liver	Kidneys	Spleen	Femur	Plasma
	mg/kg DM	mg/kg DM	mg/kg DM	mg/kg DM	µg/dl
Day 0	28.9 ± 2.3	22.6 ± 2.2	25.5 ± 1.0	172 ± 33	154 ± 55
Day 21	24.4 ± 0.8*	19.1 ± 0.8*	20.4 ± 2.7*	159 ± 7	102 ± 15

* indicates a significant difference (P < 0.05)

Table 5: Feed intake and zinc retention in rats fed different sources of zinc (average of 6 animals ± SD)[1]

	Feed intake	Zinc intake	Amount of faces produced	Zinc faecal concentration	Amount of urine produced	Zinc urine concentration	Zinc retained
	g/rat	mg/rat	g DM/rat	mg/kg DM	ml/rat	mg/l	% Zn intake
$ZnSO_4$	121 ± 4.5	2.4 ± 0.1	7.6 ± 0.4	183 ± 14.0 b	43 ± 3.5	1.2 ± 0.1	40 ± 6.6 a
Zn-MHA	107 ± 8.5	2.3 ± 0.2	6.5 ± 0.9	126 ± 15.6 a	34 ± 2.6	1.6 ± 0.2	61 ± 8.6 b

[1]Different letters within the same column indicate a significant difference (P < 0.05)

Zinc content of faeces was significantly higher when the $ZnSO_4$ diet was fed (183 vs. 126 mg/kg DM for the Zn-MHA; $P < 0.05$). The percentage of dietary zinc that was retained by the animals (calculated as the ingested zinc minus the zinc excreted with faeces and urine) was significantly higher in the rats fed the Zn-MHA diet (respectively, 61% for Zn-MHA vs. 40% for the $ZnSO_4$ diet). These results seem to show a higher bioavailability of the zinc organic source compared to zinc-sulphate, confirming in the rat what had already been observed in chicks (Wedekind *et al.*, 1992) and pigs (Hahn e Baker, 1993) when zinc chelates were fed. Nevertheless, other authors reported no difference between bioavailability of inorganic and organic sources of zinc in cattle (Spears *et al.*, 1991) and pigs (Swinkels *et al.*, 1996). These contradictory results could be explained by the fact that different organic forms of zinc have been used in the cited studies and it is well known that zinc bioavailability is strongly influenced by the chemical properties of the chelate that is used (especially the type of bond and the molecular weight (Ashmead *et al.*, 1993). In fact, all the cited authors have used chelates where the zinc cation is bound to one or two aminoacids. In our study, zinc bioavailability of zinc-MHA was much higher than that of zinc sulphate (+ 52,5%; $P < 0.05$). Zn-MHA fed rats showed higher liver Zn content than $ZnSO_4$ fed animals (+ 14%; $P < 0,05$; Table 6). Zinc in spleen, kidneys, femur, and plasma was not influenced by treatment. In conclusion, these data indicate that the use of MHA chelates could be a valuable tool to increase bioavailability of trace minerals and reduce the environmental impact of animal manure.

Table 6: Zinc content of liver, kidneys, spleen, femur and plasma in rats fed different sources of zinc (average of 6 animals ± SD)[1]

	Liver	Kidneys	Spleen	Femur	Plasma
	mg/kg DM	mg/kg DM	mg/kg DM	mg/kg DM	µg/dl
$ZnSO_4$	23.6 ± 1.4 a	24.0 ± 1.8	25.1 ± 3.0	142.5 ± 10.2	219.8 ± 74.2
Zn-MHA	26.9 ± 1.3 b	24.8 ± 0.6	26.2 ± 4.3	149.8 ± 33.7	166.0 ± 24.7

[1]Different letters within the same column indicate a significant difference ($P < 0.05$)

3.6. Analytical methods for determination of the Glycine chelates

3.6.1. Competition method

An important task of the research on metal chelates for animal nutrition is the setting up of analytical methods for rapid recognition and quantitative determination of these species.
Besides the well known classification of metal chelates proposed by *"Association of American Feed Control Officials" (AAFCO, 2001),* from the strictly analytical point of view metal chelate species can be classified in the following classes (See Introduction).

(i) Single aminoacid (AA) chelates (e. g. glycine) of well defined formula.
(ii) Single alpha-hydroxyacid chelates (e. g. mehtionine hydroxy-analogue) of well defined formula.
(iii) Chelates of a *pool* of AA's of known composition.
(iv) Chelates of protein lysates (e. g. soy beans meal).
(v) Chelates of other organic species (e. g. saccharides).

Metal glycinates belong to the firts class (i). However, a lot of metal glycinates placed on the market often do not correspond to real glycinate chelates, as expected in order to have the right nutritional performance.
Three types of sub-classes of glycinates are possible to be found on the market place:

(a) mechanical mixtures of inorganic salts with glycine; easy to recognize by macro- and micro-morphological investigations;
(b) product of reactions in water between metal sulfates (MSO_4) and glycine (HGly) (molar ratio 1:2); often referred as *monochelates*, of formula [M(Gly)(Hgly)]HSO_4; their pH in water solution is in the acidic range (3-4) (Figure 38);
(c) true metal bis-chelates of formula [$M(Gly)_2$], obtained by reaction of the

metal hydroxide with glycine (molar ratio 1:2); they are the unique bis-chelates giving in water slightly basic pH values (7-8) (Figure 39).

The identification of the two last sub-classes (b, c) is often possible by means of IR spectroscopy directly in the solid samples, taking advantage of the characteristic IR spectra of pure metal glycinates.

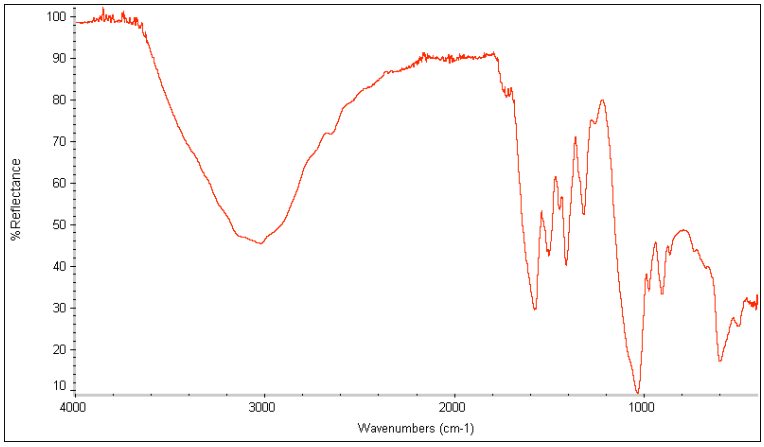

Figure 38: IR spectra of $[Cu(Gly)(Hgly)]HSO_4$

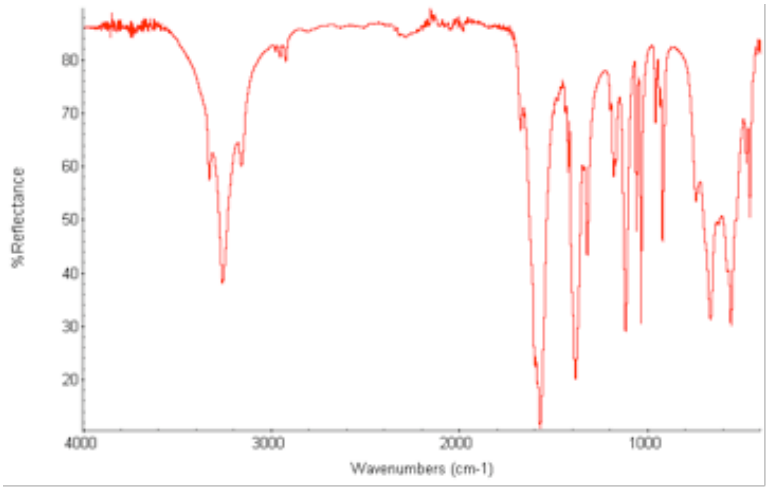

Figure 39: IR spectra of pure $Cu(Gly)_2$

Nevertheless, for complex systems containing different species, the IR method, joined with pH determinations, does not afford, in some cases, affordable results.
In order to solve these cases, we have tried to set up a rapid method useful to discriminate the chelate samples in virtue of their response in aqueous solution when faced to a mild complexing agent able to bind the metal cations to a certain extent. Strong chelates should release small amounts of metal caions, whereas weaker chelates should release higher amount of metal. The complexing agent which acts as a competitor is conveniently anchored to a solid matrix. By treating the chelate solutions with a fixed amount of the solid competitor and by measuring the extent of metal released (and captured by the complexing agent), or that remained in solution with the original chelating agent, it will be possible to estimate the chelation ability of ligands present in the real samples. Data consisting in the amount of metal present in solution will be compared with those obtained with two limit cases, that of metal sulfate (simple inorganic salt in water, no chelation) and that of metal glycinate (true bis-chelation).

Experiments have been carried out with copper chelates: $CuSO_4$, $[Cu(Gly)_2]$, and three commercial samples (*Be, MA, Cy*) were tested.
The solid matrix used was silca gel functionalized with amino groups, contained in the Supelclean™ DSC-NH_2 SPE Tube (6 ml, 0.5 g) (Supelco™, Bellefonte, PA, USA).
They were conditioned by passing methanol (5 ml), water (5 ml) and finally the buffer BES [Bis(2-hydroxyethyl)taurine - pH 7.00, Fluka™].
Solutions (5 ml) containing copper chelates (0.01 M), in water or in buffer solution, were passed through the SPE Tube by a standard SPE (solid phase extraction) apparatus.
Copper chelate concentrations, before and after the SPE run, were determined by UV-Vis spectrophotometric methods and confirmed by ICP atomic emission spectroscopy.
The results are summarized in Table 7. In order to validate this method, another set of samples nas been examined and validation results are shown in Table 8.
It is noteworthy to remark that this method (not optimized) appears promising

being able to detect differences among copper chelates in aqueous solutions used in animal nutrition.

In particular, the I_c parameters (calculated as $[A_1/A_0]*100$) is suitable to classify different chelates, being 0 in the case of copper sulfate (no chelation) and 66 in the case of the pure bis-chelate [$Cu(Gly)_2$] in buffer.

The three commercial sample display different values, one of them (*Cy* sample) being coincident with that of the pure bis-chelate. This sample gives in water a pH value (6.75) closer to that of the bis-chelate (7.53).

This method puts the *Cy* chelate in the first positions in this empirical chelation power scale, followed by *MA* and *Be* chelates.

Solution	V (ml)	A_0	C_0 (M)	A_1	C_1(M)	Ic (%)	pH_0	pH_1
$CuSO_4$ in Water	5	0,1046	0,01	0	-	0	4.37	5,63
$CuSO_4$ in Buffer*	5	0,6539	0,01	0,0443	0,0008	7	7.00	
$Cu(Gly)_2$ in Water	5	0,4160	0,01	0,2590	0,0058	62	7.53	6,48
$Cu(Gly)_2$ in Buffer*	5	0,4443	0,01	0,2920	0,0069	66	7.00	
Commercial Samples	**V (ml)**	**A_0**	**C_0 (M)**	**A_1**	**C_1(M)***	**Ic (%)**	**pH_0**	**pH_1**
Cu Be in Water	5	0,1266	0,01	0,0149	0,0012	12	2.77	6,17
Cu Be in Buffer*	5	0,6099	0,01	0,0919	0,0015	15	7.00	
Cu MA in Water	5	0,1057	0,01	0,0422	0,0040	40	2.49	6,37
Cu MA in Buffer*	5	0,3547	0,01	0,1480	0,0042	42	7.00	
Cy in Water	5	0,4276	0,01	0,2886	0,0067	67	6.75	6,26
Cy in Buffer*	5	0,4718	0,01	0,3095	0,0066	66	7.00	

Table 7: Data regarding competition experiments: V(ml): volume of sample through the SPE Tube; A_0: absorbance of the solution pre SPE; C_0: concentration of the solution pre SPE; A_1: absorbance of the solution post SPE; C_1: concentration of the solution post SPE; I_c: "Chelation Index"; * Buffer solution is BES pH 7.00 (Fluka™)

Solution	V (ml)	A_0	C_0 (M)	A_1	C_1(M)	Ic (%)	pH_0
$CuSO_4$ in Buffer*	5	0,6706	0,01	0,0075	0,0001	1	7.00
$Cu(Gly)_2$ in Buffer*	5	0,4248	0,01	0,2796	0,006	66	7.00
Commercial Samples	**V (ml)**	**A_0**	**C_0 (M)**	**A_1**	**C_1(M)***	**Ic (%)**	**pH_0**
Cu Be in Buffer*	5	0,5433	0,01	0,0522	0,0010	10	7.00
Cu MA in Buffer*	5	0,3404	0,01	0,0905	0,0027	27	7.00
Cy Cu in Buffer*	5	0,4374	0,01	0,2852	0,0065	65	7.00

Table 8: Validation data for the competition experiments: V(ml): volume of sample through the SPE Tube; A0: absorbance of the solution pre SPE; Co: concentration of the solution pre SPE; A1: absorbance of the solution post SPE; C1: concentration of the solution post SPE; Ic: "Chelation Index"; * Buffer solution is BES pH 7.00 (Fluka™)

3.6.2. MIR spectrophotometry investigations

The multivariate approach employed for the quantification of Zn-MHA chelates by means of MIR analysis was also extended to the determination of copper glycinate in premix samples. Also in this case a discriminant analysis was carried out in order to select the spectral variables correlated with the glycinate concentration.

Although a pool of variables useful for the quantification of the glycinate was extracted, the multivariate model obtained by means of multiple linear regression performed on the dataset selected by means of discriminant analyses resulted strongly influenced by the variability of the spectra obtained by samples with the same concentration of glycinate. The variability of the spectra can be ascribed to the unhomogeneity of the samples or to the use of different batches of glycinate employed for the formulation of the premix. This problem could be overcame identifying the variables discriminating different samples with the same concentration of glycinate, in order to exclude them from the dataset and develop a more robust and unbiased multivariate calibration model. These studies are currently in progress.

3.7. Conclusion

The present work has allowed to reach the following goals.

1. The effective chelation of MHA toward transition metal cations has been demonstrated in the solid state by solving the crystal structure of the zinc derivative.
2. The presence of metal chelates in solution has can demonstrated by electrochemical and NMR spectroscopic methods.
3. The limit of determination by MS spectrometric methods in water solution have been defined and a relevant analytical procedure has been set up.
4. IR spectrometric methods both in the MIR and in the NIR region have been set up and can be conveniently proposed for the determination of MHA chelates in solid commercial samples.
5. Rapid procedures for the evaluation of the chelating strenght of commercial misture have been develop for practical purpose.

4. Reference

Introduction

Association of American Feed Control Officials - (AAFCO, 2001: 282-3)

C.B. Ammerman, P.R Henry, *Anim. Health Nutr.* 41(4) (1986), 24

C.B. Ammerman, Academic Press, Sand Diego, 1995

G. Ballarini, G. Predieri, *Progress in Nutrition*, Vol.9, N.1 (2007)

J. Cao, P. R. Henry, R. Guo, R. A. Holwerda, J. P. Toth, R. C. Littell, R. D. Miles, C. B. Ammerman, *J. Anim. Sci.* 78 (2000) 2039-2054

T.J. Cunha, *Feedstuffs*, **55**(41) (1983), 39

J. J. Dibner, R. C. Durley, J. G. Kostelc, F. J. Ivey, *J. Nutrition* 120 (1990) 553-560.

F. Enjalbert, P. Lebreton and O. Salat. Journal of Animal Physiology and Animal Nutrition, 90 (2006) 459-466.

R.J. Hannam,D.J. Reuter, *Temperate Pastures: Their Production, Use and Menagement*, Australian Wool Corporation/CSIRO, Melbourn, Australia, 1987

R.J. Hannam,D.J. Reuter, *Temperate Pastures: Their Production, Use and Menagement*, Australian Wool Corporation/CSIRO, Melbourn, Australia, 1987

G.J. Judson, (D.G. Masters and C.L. White, eds), *Australian Centre for International Agricolture Research*, Canberra (1996).

R. Kincaid, *Feedstuf*, **61**(11) (1989), 22

F. H. Kratzer, P. Vohra, CRC Press Inc., Boca Raton, FL (1986).

J.P. Langlands, G.E. Donald, J.E. Bowles, *Aust. J. Exp. Agric.*, 28 (1988), 291

M.I.E. Long, W.K. Ndyanabo, B. Marshall, D.D. Thornton, *Trinidad Trop. Agr.*, 46 (1969), 201

A. MacPherson, (D.I. Givens, E. Owen, R.F.E. Axford, H.M. Omed, eds), CAB International, Wallingford, U.K. (2000)

(1976, 1996 a, 1997, 1999) L.R. McDowell, (A.J. Smith, ed.), Univ. Of Edinburgh Press, Edinburgh, Scotland, (1976)

·L.R. McDowell, *Anim. Feed Sci. Tech.*, 60 (1996 a), 247

·L.R. McDowell, University of Florida, Gainesville, FL, (1997)

·L.R. McDowell, University of Florida, Gainesville, FL, (1999)

L.R. McDowell, J.H. Conrad, *Seventh International Symposium on Trace Elements in Man and Animals (TEMA-7)*, Dubrovnik, IMI, Zagreb, Yugoslavia, (1991)

L.R. McDowell, G. Valle, (D.I. Givens, E. Owen, R.F.E. Axford, H.M. Omed, eds), CAB International, Wallingford, U.K. (2000)

J. Nelson, Western Nutrition Conference, Winnipeg, Manitoba, Canada (1988)

KC Olson, *Vet Clin Food Anim* 23 (2007) 69-90.

P. Parks, K.J. Harmston, *Feed Menagement*, **45**(10) (1994), 35

Official Journal of the European Union, OJEU, 24/3/2006, L 86/4-7.

Parere su alcuni bisglicinati come fonte di rame, zinco, calcio e magnesio e sul glicinato nicotinato come fonte di cromo in prodotti alimentari destinati alla popolazione in generale (compresi gli integratori alimentari) e in prodotti alimentari destinati a un'alimentazione particolare, *The EFSA Journal* (2008) 718, 2-3.

M.L. Scott, M.C. Nesheim, R.J. Young, *Nutrition of the Chicken*, M.L. Scott and Associates, Ithaca, NY, (1982)

J.W. Spears, *2nd Annual Florida Ruminant Nutrition Symposium*, p. 1. Uaniversity of Florida, Gainsville, FL, (1991)

J.W. Spears, *The Journal of Nutrition*. 2003

J.W. Spears, *Proceedings of the Nutrition Society* (2000), 59, 587-594.

E.J. Underwood, W. Mertz, , *5th Rev. Ed.*, Vol. 1 (W. Mertz, ed.) p. 1 Accademic Press, New York, (1987)

E.J. Underwood, *Proc. Of the Florida Nutrition Conference*, University of Florida, Gainsville, FL, (1979)

E.J. Underwood, Commonwealth Agricultural Bureaux, Slough, U.K., (1981)

Internet web site:

www.efsa.europa.eu

www.ministerodellasalute.it

Experimental

L. Alderighi, P. Gans, A. Ienco, D. Peters, A. Sabatini, A. Vacca, *Coord. Chem. Rev.* 184 (1999) 311-318

A. D. Becke, *J. Chem. Phys.* 98 (1993) 5648-5652

P.T. Callaghan, M.A.L Gros, D.N. Pinder, J. Chem. Phys., 79 (1893) 6372-6381

F. Dallavalle, G. Folesani, R. Marchelli, G. Galaverna, *Helv. Chim. Acta* 77 (1994) 1623-1630

A.J. Dingley, J.P. Mackay, B.E. Chapman, M.B Morris, P.W. Kuchel, B.D. Hambly, G.F. King, *J. Biomol. NMR.*, 6, (1995) 321-328

EURACHEM guidelines - The Fitness for Purpose of Analytical Methods (1998)

S. Ferruzza, G. Ranaldi, M. Di Girolamo, Y. Sambuy, *J. Nutrition* 125 (1995) 2577-2585

S. Ferruzza, M.L. Scarino, G. Rotilio, M.R. Ciriolo, P. Santaroni, A. Onetti-Muda, Y. Sambuy, Am. *J. Physiol.* 277 (1999) G1138-G1148

M. J. Frisch, G. W. Trucks, H. B. Schlegel, G. E. Scuseria, M. A. Robb, J. R. Cheeseman, J. A. Montgomery, Jr., T. Vreven, K. N. Kudin, J. C. Burant, J. M. Millam, S. S. Iyengar, J. Tomasi, V. Barone, B. Mennucci, M. Cossi, G. Scalmani, N. Rega, G. A. Petersson, H. Nakatsuji, M. Hada, M. Ehara, K. Toyota, R. Fukuda, J. Hasegawa, M. Ishida, T. Nakajima, Y. Honda, O. Kitao, H. Nakai, M. Klene, X. Li, J. E. Knox, H. P. Hratchian, J. B. Cross, V. Bakken, C. Adamo, J. Jaramillo, R. Gomperts, R. E. Stratmann, O. Yazyev, A. J. Austin, R. Cammi, C. Pomelli, J. W. Ochterski, P. Y. Ayala, K. Morokuma, G. A. Voth, P. Salvador, J. J. Dannenberg, V. G. Zakrzewski, S. Dapprich, A. D.

Daniels, M. C. Strain, O. Farkas, D. K. Malick, A. D. Rabuck, K. Raghavachari, J. B. Foresman, J. V. Ortiz, Q. Cui, A. G. Baboul, S. Clifford, J. Cioslowski, B. B. Stefanov, G. Liu, A. Liashenko, P. Piskorz, I. Komaromi, R. L. Martin, D. J. Fox, T. Keith, M. A. Al-Laham, C. Y. Peng, A. Nanayakkara, M. Challacombe, P. M. W. Gill, B. Johnson, W. Chen, M. W. Wong, C. Gonzalez, and J. A. Pople, Gaussian 03, *Revision B.04, 2003, Gaussian, Inc.*, Pittsburgh PA

P. Gans, A. Sabatini, A. Vacca, *Talanta* 43 (1996) 1739-1753

S. J. Gibbs, C.S. Johnson Jr, J. Magn. Reson., 93 (1991) 395-402

R. Glahn, M. Gangloff, D. Van Campen, D. Miller, E. Wieven, W. Norvell, *J. Nutrition* 125 (1995) 1833-1840

C.S. Johnson Jr, *Progress in Nuclear Magnetic Resonance*, 34 (1999) 203-256.

C. Lee, W. Yang, R. G. Parr, *Phys. Rev.* B 37 (1988) 785

M. Nardelli, *J. Appl. Cryst.*, 32 (1999) 563

G. Predieri, M. Tegoni, E. Cinti, G. Leonardi, S. Ferruzza, *J. Inorg. Biochem*. 95 (2003) 221-224

Giovanni Predieri, Diego Beltrami, Roberto Pattacini, M. Laura Parisi, Adalgisa Sinicropi Daniela Valensin, Riccardo Basosi, *Inorganica Chimica Acta* – Accepted 2008.

W.S. Price, *Concepts in Magnetic Resonance,* 10 (1998) 197-237

R. Rinda Ontiveros, William D. Shermer and Robert A. Berner, *J. Agric. Food Chem* 1987, 35, 692-694.

G. M. Sheldrick, SHELXL-97, University of Göttingen, Germany, 1997

J. Tomasi, M. Persico, *Chem. Rev*. 94 (1994) 2027-2094

D. Wu, A. Chen, C.S. Johnson Jr. J. Magn. Reson. A. 115 (1995) 260-264

L. Zékány, I Nagypál, G. Peintler, PSEQUAD 5.01 (2001)

Results and discussion

J. Anderson, M. Balda, A. Fanning, Curr. Opin. Cell. Biol. 5 (1993) 772-778

H.D. Ashmead, H. Zuninho in H.D. Ashmead, H. DeWaine (eds), Moyes Publ., Park Ridge, NJ (1993) 21-40

M. J. S. Apines, S. Satoh, V. Kiron, T. Watanabe, T. Aoki, Aquacult. 225 (2003) 431-444

S. Ballard, J. Hunter, A. Taylor*, Annu. Rev. Nutr. 15 (1995) 35-55*

A.T. Blades, M.G. Ikonomou, P. Kebarle, *Anal. Chem.* 63 (1991) 2109-2114

Alessandra Bello, Federica Bianchi, Maria Careri, Marco Giannetto, Giovanni Mori, Marilena Musci, *Analytica Chimca Acta.* 603 (2007) 8-12.

D. J. Bobilya, G.L. Johanning, T. L. Veum, *Am. J. Clinical Nutr.* 59 (1994) 649-653

E.J. Cabrita, S. Berger. *Magnetic Resonance in Chemistry* 39 (2001) S142-S148

J. Cao, P. R. Henry, R. Guo, R. A. Holwerda, J. P. Toth, R. C. Littell, R. D. Miles, C. B. Ammerman, *J. Anim. Sci.* 78 (2000) 2039-2054.

R. Carballo, A. Castiñeiras, B. Covelo, E. García-Martínez, J. Niclós, E. M. Vázquez-López, Polyhedron 23 (2004) 1505

Z.-F. Chen, J. Zhang, R.-G. Xiong, X.-Z. You, *Inorg. Chem. Commun.* 3 (2000) 493

J. J. Dibner, R. C. Durley, J. G. Kostelc, F. J. Ivey, *J. Nutrition* 120 (1990) 553-560

S. Ferruzza, M.L. Scarino, G. Rotilio, M.R. Ciriolo, P. Santaroni, A. Onetti-Muda, Y. Sambuy, *Am. J. Physiol.* 277 (1999) G1138-G1148

S. Ferruzza, M. Scacchi, M. L. Scarino, Y. Sambuy, *Toxicol. In Vitro* 16 (2002) 399-404

S. Ferruzza, M. L. Scarino, L. Gambling, F. Natella, Y. Sambuy, *Cell. Mol. Biol.* 49 (2003) 89-99

A. Fischinger, A. Sarapu, A. Companion, *Can. J. Chem.* 47 (1969) 2629-2637

A. J. Fischinger, L. E. Webb, *J. Chem Soc.* D (1969) 407

M. Fleck, E. Tillmanns, L. Bohaty, Z. Kristallogr. 216 (2001) 633

J. G. Forrest, C. K. Prout, F. J. C. Rossotti, *Chem. Commun.* (1968) 2791-2792

R. Freeman, H. D. W. Hill, L.D. Hall, B.L. Tomlinson, *J. Chem. Phys* 61 (1974) 4466-4473

J.D. Hahn, D.H. Baker, *J. Anim. Sci.* 71 (1993) 3020-3024

L. D. Hall, H. D. W. Hill, *J. Am. Chem. Soc.* 98 (1976) 1269-1270

F. H. Kratzer, P. Vohra, *Chelates in Nutrition*, CRC Press Inc., Boca Raton, FL (1986).

R. O. Kwock, C. L. Keen, J. Hegenauer, P. Saltman, L. S. Hurley, B. Lönnerdal, *J. Nutr.* 114 (1984) 1454-1461

Y. Inomata, T. Haneda, F. S. Howell, *J. Inorg. Biochem.* 76 (1999) 13

A.E. Martell, R.M. Smith, NIST Standard Reference Database 46 Version 6.0, Gaithersburg, MD, 2001

G. Melikyan, F. Amiryan, M. Visi, K. Hardcastle, B. L. Bales, G. Aslanyan, S. H. Badanyan, *Inorg. Chim. Acta* 308 (2000) 45-50

A. Nusrat, J. Turner, J. Madara, *Am. J. Physiol.*, 279 (2000) G851-G857

P. Pastore, A. Gallina, P. Lucaferro, F. Magno, *Analyst* 124 (1999) 837-842

M. Pinto, S. Robine-Leon, M. Appay, Biol. Cell. 47 (1983) 323-330

G. Predieri, M. Tegoni, E. Cinti, G. Leonardi, S. Ferruzza, *J. Inorg. Biochem.* 95 (2003) 221-224

Giovanni Predieri, Diego Beltrami, Roberto Pattacini, M. Laura Parisi, Adalgisa Sinicropi Daniela Valensin, Riccardo Basosi, *Inorganica Chimica Acta* – Accepted 2008.

R. Rinda Ontiveros, William D. Shermer and Robert A. Berner, *J. Agric. Food Chem* 1987, 35, 692-694.

A. Rossi, R. Poverini, G. Di Lullo, A. Modesti, A. Modica, M.L. Scarino, *Toxicol. In Vitro* 10 (1996) 27-36

Y. Sambuy, S. Ferruzza, G. Ranaldi, I. De Angelis, *Cell. Biol. Toxicol.*, 17 (2001) 301-317

K. D. Singh, S. C. Jain, T. D. Sakore, A. B. Biswas, *Acta Crystallogr.*, Sect. B 31 (1975) 990

G. Smith, E. J. O'Reilly, C. H. L. Kennard, T. C. W. Mak, *Inorg. Chem*. 24 (1985) 2321

J. W. Spears, D. P. Hutcheson, N. K. Chirase, E. B. Kegley, *J. Anim. Sci*. 69 (Suppl. 1) (1991) 552

J.W. Spears, *Anim. Feed Sci. Technol*. 58 (1996) 151-163

Stilbs e Lindman 1981, P. Stilbs, B. Lindman, *J. Phys. Chem.*, 85 (1981) 2587-2589

J.W., Swinkels, E.T. Kornegay, W. Zhou, M.D. Lindemann, K.E. Webb, M.W. Verstegen, *J. Anim. Sci*. 74 (1996) 2420-2430

L. K. Templeton, D. H. Templeton, D. Zhang, A. Zalkin, Acta Crystallogr., Sect. C: *Cryst. Struct. Commun*. 41 (1985) 363

S. Tsuji, T. Shibata, Y. Ito, S. Fujii, K.-I. Tomita, Acta Crystallogr., Sect. C: *Cryst. Struct. Commun*. 47 (1991) 528

G. J. Van Berkel, S.A. McLuckey, G.L. Glish, *Anal. Chem*. 63 (1991) 1971-1978

K. J. Wedekind, A. E. Hortin, D. H. Baker, *J. Anim. Sci*. 70 (1992) 178-187

R.-G. Xiong, J.-L. Zuo, X.-Z. You, H.-K. Fun, S. S. Raj, *New J. Chem.*, 23 (1999) 1051

F. Zucco, I. De Angelis, F. Delie, W. Rubas, *Crit. Rev. Therap. Drug Carrier Syst*. 14 (1997) 221-286